Application of Boron Doped Diamond Electrodes to Electrochemical Gas Sensors

February 2022

Yunita Triana

A Thesis for the Degree of Ph.D. in Engineering

Application of Boron Doped Diamond Electrodes to Electrochemical Gas Sensors

February 2022

Graduate School of Science and Technology
Keio University

Yunita Triana

Table of Contents

Chapter 1

General Information

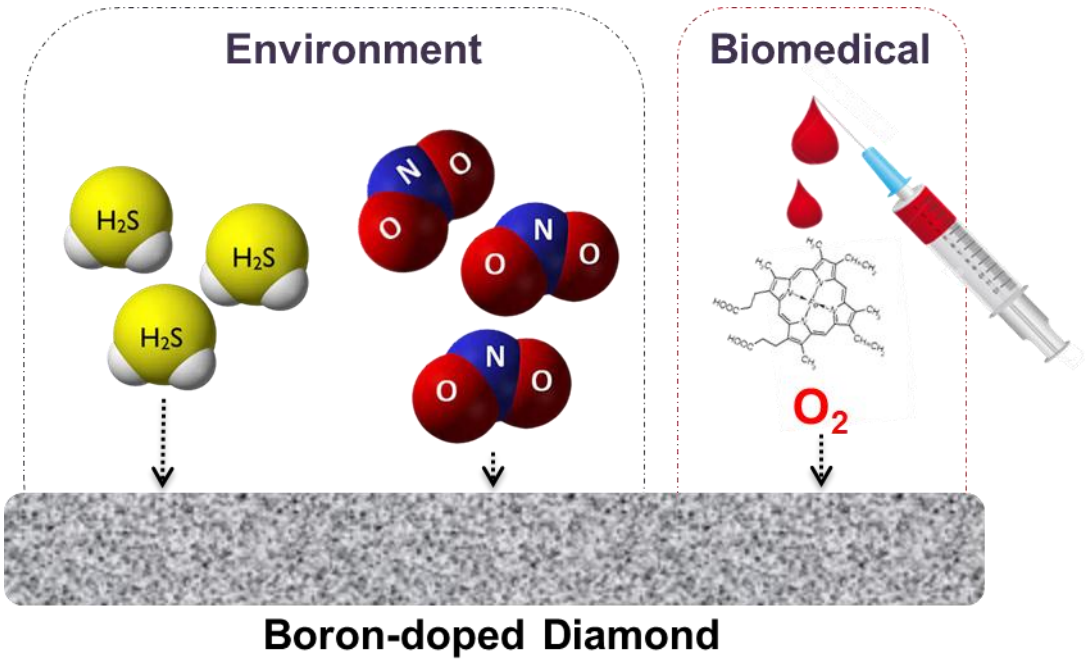

CHAPTER 1.
General Information

1. Development of Gas Sensor

A device, module or machine that detects events or changes and relays the information to other electronics is called sensor. A sensor reads physical phenomena and converts into a measurable digital signal, which can then be displayed, read, or processed further[1]. There is a range of sources, including light, temperature, movements, and pressure etc. Sensors are embedded in everything we come into contact with in our everyday lives. Subsequent subsections show some of the critical sensors used in our daily life are level, temperature, proximity, pressure, chemical, infra-red, and many other sensors[2].

Among them, there is gas sensor which similar to chemical sensors, except that they monitor air quality and detect various gases. Gas sensor provides a vital way to monitor gas concentration and gives safety information. Gas sensor technologies have improved the everyday life of human beings through their applications in almost all fields[3]. They are used for air quality monitoring, toxic or combustible gas detection, hazardous gas monitoring and medical application.

1.1 Application of Gas Sensor to Improve Environmental Monitoring

Biotic and abiotic factors are the composition of our atmosphere. In fact, abiotic factor is quite essential for life on the planet. The abiotic factors are such as gases, moisture, humidity, and temperature. The hazardous gases should not increase beyond a critical level shoud be maintained to keep oxygen in an adequate level. Atmospheric pollution can create a high level of health and life loss within the short span of time. Environmental pollution, urbanization, use of automobiles, fuel burning, and industrial wastes are the main source for the increasing of hazardous gas concentration in the air. Six pollutants have been identified as the main source of air pollution. The particulate matter consists of lead and gases like oxides of carbon and oxides of nitrogen[4]. There are several diseases which result from pollution and threaten human health. Seven million deaths take place due to pollution[5]. This is because respiratory organ diseases are mainly ascribed to poor air quality. The major diseases resulting from air pollution are stroke, ischemic heart diseases, lower respiratory infections and lung cancer[6]. For the environmental effect may cause acid rain. Air quality control is the main aspect in the field of environmental monitoring. Gas sensing devices are used to protect plants and personnel from inflammable and toxic gases. They can cause hazard to human and their belongings due to its toxic nature such as hydrogen sulfide and nitrogen dioxide.

a. Hydrogen Sulfide (H_2S)

Today the rapid expansion of industries gives contribution as a serious problem to the environment and human health safety. Especially, waste gas such as hydrogen sulfide (H_2S) attracts much interest due to the dangerous characteristics. Hydrogen sulfide (H_2S) is known to be a corrosive, poisonous, and gaseous compound. Hydrogen sulfide is basically a gas state chemical that also found in the dissolved form[7].

It is widely found in several water pollutant resources such as sewage treatment plants, electric power waste, coal processing plants, sulfur production processes, commercial

hydrogen sulfide production, and other resources[8]. At concentrations greater than 500 parts per million, inhalation of hydrogen sulfide can lead to immediate collapse and unconsciousness. Unconsciousness and death have occurred in situations of prolonged exposure to hydrogen sulfide at concentrations of 50 ppm. The estimated global release of hydrogen sulfide from saline marshes into the atmosphere is 8.3×10^5 ton per year. The Occupational Safety and Health Administration (OSHA) define Permissible Exposure Limits (PELs) to H_2S gas: 20 ppm for ceiling industry, 50 ppm (up to 10 minutes if no other exposure during shift) for general industry, 10 ppm for construction and shipyard[9].

The strict implementation of industrial gas waste regulations is required the highly reliable and accurate gas sensors devices. High-performance liquid chromatography[10,11] and gas chromatography[12,13] are used to detect H_2S. There are some weaknesses of the methods such as long incubation times due to the process in the column and these instruments are expensive.

Recently, electrochemical sensor has been growing interest to detect H_2S due to the sensitivity, selectivity, real-time detection and low detection limit[14]. By electrochemical method, there are potentiometric[15] and amperometric[16] techniques to detect H_2S. However, the main problem is durability of the working electrode (*eg*. glassy carbon and platinum electrodes) due to sulfur (S^0) layer as an oxidation product via 2 electrons can degrade the analytical performance. Therefore, a redox mediator is needed to prevent sulfur deposited on the surface of working electrodes such as room temperature ionic liquids (RTILs), hydroxyl-functionalized ionic liquids, phenol, phenylenediamine, and eugenol. However, organic solutions are expensive and harmful for the environment. Therefore, researches on high sensitivity, selectivity and high durability material for electrochemical H_2S sensor have become a hot issue.

b. Nitrogen Dioxide (NO_2)

Nowadays, road traffic and automobiles activities are sources of pollution released into the atmosphere since the beginning of the twentieth century. Our urban and rural areas are currently subject to pollution peaks such as ozone, nitrogen dioxide, and carbon monoxide. One of six criteria air pollutants designated by the United States Environmental Protection Agency (USEPA) is nitrogen dioxide (NO_2). It is formed in the atmosphere from nitrogen monoxide (NO), which is mainly released during the combustion of fossil fuels[17].

NO_2 is a reddish-brown flammable gas with a characteristic odor. At low concentrations of NO_2, medical consequences include difficulty in breathing, chest pain and chronic respiratory problems. This gas is extremely toxic at high concentrations above 360 ppb. From an environmental point of view, nitrogen dioxide is converted into nitric acid in the presence of water molecules and contributes to form as acid rain. Therefore, the monitoring of air quality and gaseous pollutants is the goal of several researchers around the world. The most difficult pollutants to control is NO_2[18].

Maximum 30-minute or 1-hour average and maximum 24-hour average outdoor nitrogen dioxide concentrations of up to 0.5 ppm and 0.21 ppm, respectively. In Japan, the short-term exposure limit for NO_2 gas is 500 ppb, and the environmental standard value is 40 to 60 ppb[19].

It leads to urgent needs for sensitive, selective, and responsive NO_2 sensors. High performance liquid chromatography (HPLC)[20] and gas chromatography[21] are used for NO_2 detection. However, it caused cost ineffectiveness, insufficient sensitivity for detection, and time consuming sample incubation. Chemiluminescence[22,23] combined with HPLC and gas chromatography is also widely used but the response time is limited.

In the last decades, electrochemical sensors have presented a promising way forward for the detection of NO_2 gas, since they offer real time measurement, simplicity with a low limit of detection (LOD) and good selectivity[24,25]. By electrochemical technique, metal electrodes such as Pt (platinum) and gold (Au) are modified with nafion[26], yttria-stabilized zirconia (YSZ)[27], and teflon[25] to increase the performance. However, surface modification is difficult and many optimizations to prepare. In other hand, carbon based electrodes such as glassy carbon[28], graphite[29], and carbon nanotubes[30] have disadvantages of limited sensitivity, poor precision and lack of durability. Further investigation of good performance material for electrochemical NO_2 sensor attracts much attention recently.

1.2 Application of Gas Sensor in Biomedical Diagnostic

The intake of oxygen (O_2) and the release of carbon dioxide (CO_2) are the most important activities for human health. Respiration provides a constant flow of O_2 molecules to our brain, organs and tissues while providing a way to remove the waste CO_2 molecules that are created in the cells[31]. Without respiration, our bodies will shut down within seconds. Therefore, regardless of the procedure, wound, disease or illness, one of the first priorities of a physician is to insure continuous respiration. For this reason, gas sensor is critical instruments in medical applications. In order to measure respiration, physicians and health care workers use several O_2 and CO_2 gas sensors. These gases are measured in 2 areas: the breath and the blood.

Blood O_2 monitoring can play as an essential role of disease biomarker such as hypoxemia, COVID-19 infection, heart failure, cancers and other diseases related to O_2 concentration in human body[32]. Oxygen is measured 3 ways, as partial pressure of oxygen (PaO_2), as oxygen saturation (O_2 Sat) and for oxygen content (O_2CT) in the blood. Normal O_2 concentration in human body is around 40 – 100 mmHg[33].

Optical detection is commonly used for O_2 concentration in daily life for example oximeter[34] and diffuse optical tomography[35]. These instruments show O_2 concentration in saturated O_2 in percentage (% SpO_2). However, oximeter has lack of sensitivity due to its limitations of the arterial pulse strength, body movement, lipids and bilirubin, color of the skin, and other physical factors[36] from the patients. So, it cannot show the real condition of the patients. Resonance[37] methods also can detect O_2 but expensive and difficult to calibrate.

Electrochemical sensors have been attracted much attention due the real-time measurement and sensitivity. By electrochemical methods, there are polarographic[38] and conductometry[39]. However, the techniques are difficult to be applied due to ineffectiveness and lack of accuracy. Therefore, developing of design material for electrochemical O_2 gas sensor is challenging and increasing in biomedical application.

2. Boron Doped Diamond (BDD) Electrodes

Diamond offers many unique properties, such as chemical inertness, extreme hardness and thermal conductivity, low friction coefficients, and high charge carrier mobility. However, natural diamond cannot be used as an electrode material, as it is a very wide band gap semiconductor, with extremely high inherent electrical resistivity (1016 Ω cm)[40]. Charge carriers into diamond surface can make it conductive. Boron has one less electron than carbon and has a small atomic radius and easily incorporated into diamond as a charge acceptor, providing a p-type semiconducting characteristic to diamond. Thus, doping with boron enhances conductivity and electron-transfer reactivity[40].

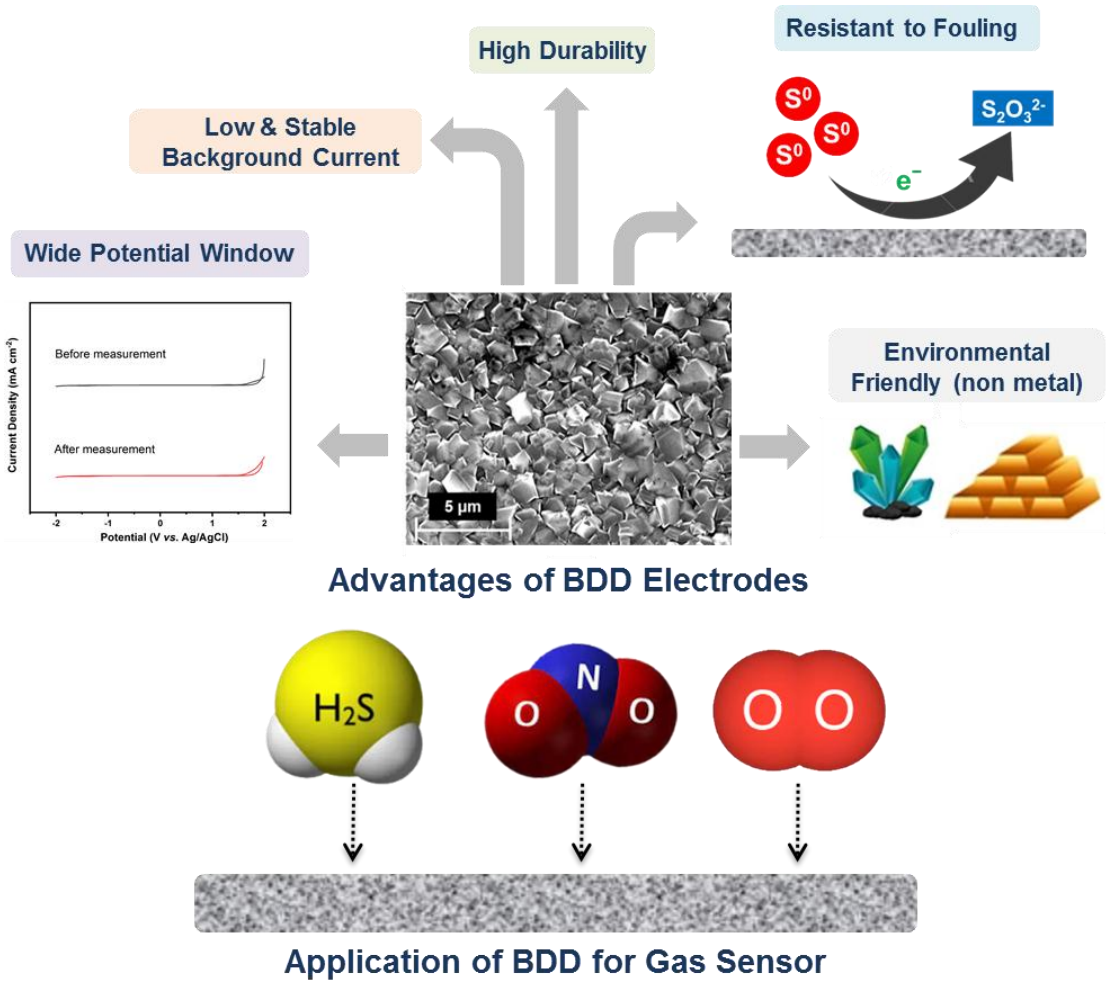

Figure 1.1. Purpose of thesis study

Boron doped diamond (BDD) thin films are the subject of considerable interest as an electrode material[41]. In comparison with other electrode materials, such as gold, platinum and glassy carbon, BDD has advantages:

a. The largest electrochemical potential window for aqueous (~3–3.5 V) and non-aqueous media (~5.0–7.5 V)[40]

b. A small and stable background current, which is attributed to the low capacitance of the BDD material (10 μF cm^{-2}), compared to conventional electrode materials, such as Pt and Au (~30 μF cm^{-2})[42].
c. A broad electromagnetic transparency window ranging from the UV-Vis region to the far-infrared region.
d. Low magnetic susceptibility compared to other electrode materials such as Pt.
e. Electrochemical properties tunable by the boron concentration in the diamond lattice, presence of sp^2 carbon, and surface termination.
f. The sp^3 hybridized structure of BDD is resistant to biofouling and biocompatible with organisms. These properties make it possible for *in vivo* real-time detection[43,44].

There are some important factors which affecting the electroanalytical properties of BDD electrodes. The first feature is the concentration of boron doping level (boron/carbon ratio). Increasing the B/C ratio leads to decrease in the overall width of the potential window because boron-rich sites are directly involved in the adsorption steps needed for gas evolution reactions. For electrochemical applications, a high boron concentration in diamond is usually preferable owing to its higher conductivity[45] as shown in Table 1.1.

Tabel 1.1 Effect of boron doping level

Boron Doping Level	Signal (Conductivity)	Potential window	Background Current
0.1%			
0.5%			
1%			
2%			

Second feature is the ratio of sp^3/sp^2. The deposition conditions are usually selected to minimize the incorporation of sp^2-bonded non-diamond carbon impurities; however, these impurities can be introduced in a controlled manner by adjusting the deposition conditions. The presence of sp^2 carbon impurities in diamond has several main effects on the electroanalytical performance of BDD electrodes[46]. Sp^2 carbon has a higher density of electronic states than sp^3 carbon and thus leads to faster electron transfer[47]. Moreover, sp^2 hybridized materials react with oxygen and water to form oxygen-containing functional groups. sp^2 carbon catalyzes redox reactions, providing adsorption sites for reactants and reaction intermediates. In addition, sp^2 carbon at the electrode surface results in surface-bound quinone groups, which show a pH dependent redox signature when appropriately activated.

The last feature is BDD surface termination/pre-treatment (*e.g.* hydrogen or oxygen). Amongst all the factors that can influence the electrochemical response of BDD electrodes,

possibly the most complex is the effect of the surface termination (H, O) due to its influence on the physical, chemical and electronic characteristics of the BDD surface[48]. Consequently, H, O termination of the BDD electrode surface[49] influences the electrochemical activity for both outer-sphere and inner-sphere redox processes[50].

These characteristics have led BDD to be used as electrochemical sensing such as free chlorine[51], oxalic acid[52], protein[53], imunosensor[54]. BDD electrodes are not only used in the aqueous electrolyte[55], but also in nonaqueous and solid electrolytes[56] state such as room temperature ionic liquid (RTIL)[57], nafion[58] or polymer[59]. Therefore, we proposed BDD as working electrodes for electrochemical gas sensing without any mediator or modification, simple procedure, cheap, high durability and environmental friendly to detect gas due to its special characteristic in this thesis as shown in Figure 1.1. So far, we reported on using BDD electrodes as gas sensor for arsine (AsH_3)[60], H_2S[61] and NO_2[62] sensor. Publication of BDD electrodes as O_2 sensor in blood solution is under submission process.

2.1 Pretreatment of BDD Electrodes

As we mentioned above the importance of BDD surface termination influence the electroactive surface on BDD electrodes. There are hydrogen termination (H-BDD) and oxygen termination (O-BDD). Conversion from hydrogen to oxygen-termination can be achieved by exposing the BDD to an oxygen plasma[63], anodic oxidation (AO)[64] or other methods[65]. On the other hand, conversion from oxygen to hydrogen-termination can be done by exposing it to a hydrogen plasma[66,67] or cathodic reduction (CR)[68].

In this research, the BDD was cleaned by chronoamperometry (+3 V vs. Ag/AgCl for 5 minutes and -3 V *vs*. Ag/AgCl for 15 minutes in 0.1 mol L^{-1} H_2SO_4) to be H-BDD. For O-BDD, the BDD was cleaned by chronoamperometry (-3 V vs. Ag/AgCl for 5 minutes and +3 V *vs*. Ag/AgCl for 15 minutes in 0.1 mol L^{-1} H_2SO_4)[69].

Based on the previous report[70], electrochemical H-termination generates a clean surface with virtually no carbon–oxygen bonds (x-ray photoelectron spectroscopy), a reduced electron affinity (scanning electron microscopy), a highly hydrophobic surface (water contact angle), and a fast electron exchange. H-BDD promotes positive dipole on the surface of BDD electrodes due to OH^- is replaced by H^+. It gives advantages for gas sensing application which have negative dipole especially H_2S, NO_2 and O_2. O-BDD is more negative dipole since OH^- is existing on the surface[69]. Moreover, under the open circuit condition, the H-BDD band position is very high with respect to the valence band maximum (VBM) of water than O-BDD[42,71]. It can increase the electroactive area on BDD to give higher sensitivity to analytes.

In this book, we studied about the effect of H-BDD and O-BDD to the electrochemical behavior. By using H-BDD, interaction between analytes and the surface can reach higher signal than O-BDD which will be discussed on the next chapter.

2.2 Preparation and Characteristic of BDD Electrodes

In this research, the BDD electrodes were deposited onto Si(111) wafer substrates by a microwave plasma-assisted chemical vapor deposition (MP-CVD) system (AX5250M; Cornes Technologies Ltd.). The boron and carbon sources were trimethyl borate and acetone, respectively. The boron-to-carbon ratio in the feed gas was 1% (1% BDD). A boron-carbon

ratio of 1% was generally selected as these values had been reported to be the most suitable for sensor applications due to wide potential window and high conductivity[45,72]. Deposition was carried out for 6 h at 5 kW. Details of the BDD fabrication process have been presented elsewhere[55]. The BDD electrodes were characterized by Raman spectroscopy (excitation wavelength: 532 nm). Details of the BDD characterization are shown in Figure 1.2.

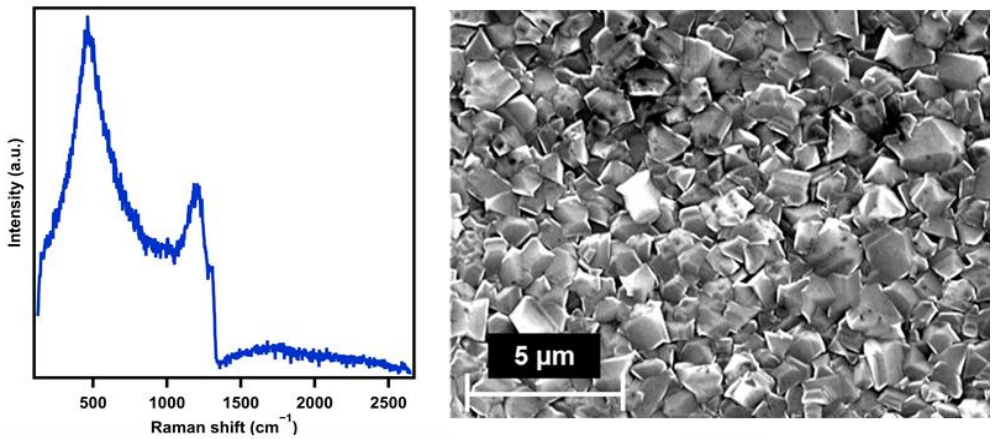

(A) (B)

Figure 1.2. Raman spectra (A) and SEM images (B) of BDD electrodes.
(Reprinted with permission from ref. [55]. Copyright 2020 Elsevier.)

The Raman spectrum of the 1% BDD electrode has a peak around 1300 cm^{-1}, indicating a diamond structure based on Figure 1.2A. Typical spectrums of 500 cm^{-1} and 1200 cm^{-1} showed sp^3 carbon and two peaks for boron while sp2 carbon as impurities at 1600 cm^{-1} was not appeared in peak. This information indicated that BDD was in high quality electrodes. Based on Figure 1.2B, SEM images of the electrodes showed polycrystalline morphology with a grain size of around 5 µm.

3. Purpose of the Thesis

This thesis will describe the study of **(1) electrochemical behavior, (2) reaction mechanism, and (3) analytical performance** of gas detection by using boron doped diamond for hydrogen sulfide, nitrogen dioxide, and oxygen gas.

In **Chapter 2**, we studied an oxidation reaction of dissolved H_2S in aqueous solution using boron doped diamond (BDD) electrodes. In order to study the oxidation behavior, the effects of pH and the scan rate were investigated. Sulfur fouling was detected on the BDD surface by X-ray photoelectron spectroscopy. Moreover, we showed the comparison of analytical performance with glassy carbon and platinum.

In **Chapter 3**, the electrochemical oxidation reaction of NO_2 in aqueous solution using boron doped diamond (BDD) electrodes is presented. The pH and scan rate dependences were investigated to study the oxidation mechanism. In addition, the analytical performance was compared with glassy carbon, platinum and stainless steel.

In **Chapter 4**, the electrochemical reduction behavior of oxygen (O_2) in blood was studied using boron doped diamond (BDD) electrodes. The scan rate dependence was investigated to study the reduction reaction mechanism. The analytical performance was

compared with glassy carbon or platinum electrodes as the working electrode. In addition, an application to bovine blood was performed. The O_2 concentration in the blood measured on the BDD electrodes was compared to that measured using the OxyLite Pro™ fiber-optic oxygen sensor device.

Chapter 2

Oxidation Reaction of Dissolved Hydrogen Sulfide Using Boron Doped Diamond

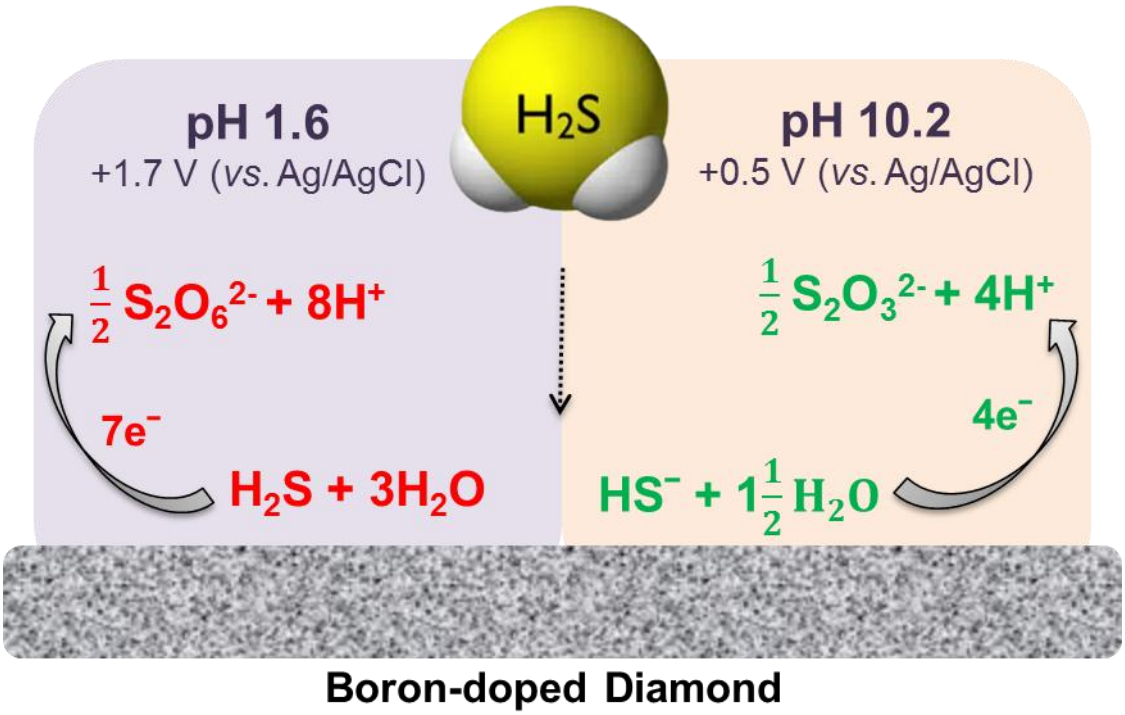

CHAPTER 2.
Oxidation Reaction of Dissolved Hydrogen Sulfide Using Boron Doped Diamond

1. Introduction

Hydrogen sulfide (H_2S) is a flammable, water soluble and colorless gas with a strong smell of rotten eggs. It is also harmful when emitted into the air [73]. H_2S is a by-product of natural biological activities and an industrial pollutant [74–76]. Various methods have been developed to detect H_2S. High-performance liquid chromatography[10,11] and gas chromatography[12,13] are used to detect H_2S; however the incubation times are long because of the process in the column and it can turn into sulfur dioxide under specific conditions. Furthermore, these instruments are expensive.

Electrochemical sensors have some advantages for H_2S detection. The sensitivity, selectivity, and stability are high, and detection is in real time, with a low-detection limit (LOD) and good reproducibility[77]. There are some options for the detection of sulfide and H_2S by electrochemical methods such as potentiometric[78] and amperometric[79–81] techniques. However, the lack of durability is a problem. A layer of sulfur produced on the surface of the electrodes after a measurement can degrade the analytical performance[82]. Sulfur (S^0) is a possible product via two-electron oxidation from H_2S and HS^-[83].

$$H_2S \rightarrow S^0 + 2e^- + 2H^+ \quad (1)$$

$$HS^- \rightarrow S^0 + 2e^- + H^+ \quad (2)$$

Thus, many methods require a redox mediator to prevent sulfur from being deposited on the surface. An electron is received from H_2S or HS^- and is regenerated on the working electrode and a measurable current can be observed[84]. Room temperature ionic liquids (RTILs)[85] and hydroxyl-functionalized ionic liquids[86] are used as mediators. Moreover, phenol, phenylenediamine, and eugenol are used to modify the surface of the electrodes[87]. However, organic solutions are expensive and harmful for the environment. Other than that, surface modification is not easily achieved.

In this paper, we propose a simple, environmentally friendly procedure using reusable boron doped diamond (BDD) electrodes. BDD electrodes have a wide potential window in aqueous solutions, low background currents, and chemical and mechanical stability. The surface of BDD can be easily controlled by an electrochemical treatment[88]. These characteristics have led BDD to be used in electrochemical sensing applications[89] such as for detecting drugs[90], measuring pH[91] and so on. So far, an arsine (AsH_3) gas detection has been reported as gas sensors utilizing BDD electrodes [60]. Although several works on H_2S detection by BDD electrodes have been reported [92,93], they have not studied in detail on the oxidation mechanisms.

In this work, we attempted to study the electrochemical oxidation reaction of dissolved hydrogen sulfide using BDD electrodes and to detect H_2S or HS^- without using a mediator or modifying the surface. Especially, the pH of the electrolyte and the scan rate of the CV measurement were varied to investigate the electrochemical reaction. Then, the performance was examined, and an interference test was conducted. The performance was compared with that of two other commonly used electrodes for hydrogen sulfide sensing: glassy carbon and platinum electrodes.

2. Experimental

2.1 Preparation of H_2S Gas

H_2S gas was produced from the reaction between 1 g FeS (Purity: 50%) and 1 mol L^{-1} HCl 20 mL in a closed system. The reaction is as follows:

$$FeS(s) + 2HCl(aq) \rightarrow H_2S(g) + FeCl_2(aq) \quad (3)$$

The gas was bubbled into 1 mol L^{-1} $KClO_4$ 20 mL aqueous solution, and this solution was used for electrochemical and methylene blue measurements. The scheme is shown in Figure 2.2.

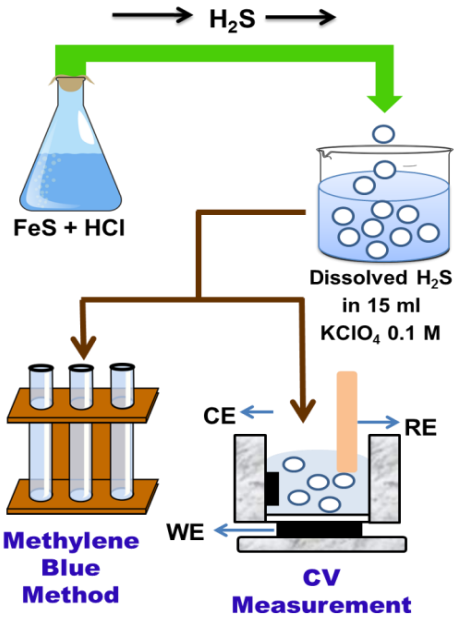

Figure 2.1. Schematic of dissolved H_2S detection by using BDD electrodes. (Reprinted with permission from ref. [55]. Copyright 2020 Elsevier.)

2.2 Methylene Blue Method

The procedure to determine the concentration of H_2S was as follows[94]. Na_2S was used as a stock solution. The stock solution concentration was verified by iodometric titration[95]. The following solutions were prepared:

Reagent A: 0.125 g $Zn(CH_3COO)_2$ in 250 mL of 0.25 mol L^{-1} NaOH

Reagent B: 0.1 g N-N-dimethyl-p-phenylenediamine in 100 mL of 5.5 mol L^{-1} HCl

Reagent C: 0.023 mol L^{-1} $FeCl_3$ in 1.2 mol L^{-1} HCl

Sample: 0.1 mol L^{-1} $KClO_4$ (20 mL) aqueous solution in which H_2S gas was dissolved.

Reagent A (10 mL) was added to the sample to precipitate ZnS which floated in the solution. Reagent B (2 mL) and reagent C (2 mL) were added to that solution. The optical density of this solution was measured by an ultraviolet-visible (UV-Vis) spectrophotometer (V-570, JASCO) at a wavelength of 670 nm.

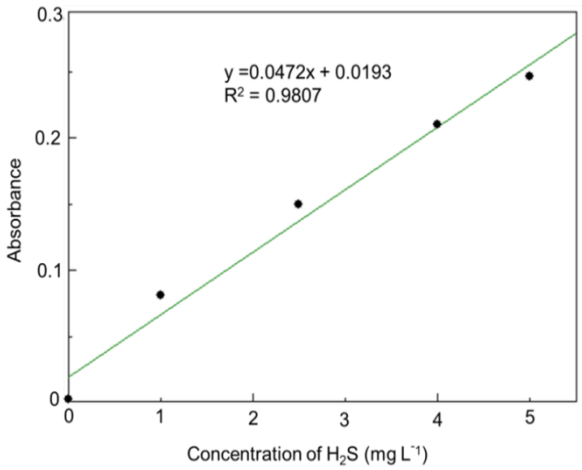

Figure 2.2. A plot of the concentration of Na_2S (sulfide standard solution) against the absorbance. (Reprinted with permission from ref. [55]. Copyright 2020 Elsevier.)

Na_2S which concentration was 0, 1, 2.5, 4, and 5 mg L^{-1} was added into NaOH with $Zn(CH_3COO)_2$ to precipitate ZnS. Then, *N*-*N*-dimethyl-*p*-phenylenediamine and $FeCl_3$ were added into the solution and methylene blue color appeared. The optical density of this solution was measured by ultraviolet-visible (UV-Vis) spectrophotometer at wavelength of 670 nm. The concentration of Na_2S and the absorbance of solutions were plotted (Figure 2.2). Concentration of H_2S bubbled into solutions was determined from the calibration curve obtained from Na_2S measurements.

2.3 Chemicals and Materials

All of the chemicals were purchased from FUJIFILM Wako Pure Chemical Corporation and used without further purification. Ultrapure water with a resistivity of 18.2 MΩ cm at 25^0C was obtained from a Simply-Lab water system (DIRECT-Q UV3 system, Millipore Corp.).

2.4 Electrochemical Measurements

All measurements were conducted at room temperature (25^0C). 0.1 mol L^{-1} $KClO_4$ was used as an electrolyte. $HClO_4$ and KOH were used to obtain solutions with pHs of 1.6, 7.0 and 10.2. A three-electrode cell was used for electrochemical measurements. 1% BDD was used as the working and counter electrodes and Ag/AgCl (saturated KCl) was used as the reference electrode. The geometric surface area of the working electrode was 0.08 cm^2 (r = 0.16 cm). Before each measurement, the following pretreatment of the BDD electrodes was conducted. First, the BDD was soaked in aqua regia for 30 minutes. Next, it was ultrasonicated in pure water for 15 minutes and dried with N_2 gas. Finally, the BDD was cleaned by chronoamperometry (+3 V vs. Ag/AgCl for 5 minutes and -3 V *vs*. Ag/AgCl for 15 minutes in 0.1 mol L^{-1} H_2SO_4) to be hydrogen terminated BDD (H-BDD)[69]. Glassy carbon (GC) and platinum (Pt) working electrodes were also used and the performance compared with that of the BDD electrode with the same geometric surface area and electrochemical setup. Before each measurement, the surfaces of the GC and Pt electrodes were polished with alumina slurry (0.05-1.0 μm). After polishing, they were ultrasonicated in ethanol for 15 minutes, cleaned with pure water and dried with N_2 gas. Chronoamperometry

and cyclic voltammetry (CV) measurements were carried out with a Versa STAT 4 Potentiostat/Galvanostat (Ametek Inc.).

2.5 Sulfur Analysis

X-ray photoelectron spectroscopy (XPS) was used to observe passivation by sulfur on the surface of the electrodes. XPS spectra were obtained with a JPS-9010TR (JEOL Ltd.). The background was subtracted from the spectra, and peaks were found and fitted using Origin 2020. S 2p spectra were assigned to the following components: 168 eV (S 2p) and 164 eV ($C-SO_x$). These binding energies were fixed for all of the analyses.

3. Result and Discussion

3.1 Effect of BDD Pretreatment to H_2S Detection

First, we investigated the effect of surface termination on BDD electrodes to detect H_2S in 0.1 M $KClO_4$ at pH 7. The CVs were recorded at 0.1 V s^{-1}, over the potential range 0 V to 2.0 V (*vs.* Ag/AgCl). For hydrogen termination (H-BDD), the BDD was cleaned by chronoamperometry (+3 V vs. Ag/AgCl for 5 minutes and -3 V *vs*. Ag/AgCl for 15 minutes in 0.1 mol L^{-1} H_2SO_4). For oxygen termination (O-BDD), the BDD was cleaned by chronoamperometry (-3 V vs. Ag/AgCl for 5 minutes and +3 V *vs*. Ag/AgCl for 15 minutes in 0.1 mol L^{-1} H_2SO_4). As shown in Figure 2.3, both CV's show similar oxidation peak at around +0.5 V, broad peak +1.3 V and +1.6 V (*vs*. Ag/AgCl). In the other hand, the current density is higher on H-BDD blue line) than O-BDD (red line). It is due to the higher conductivity of H-BDD as reported[48]. Based on this result, H-BDD was used as the following pretreatment to detect H_2S.

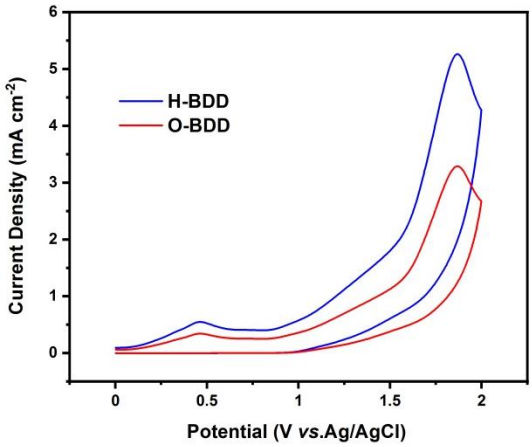

Figure 2.3. CVs of 1.30 mg L^{-1} H_2S at pH 7 in 0.1 mol L^{-1} $KClO_4$ using BDD for the working electrode with H-BDD (blue line) and O-BDD (red line) pretreatment.

3.2 Oxidation Reaction of Dissolved H_2S

We carried out cyclic voltammograms at various pH values. Figure 2.4A shows a cyclic voltammogram for dissolved H_2S in 0.1 mol L^{-1} $KClO_4$ at pH 7.0 using BDD for the working electrode. The CVs were recorded at 0.1 V s^{-1}, over the potential range 0 V to 2.0 V (*vs.* Ag/AgCl) (CVs were scanned in the positive direction from 0 V to +2.0 V and then back to 0

V). Note that, at this pH, the ratio of H_2S/HS^- is balanced in the electrolyte[96]. Sharp oxidation features can be seen at +0.5 V and +1.7 V (*vs.* Ag/AgCl) while a prominent shoulder appears at +1.3 V (*vs.* Ag/AgCl). In the CV performed at pH 7 the oxidation profiles of both species are combined.

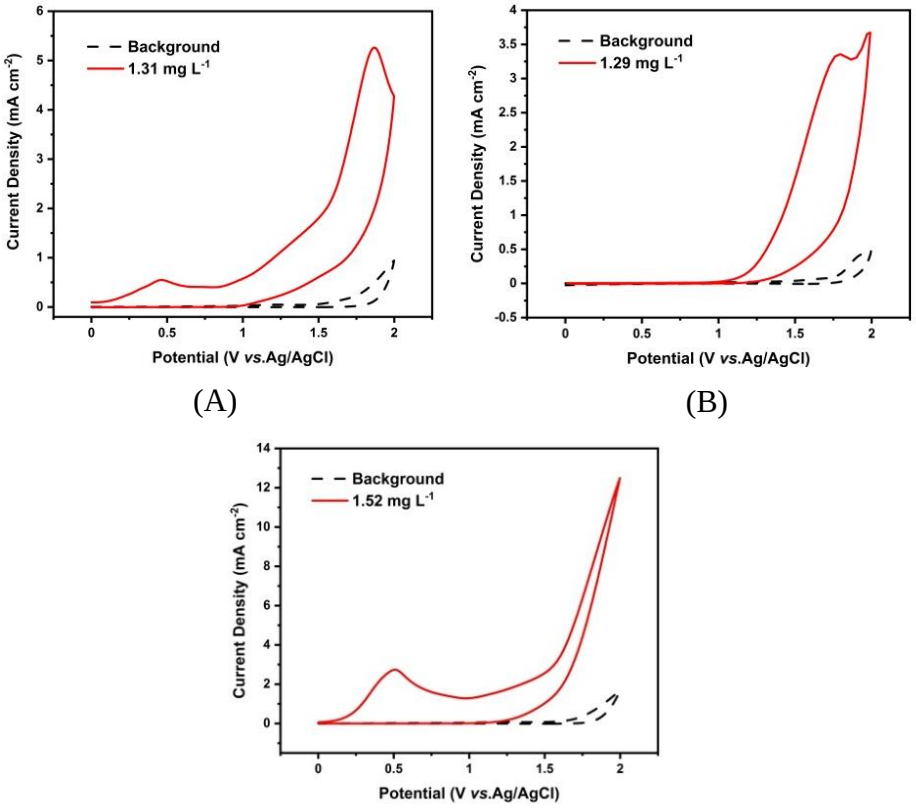

Figure 2.4. CVs of dissolved H_2S at pH 7.0 (A), pH 1.6 (B), and pH 10.2 (C) in 0.1 mol L^{-1} $KClO_4$ using BDD for the working electrode.
(Reprinted with permission from ref. [55]. Copyright 2020 Elsevier.)

We varied the pH to confirm the oxidation behavior. The electrolyte pH was adjusted to 1.6 and 10.2 in order to individually characterize the CVs for H_2S and HS^-. H_2S is the dominant species at pH 1.6 and HS^- at 10.2[96]. At pH 1.6, a single oxidation peak at +1.7 V (*vs.* Ag/AgCl) is clearly observed using a BDD electrode (Figure 2.4B), which is owing to the high overpotential for the water electrochemical reaction[44]. At pH 10.2, an oxidation peak at +0.5 V (*vs.* Ag/AgCl) was observed (Figure 2.4C), which is consistent with a previous work[97]. No reduction peaks were observed in the reverse scan under acidic conditions. The results of this experiment showed that dissolved hydrogen sulfide is oxidized on BDD electrodes as reported[93], and, moreover, suggest that oxidation of dissolved H_2S can be detected individually at different pH values using BDD electrodes.

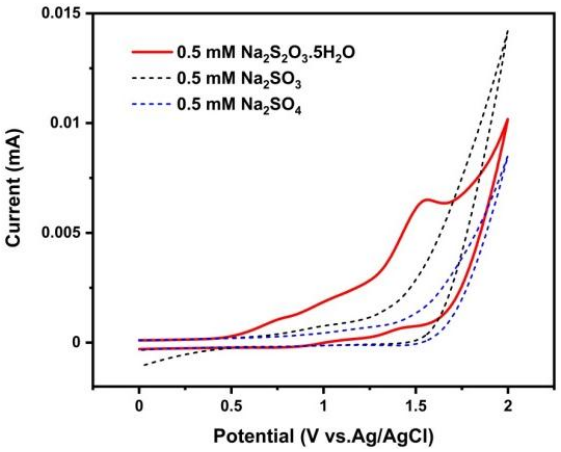

Figure 2.5. Oxidation Peak of Thiosulfate Solution.
(Reprinted with permission from ref. [55]. Copyright 2020 Elsevier.)

Note that, although the oxidation peaks are expected to be shifted depending on pH based on Nernst equation, the observed peak shifts were very small. Here, it was observed at +0.46 V (vs Ag/AgCl) at pH=7.0, while at +0.50 V (vs. Ag/AgCl) at pH=10.2. This might be due to the specific surface properties of BDD electrodes, which could be affected by boron doping level[98], surface termination[69], small sp^2 species (impurity) and grain boundary.[88]

Then, we turned our attention to the broad oxidation shoulder obtained at +1.3 V (*vs.* Ag/AgCl) when using an electrolyte with pH 10.2 (Figure 2.4C) which also appeared when the electrolyte with pH 7.0 was used. We analyzed the oxidation behavior using thiosulfate, sulfite and sulfate aqueoues solutions in the electrolyte. In fact, an oxidation peak was observed for thiosulfate ($S_2O_3^{2-}$) as shown in Figure 2.5. The indication is that the peak at +1.3 V (*vs.* Ag/AgCl) is due to an oxidation product. Another possibility is that this is due to oxidation by hydroxide ions. It was found that the surface conditions affected the BDD electrode as reported previously[99]. So, this unique feature might be an overlap effect between both conditions.

Table 2.1. Electro number calculation of variable scan rate.
(Reprinted with permission from ref. [55]. Copyright 2020 Elsevier.)

pH	Bubbling Time (minutes)	mg L^{-1}	Scan Rate (V s^{-1})	Square Root of Scan Rate (V s^{-1})	Potential (V *vs*.Ag/AgCl)	Current (A)	n	Average of n
1.6	5	1.02	0.01	0.10	1.65	0.00010	6.7	7.05
		1.18	0.02	0.14	1.69	0.00018	7.1	
		1.33	0.03	0.17	1.70	0.00023	6.9	
		1.34	0.04	0.20	1.72	0.00029	7.2	
		1.33	0.05	0.22	1.73	0.00033	7	
		1.39	0.06	0.24	1.75	0.00038	7.4	
10.2	10	2.75	0.06	0.24	0.49	0.00024	4.3	4.38
		2.78	0.05	0.22	0.50	0.00024	4.5	
		2.89	0.04	0.20	0.49	0.00021	4.3	
		2.46	0.03	0.17	0.46	0.00015	4.3	
		2.83	0.02	0.14	0.47	0.00015	4.4	
		2.58	0.01	0.10	0.41	0.00010	4.5	

In order to study the oxidation mechanism, CVs at various scan rates were conducted. The electron number was calculated from the slope of the linear relationship between the peak current and the scan rate, as represented by the Randles Sevcik Equation[100,101] for irreversible process (4):

$$I_p = (2.99x10^5)\, n\, (\alpha\, n_\alpha)^{1/2}\, A\, D^{1/2}\, v^{1/2}\, C_A \qquad (4)$$

in which I_p is the peak current (ampere), *n* is the number of electrons, α is the charge transfer coefficient, n_α is the number of electrons involved in the charge transfer step, *D* is the diffusion coefficient ($cm^2\ s^{-2}$) or slope value, *A* is the area of the electrode surface (0.0855 cm^2), *v* is the scan rate (V s^{-1}) and *C* is the concentration in the bulk solution (mol cm^{-3}). Detailed calculations are summarized in Table 2.1.

In this regard, the oxidation current increased linearly with the square root of the scan rate over the range 0.01 – 0.06 V s^{-1}, indicating that the process is transport controlled with little or no fouling of the electrode[102]. At pH=1.6, as shown in Figure 2.6A, the slope as diffusion coefficient was 0.0019 (R = 0.998) and the calculated value for *n* was about ~7 electrons (Table 2.1). This can be attributed to the total oxidation reaction of hydrogen sulfide to $S_2O_6^{2-}$ via the transfer of ~7 electrons[103], although the detailed mechanisms involving intermediates such as S, $S_4O_6^{2-}$, SO_2 are not clear at present. Based on the behavior, we propose the following equation for the electrochemical reaction at +1.7 V (*vs.* Ag/AgCl):

$$H_2S + 3H_2O \rightarrow \frac{1}{2}S_2O_6^{2-} + 8H^+ + 7e^- \qquad (5)$$

Next, at pH=10.2, the potential range from 0 V to 0.8 V (*vs.* Ag/AgCl) was used in order to avoid overlapping of the oxidation peak at +1.3 V (*vs.* Ag/AgCl) as shown in Figure 2.6B. The slope as diffusion coefficient was 0.01 (R = 0.96) and the value of *n* was ~4 electrons (Table 1). A possible reaction pathway is oxidation of HS^- to thiosulfate ($S_2O_3^{2-}$). From this experiment, we attributed the oxidation reaction at +0.5 V (*vs.* Ag/AgCl) to:

$$HS^- + 1\frac{1}{2}\ H_2O \rightarrow \frac{1}{2}S_2O_3^{2-} + 4H^+ + 4e^- \qquad (6)$$

Then, $S_2O_3^{2-}$ could be further oxidized to $S_2O_6^{2-}$ at higher than +1.3V (vs. Ag/AgCl).

The results of these experiments are in agreement with those from previous research in which the applied potentials at which the byproducts of H_2S oxidation were determined. At low potentials (<+0.2 V) the byproduct is sulfur (S^0), while at high potentials sulfur oxides are formed[104]. In this case, sulfate or thiosulfate readily diffuses into the aqueous solution resulting in the specific surface properties of the BDD electrodes[105] which can support the transfer of a high number of electrons.

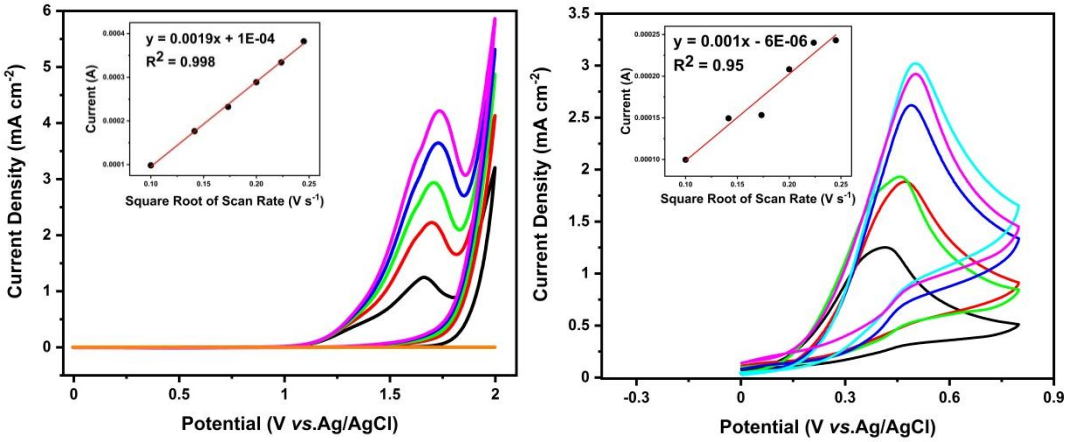

(A) (B)

Figure 2.6. CVs of scan rate dependence at pH 1.6 (A) and pH 10.2 (B) for dissolved H_2S in 0.1 mol L^{-1} $KClO_4$. (Inset: The current as a function of square root of scan rate). (Reprinted with permission from ref. [55]. Copyright 2020 Elsevier.)

3.3 Electrodes Materials

Table 2.2. Signal to background noise ratio of oxidation current on BDD, GC, and Pt. (Reprinted from ref. [55]. Copyright 2020 Elsevier.) electrodes.

pH	Electrodes	Concentration of Dissolved H_2S (mg L^{-1})	S/B
1.6	BDD	0.32	18
	GC	0.31	2.4
	Pt	0.35	4.3
10.2	BDD	0.31	21.7
	GC	0.29	3.4
	Pt	0.32	Not Detected

The same measurements were also done using GC and Pt electrodes. However, the signal to background ratios (S/B) using GC and Pt electrodes were apparently lower than that when a BDD electrode was used as shown in Table 2.2. These results imply that the oxidation signal overlaps the oxygen generation signal due to the low overpotential for oxygen generation on these electrodes.

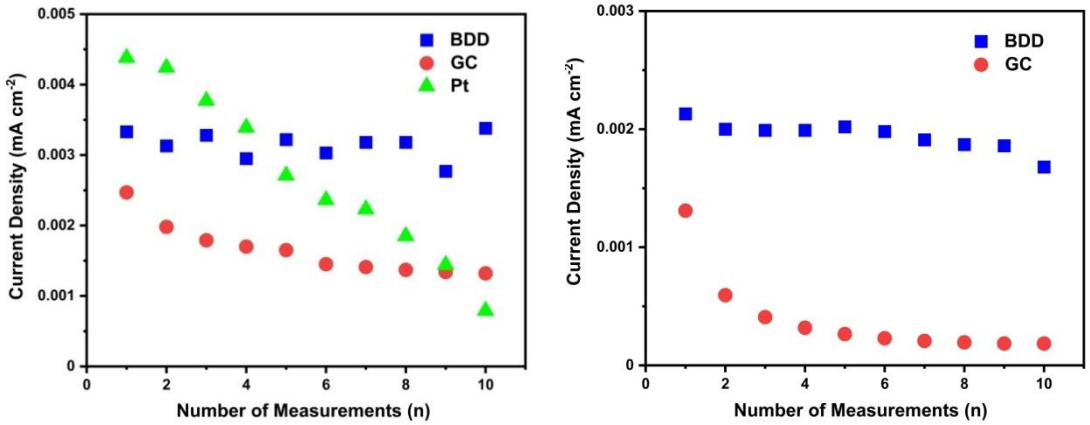

(A) (B)

Figure 2.7. Repeatability at pH 1.6 (A) and pH 10.2 (B) without pretreatment. (Reprinted with permission from ref. [55]. Copyright 2020 Elsevier.)

Moreover, we investigated the stability of BDD, GC and Pt electrodes by monitoring the peak currents. Ten measurements were made without pretreatment. As shown in Figure 2.7A, constant currents were obtained on BDD electrodes even without pretreatment at pH 1.6. On the other hand, poor durability was found with the GC and Pt electrodes as the current decreased with successive measurements. At pH 10.2, the current density with BDD was also more stable than with a GC electrode as shown in Figure 2.7B. Good repeatability can be obtained with GC and Pt electrodes by polishing before each measurement. However,

polishing in an enclosed electrochemical set up is difficult. That is, the concentration of H_2S may change over time due to equilibration with the surrounding gas phase when we keep removing the electrodes during the polishing process.

Although many electrodes such as platinum and glassy carbon electrodes have the ability to detect hydrogen sulfide, the adsorption of elemental sulfur via two-electron oxidation on these electrodes prevents detection by reducing the available electroactive surface area and decreasing sensitivity[106]. Therefore, we investigated passivation after the measurement. The results are shown in Figure 2.8. X-ray photoelectron spectroscopy was used to evaluate fouling of the surface of the electrodes.

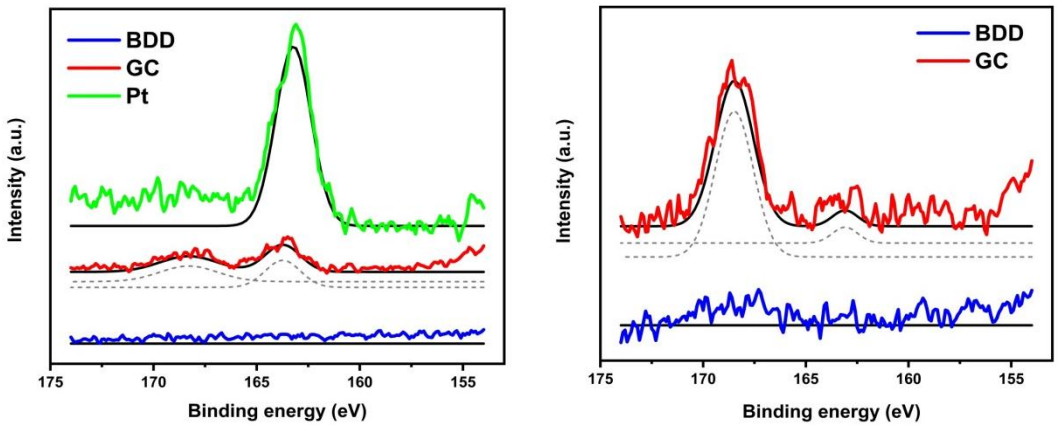

Figure 2.8. XPS spectra of S 2p region for BDD (blue), GC (red) and Pt (green) electrodes and spectra analyzed (black) at pH 1.6 (A) and 10.2 (B).
(Reprinted with permission from ref. [55]. Copyright 2020 Elsevier.)

As expected, it was found there was no sulfur fouling on BDD as shown in Figure 2.8. This is consistent with a previous investigation in which sulfate and thiosulfate were produced in the oxidation process. Different products were found using GC and Pt electrodes. Sulfur oxide at around 168 eV and sulfur at 163 eV were observed at pH 1.6 (Figure 2.8A) and 10.2 (Figure 2.8B) on GC electrodes. Oxidation of H_2S in contact with the surface of the sulfur layer forms polysulfide[107]. In contrast to the GC electrode, sulfur 2p at 163.1 eV was observed with a Pt electrode at pH 1.6 as shown in Figure 2.8A. Based on a previous study, the main product adsorped on the Pt was platinum (II) sulfide (PtS)[108]. In this case, the sp^3 hybridized structure of BDD gives it high chemical and physical stability, making it resistant to fouling. Therefore, it is difficult for chemicals to be adsorbed and grow on it[109]. Thus, BDD electrodes provide an efficient integrated sensor.

3.4 Analytical Performance

Figure 2.9 shows the concentration dependence of the current density. The electrolyte with pH 10.2 was used for these calibration curves since HS^- is a more stable species than H_2S in the electrolyte. The current at +0.5 V (*vs.* Ag/AgCl) is plotted as a function of the concentration of dissolved H_2S determined by the methylene blue method. The curves have

good linearity (r^2 = 0.99) and the curve for the BDD electrodes is given by the linear equation y = 0.0011x + 0.000002 in the concentration range of 0.22 – 2.34 mg L^{-1}.

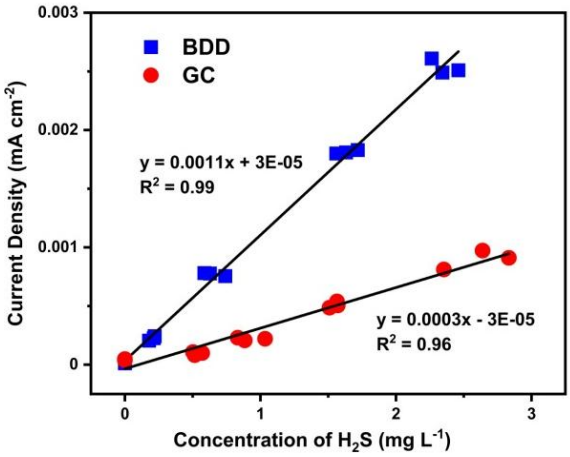

Figure 2.9. Calibration Curve of concentration of dissolved H_2S against oxidation current using BDD and GC electrodes.
(Reprinted with permission from ref. [55]. Copyright 2020 Elsevier.)

The llimit of detection (LOD) was determined on the basis of the equations of LOD = 3 SD/slope, where SD is the standard deviation of three background current of blank samples and the slope is obtained from the calibration curve[110]. As Figure 2.9 shows a lower detection limit, 0.82 µg L^{-1} (S/N=3), was obtained with the BDD electrodes compared with the GC electrodes. It might be due to the characteristic of BDD electrodes which have low background current and inert surface[72]. GC electrodes have pores surfaces and can easily adsorb species[111]. Moreover, the sensitivity is higher for BDD than for GC, and definitely satisfies the WHO requirements.

3.5 Interference Test

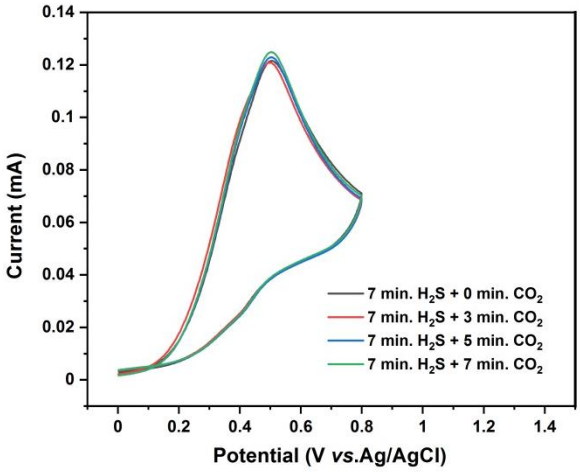

Figure 2.10. Calibration Curve of concentration of dissolved H_2S against oxidation current using BDD and GC electrodes.

Interference by other gas was then examined. CO_2 gas, which is generally found in the same systems as H_2S in some industries (e.g., the electrical industry), was investigated as shown in Figure 2.10. H_2S and CO_2 were introduced into the sensor together by using various bubbling times. We observed the peak currents when CO_2 was in contact with the sensor. As shown in Table 2.3, there was no significant interference by CO_2 as demonstrated by the constant oxidation current. It might be due to oxidation potential of H_2S and reduction potential of CO_2[112] on BDD electrodes.

Table 2.3. Investigation data of interference test by CO_2 gas to sensor.
(Reprinted with permission from ref. [55]. Copyright 2020 Elsevier.)

Bubbling Time (Minutes)		Concentration of Dissolved H_2S (mg L^{-1})	Oxidation Current (mA)
H_2S	CO_2		
7	0	1.32	0. 125
7	3	1.34	0. 126
7	5	1.32	0. 125
7	7	1.39	0. 132

4. Conclusion

Here, we report on an electrochemical behavior of dissolved hydrogen sulfide using BDD electrodes and to apply to the sensor for measuring the concentration of them. BDD electrodes have several advantages over GC and Pt electrodes: (1) the detection target can be controlled by the oxidation potential based on sulfur containing species (H_2S/HS^-), (2) the high oxidation potential due to the electroactive surface area promotes oxidation to sulfate or sulfur oxides without sulfur passivation and (3) a low detection limit which cannot be achieved using GC and Pt electrodes. These results suggest that BDD electrodes can be used in detecting hydrogen sulfide.

Chapter 3

Electrochemical Oxidation Behavior of Nitrogen Dioxide for Gas Detection Using Boron Doped Diamond

CHAPTER 3.
Electrochemical Oxidation Behavior of Nitrogen Dioxide for Gas Detection Using Boron Doped Diamond

1. Introduction

Nitrogen dioxide (NO_2) is a reddish-brown gas above 21.15ºC; a brown liquid below 21.15ºC; and a colorless solid at about -11ºC[113]. Among the several oxides of nitrogen involved in air pollution, NO_2 is the most dangerous and toxic both presenting a health risk and causing environmental damage. Recently, because of this, there has been a growing interest in NO_2 gas detection.

High performance liquid chromatography (HPLC)[114] and gas chromatography[21,115] are employed for NO_2 detection. However, each method suffers from diverse disadvantages such as cost ineffectiveness, insufficient sensitivity for detection, and time consuming sample incubation. Chemiluminescence[116,117] is also widely used to detect NO_2 gas and is combined with HPLC or gas chromatography, but the response time is limited. In the last decades, electrochemical sensors have presented a promising way forward for the detection of NO_2 gas, since they offer real time measurement, simplicity with a low limit of detection (LOD) and good selectivity[24,25].

The electrochemistry of NO_2 gas detection at some electrode materials has been studied. Most of the investigations have been carried out using inert metallic materials such as platinum (Pt)[118] and gold (Au)[119]. Modifying electrodes with supporting membranes is one of the techniques used to enhance the performance. Pt/Nafion[120,121], Pt/yttria-stabilized zirconia (YSZ)/$LaFeO_3$[122], Au/Teflon[25,123] and PAn/Au/Nafion[26] have all been studied. Furthermore, some interest has been shown in carbon based electrodes such as glassy carbon (GC)[124], graphite[29] and carbon nanotubes[125,126]. However, there are often problems with these approaches, such as limited sensitivity, poor precision, long procedures and lack of durability.

In this work, we use boron doped diamond (BDD) as an electrode material. BDD electrodes have some excellent properties, including a wide potential window in aqueous solutions and low background current, which enables them to be used with an exceptional potential sweep[127]. BDD also has excellent chemical and mechanical stability, thereby improving the reproducibility of the signals[128]. The surface of BDD can be easily controlled by an electrochemical treatment[69,88]. These characteristics have led BDD to be used in electrochemical sensing applications[89] such as for detecting drugs[43,90], measuring pH[91] and so on. Recently, we reported on utilizing BDD electrodes for detecting arsine (AsH_3)[60] and hydrogen sulfide (H_2S)[61].

Although previous work on NO_2 gas detection using BDD electrodes has been reported[28], the oxidation reaction was not clearly explained. This present work focuses on a detailed examination of the oxidation behavior of NO_2 gas using cyclic voltammetry (CV) combined with highly boron doped diamond electrodes. First, we carried out a fundamental study of the oxidation mechanism with NO_2^-. Specifically, the pH of the electrolyte and the scan rate dependence were varied to investigate the oxidation reaction. Then, we applied this to NO_2

gas to confirm the oxidation behavior and measure the analytical performance. In this paper we also give some preliminary results of a comparison between BDD and glassy carbon, platinum and stainless steel electrodes.

2. Experimental

2.1 Azo Dye Method

Aliquots of stock solution containing 1 – 4 mM of nitrite were transferred into a series of 10 mL calibrated flasks. To each flask, 1 mL of 0.5% sulfanilic acid and 1 mL of 2 M hydrochloric acid solutions were added and the solution was shaken thoroughly for 5 min to allow the diazotization reaction to go to completion. Then, 1 mL of 0.5% methyl anthranilate and 2 mL of 2 M sodium hydroxide solution were added to form an azo dye and the contents were diluted to 10 mL using water. After dilution, the absorbance of the red colored dye was measured at 493 nm against the corresponding reagent blank and the calibration graph was constructed[129].

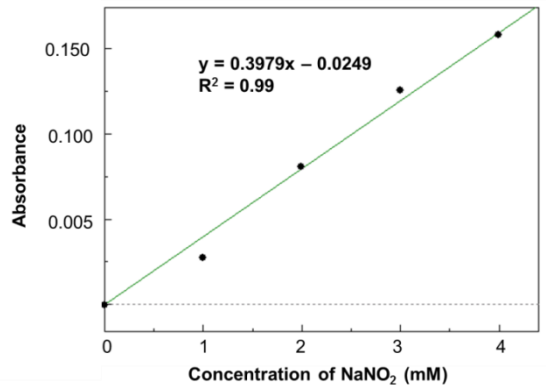

Figure 3.1. A plot of the concentration of $NaNO_2$ (sodium nitrite solution) against the absorbance. (Reprinted with permission from ref. [56]. Copyright 2021 John Wiley and Sons.)

$NaNO_2$ which concentration was 0, 1, 2, 3 and 4 mM was added into sulfanilic acid with hydrochloric acid. Then, methyl anthranilate and sodium hydroxide were added into the solution and red color dye color appeared. The optical density of this solution was measured by ultraviolet-visible (UV-Vis) spectrophotometer at wavelength of 493 nm. The concentration of $NaNO_2$ and the absorbance of solutions were plotted (Figure 3.1). Concentration of NO_2 gas bubbled into solutions was determined from the calibration curve obtained from $NaNO_2$ measurements.

2.2 Chemicals and Materials

All of the chemicals were used without further purification and purchased from FUJIFILM Wako Pure Chemical Corporation. All the solutions were prepared with pure water with a resistivity of 18.2 MΩ cm at 25°C supplied from a DIRECT-Q 3 UV system (Merck Millipore Corporation).

2.3 Electrochemical Measurement

0.1 M $KClO_4$ was used as the electrolyte. $HClO_4$ and KOH were used to obtain solutions with pHs of 1 to 7. Electrochemical measurements were conducted at room temperature (25°C) using a three-electrode system in a 5 mL acrylic cell. BDD, GC, Pt and stainless steel were used as working electrodes, while 1% BDD was used as the counter electrode and Ag/AgCl (saturated KCl) was used as the reference electrode. The geometric surface area of the working electrode was fixed with an O-ring with an area of 0.636 cm^2 (r = 0.45 cm). This was connected to a potentiostat through a copper plate. Before each measurement, the following pretreatment of the BDD electrodes was conducted. First, the BDD was soaked in aqua regia for 30 min. Next, it was ultrasonicated in pure water for 15 min and dried with N_2 gas. Finally, the BDD was cleaned by chronoamperometry (+3 V *vs*. Ag/AgCl for 5 min and −3 V *vs*. Ag/AgCl for 15 min in 0.1 M H_2SO_4) in order to obtain hydrogen terminated BDD (H-BDD)[69]. The surfaces of the GC, Pt and stainless steel electrodes were polished with alumina slurry (0.05–1.0 μm). After polishing, they were ultrasonicated in ethanol for 15 min, cleaned with pure water and dried with N_2 gas. Data was recorded by a Versa STAT 4 Potentiostat/Galvanostat (Ametek Inc.).

2.4 In Situ Attenuated Total Reflectance – Infra Red (ATR-IR) Measurements

A sub micrometer-thick BDD film was deposited onto a Si ATR-IR prism using a microwave plasma chemical vapor deposition method system. Acetone and trimethylborate were used as the carbon and boron sources, respectively. These were mixed with a B/C ration of approximately 0.5%. The steps are described in detail in a previous report[130]. In situ FTIR measurements were conducted with a FT/IR-6600 spectrometer (JASCO) using a liquid nitrogen cooled MCT detector. An electrochemical glass cell was connected to the spectrometer. The BDD thin film on the Si prism, a glassy carbon rod and Ag/AgCl (saturated KCl) were used as the working, counter and reference electrodes, respectively.

3. Result and Discussion

3.1 Effect of BDD Pretreatment to NO_2^- Detection

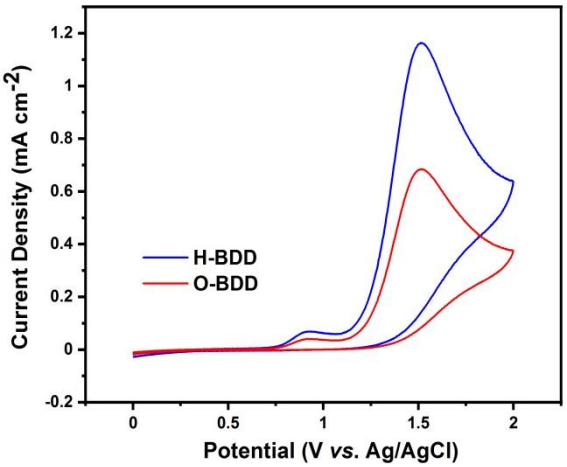

Figure 3.2. Electrochemical behavior of 4.00 mM $NaNO_2$ using BDD electrodes at pH 3 in 0.1 M $KClO_4$ using BDD for the working electrode with H-BDD (blue line) and O-BDD (red line) pretreatment.

First, we investigated the effect of surface termination on BDD electrodes to detect NO_2 in 0.1 M $KClO_4$ at pH 3. The CVs were recorded at 0.1 V s^{-1}, over the potential range 0 V to 2.0 V (*vs.* Ag/AgCl). The same procedures were done for hydrogen termination (H-BDD) and oxygen termination (O-BDD) preparation as mentioned in chapter 2. As shown in Figure 3.2, the CV's shows similar oxidation potential at +1.0 V and +1.5 V (*vs*. Ag/AgCl). However, the current density is higher on H-BDD blue line) than O-BDD (red line). H-BDD has good performance of electrochemical activity and higher response than O-BDD[48]. Based on this result, H-BDD was used as the following pretreatment to study the oxidation behavior of NO_2.

3.2 Oxidation Behavior of NO_2^-

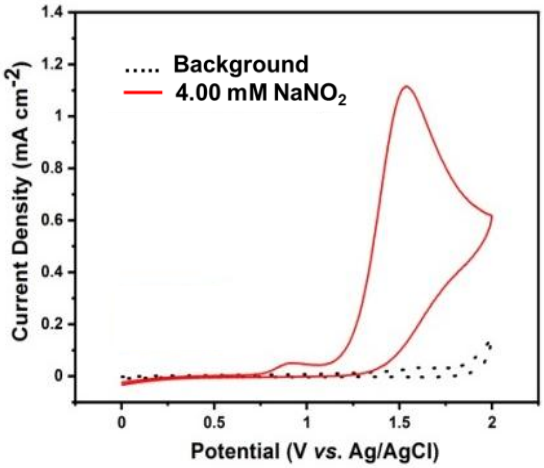

Figure 3.3. Electrochemical behavior of $NaNO_2$ using BDD electrodes at pH 3.
(Reprinted with permission from ref. [56]. Copyright 2021 John Wiley and Sons.)

The electrochemical behavior of NO_2^- was studied using cyclic voltammetry (CV). Figure 3.3 show CVs for a 0.1 M $KClO_4$ solution at pH 3 in the absence and presence of 4 mM $NaNO_2$ using BDD for the working electrode. A scan rate of 100 mV s^{-1} was applied. The CVs were recorded over the potential range from 0 V to 2 V (*vs*. Ag/AgCl) (CVs were scanned in the positive direction from 0 V to 2 V and then back to 0 V). Whereas no peak appears in the absence of $NaNO_2$, well-defined oxidation peaks in the presence of $NaNO_2$ can be seen at +0.9 V and +1.5 V (*vs*. Ag/AgCl). Note that, at this pH, some of the NO_2^- species becomes HONO. The ratio of HONO/NO_2^- is balanced in the electrolyte[131–134]. In the CV performed at pH 3 the oxidation profiles of both species are combined.

First, we carried out CVs at various pH values to investigate the oxidation behavior. The electrolyte pH was varied from 1 to 7 in order to individually characterize the CVs for the HONO and NO_2^- species. A single oxidation peak at +1.1 V (*vs*. Ag/AgCl) can clearly be seen at pH 1 (Figure 3.4A) and pH 2 (Figure 3.4B). These peaks are assigned such that the dominant fraction at pH 1 is H_2ONO^+ and that at pH 2 is HONO[131–134]. On the other hand, it is suggested that the reaction that converts H_2ONO^+ to HONO is reversible at very low pH[131]. So, this result suggests that HONO is oxidized at BDD electrodes at pH 1 and 2.

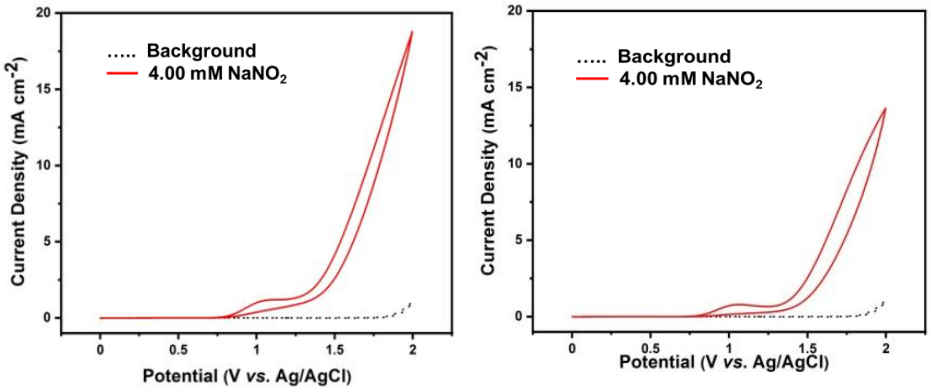

Figure 3.4. Electrochemical behavior of $NaNO_2$ using BDD electrodes at pH 1 (A) and pH 2 (B) (Reprinted with permission from ref. [56]. Copyright 2021 John Wiley and Sons.)

When, at pH 1, cyclic voltammetry was applied over the wider potential range of 0 V to 3 V (*vs*. Ag/AgCl), in addition to the peak at +1.1 V (*vs*. Ag/AgCl), a sharp oxidation feature appeared at +2.5 V (*vs*. Ag/AgCl) (Figure 3.5). This signal might be due to a combination of the oxygen evolution reaction and the oxidation of radical nitrates ($NO_3^{\bullet}$)[135].

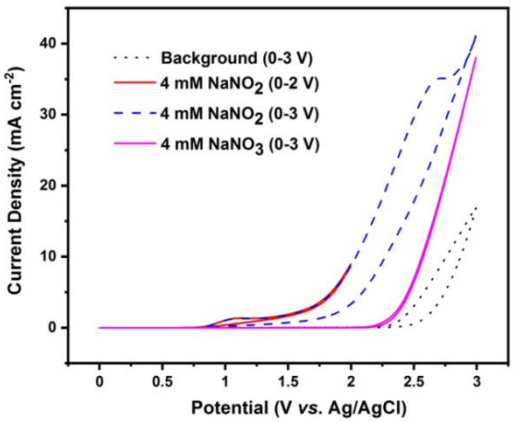

Figure 3.5. Cyclic voltammograms in the presence of 4 mM $NaNO_2$ at potential range 0 – 2 V (*vs.* Ag/AgCl) (red line), 4 mM $NaNO_2$ at potential range 0 – 3 V (*vs.* Ag/AgCl) (blue line) and 4 mM $NaNO_3$ at potential range 0 – 3 V (*vs.* Ag/AgCl) (purple line) at pH 1 in 0.1 M $KClO_4$ using BDD for the working electrode.
(Reprinted with permission from ref. [56]. Copyright 2021 John Wiley and Sons.)

In order to study the oxidation mechanism at +1.1 V (*vs*. Ag/AgCl), CVs at various scan rates were conducted. The potential range from 0 V to 1.3 V (*vs.* Ag/AgCl) was used as shown in Figure 3.6. The electron number was calculated from the slope of the linear relationship between the peak current and the scan rate, as represented by the Randles Sevcik Equation[100,101] for irreversible processes (1):

$$I_p = (2.99\text{x}10^5)\, n\, (\alpha\, n_\alpha)^{1/2}\, A\, D^{1/2}\, \nu^{1/2}\, C_A \qquad (1)$$

in which I_p is the peak current (ampere), *n* is the number of electrons, α is the charge transfer coefficient, n_α is the number of electrons involved in the charge transfer step, *D* is the diffusion coefficient ($cm^2\ s^{-2}$), *A* is the area of the electrode surface (0.636 cm^2), *v* is the scan rate ($V\ s^{-1}$) and *C* is the concentration in the bulk solution ($mol\ cm^{-3}$).

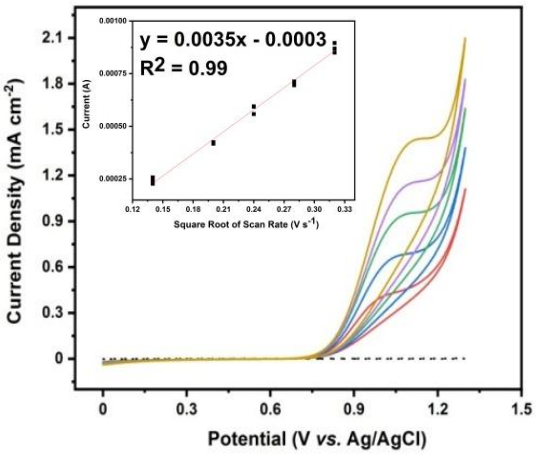

Figure 3.6. Cyclic voltammograms at various scan rates with the electrolyte at pH 1.
(Reprinted with permission from ref. [56]. Copyright 2021 John Wiley and Sons.)

As shown in the inset in Figure 3.6, the oxidation current increases linearly with the square root of the scan rate over the range 20 – 100 mV s^{-1}. The slope here is 0.0035 (R^2 = 0.99) and the calculated value for *n* is ~3 electrons (Table 3.1). This can be attributed to the total oxidation reaction of HONO to $NO_3^{\bullet}$ via the transfer of ~3 electrons. Based on this behavior, we propose the following equation for the electrochemical reaction at +1.1 V (*vs.* Ag/AgCl) in two steps:

First step, NO_2 gas is hydrolyzed[136] in the water as follows:

$$NO_2 + H_2O \rightarrow HNO_3 + HONO \qquad (2)$$

Then, HONO species is oxidized on BDD electrodes via ~3 electrons:

$$HONO + H_2O \rightarrow NO_3^{\bullet} + 3H^+ + 3e^- \qquad (3)$$

Table 3.1. Electro number calculation of variable scan rate at pH 1.
(Reprinted with permission from ref. [56]. Copyright 2021 John Wiley and Sons.)

Scan Rate ($V\ s^{-1}$)	Square Root of Scan Rate	Potential (V *vs.* Ag/AgCl)	Current (A)	Electron Number (n)	Average of (n)
0.02	0.14	1.00	0.000195	3.31	2.91
0.04	0.20	1.04	0.000278	3.19	
0.06	0.24	1.06	0.000339	2.64	
0.08	0.28	1.07	0.000372	2.19	
0.10	0.32	1.10	0.000456	2.21	

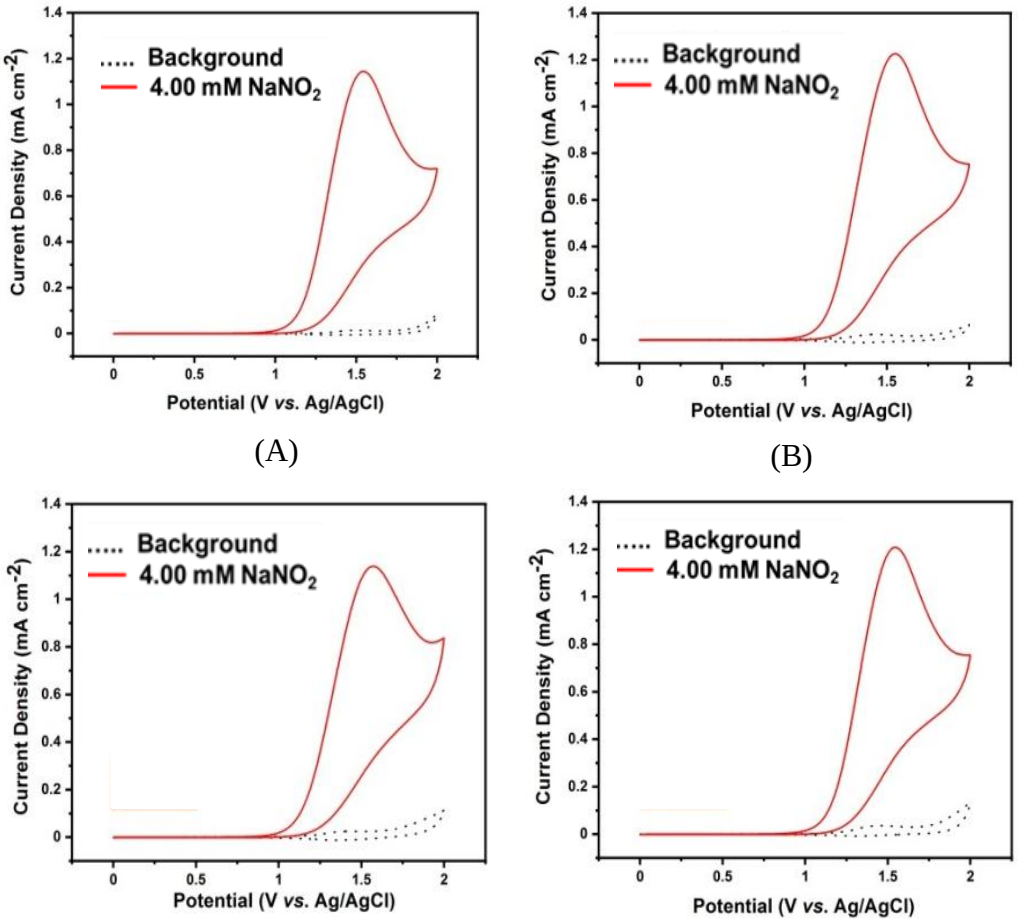

Figure. 3.7. Electrochemical behavior of $NaNO_2$ using BDD electrodes at pH 4 (A), pH 5 (B), pH 6 (C) and pH 7 (D). Table 1. Electro number calculation of variable scan rate at pH 1. (Reprinted with permission from ref. [56], Copyright 2021 John Wiley and Sons.)

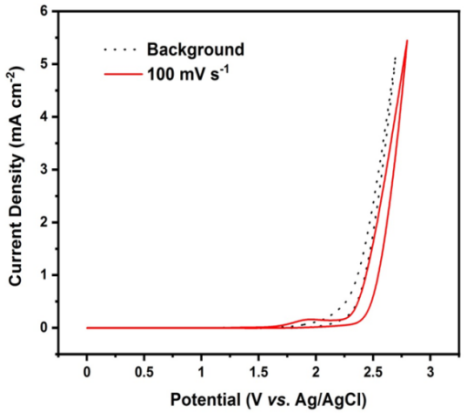

Figure 3.8. Cyclic voltammograms in the absence (dashed line) and presence (red line) of 4 mM $NaNO_2$ at potential range 0 – 3 V (*vs.* Ag/AgCl) at pH 7 in 0.1 M $KClO_4$ using BDD for the working electrode.
(Reprinted with permission from ref. [56]. Copyright 2021 John Wiley and Sons.)

Next, for pH 4 to 7 (Figure 3.7A to 3.7D), no peak appears in the absence of $NaNO_2$. In contrast, a well-defined oxidation peak at +1.5 V (*vs*. Ag/AgCl) is observed in the presence of $NaNO_2$. It is assumed that NO_2^- [131–134] is oxidized at the BDD electrode at these pH values. Moreover, at pH 7, when cyclic voltammetry was applied over the wider potential range of 0 V to 3 V (*vs*. Ag/AgCl), no oxidation signal was observed; however, the oxygen evolution signal was evident (Figure 3.8).

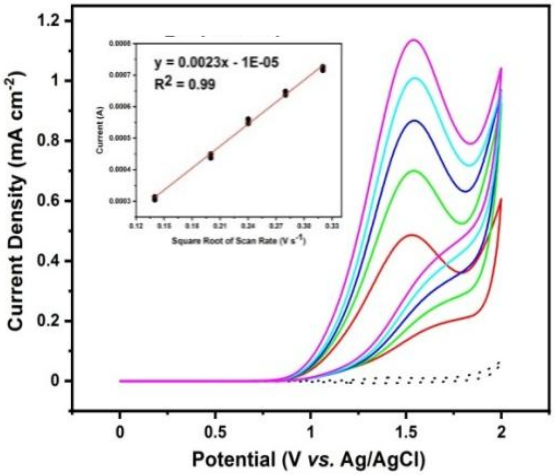

Figure 3.9. Cyclic voltammograms at various scan rates with the electrolyte at pH 7.The range of scan rates is 20 – 100 mV s^{-1}using a 0.1 M $KClO_4$ solution with 4 mM $NaNO_2$ and BDD electrodes. (Inset: The current as a function of square root of scan rate).
(Reprinted with permission from ref. [56]. Copyright 2021 John Wiley and Sons.)

Furthermore, to study the oxidation reaction in detail, the electron number at a potential of +1.5 V (*vs*. Ag/AgCl) was investigated at pH 7. The scan rate ranged from 20 to 100 mV s^{-1}, and the potential from 0 V to 2 V (*vs.* Ag/AgCl) as shown in Figure 3.9. The slope of the curve of the current versus the square root of the scan rate was 0.0023 (R^2 = 0.99) and the value of *n* was ~2 electrons (Table 3.2)[137].

Table 3.2. Electro number calculation of variable scan rate at pH 7.
(Reprinted with permission from ref. [56]. Copyright 2021 John Wiley and Sons.)

Scan Rate (V s^{-1})	Square Root of Scan Rate	Potential (V *vs.* Ag/AgCl)	Current (A)	Electron Number (n)	Average of (n)
0.02	0.14	1.53	0.000314	2.65	1.76
0.04	0.20	1.55	0.000450	1.92	
0.06	0.24	1.54	0.000561	1.59	
0.08	0.28	1.55	0.000649	1.39	
0.10	0.32	1.54	0.000727	1.24	

Moreover, we investigated the oxidation mechanism using ATR-IR measurements. Figure 3.10 shows the ATR-IR spectra for a 0.1 M $KClO_4$ solution with 4 mM $NaNO_2$ in the cell with BDD electrodes after oxidation for 10 minutes. The potential range was from +0.3 V to +1.7 V (*vs.* Ag/AgCl). The ATR-IR spectra at potentials from +0.9 V to +1.7 V (*vs.* Ag/AgCl) have strong peaks at 1388 cm^{-1}, 1226 cm^{-1} and 1092 cm^{-1}. In contrast, no peaks appear around these wavenumbers at potentials from +0.3 V to +0.7 V (*vs.* Ag/AgCl). On the basis of previous studies[138,139], the peaks around 1400 – 1000 cm^{-1} can be assigned to nitrate.

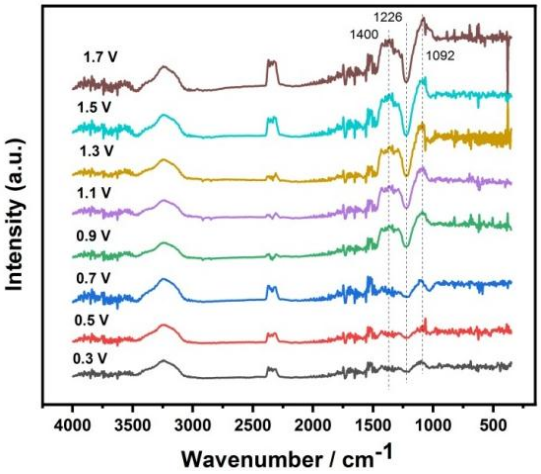

Figure 3.10. In situ ATR-IR spectra during electrochemical oxidation of 4 mM $NaNO_2$ in 0.1 M $KClO_4$ solution on BDD electrodes.
(Reprinted with permission from ref. [56]. Copyright 2021 John Wiley and Sons.)

A possible reaction pathway is oxidation of NO_2^- to nitrate (NO_3^-) which is consistent with a previous report[140]. From this experiment, we attributed the oxidation reaction at +1.5 V (*vs.* Ag/AgCl) to the following reaction: First, NO_2 gas forwards to the nitrite species in the water at pH 7. Then, NO_2^- is oxidized on BDD electrodes via 2 electrons:

$$NO_2^- + H_2O \rightarrow NO_3^- + 2H^+ + 2e^- \quad (4)$$

In these experiments no reduction peaks were observed in the reverse scan under acidic and neutral conditions. The results show that NO_2 is oxidized at BDD electrodes as reported[28]. Moreover, both HONO and NO_2^- can be distinguished by pH at specific oxidation potentials. This is facilitated by the surface properties of the BDD electrodes[105].

3.3 Oxidation Behavior of NO_2 Gas

First, we prepared NO_2 gas from the reaction between a Cu wire and 2.5 mL of concentrated HNO_3 in a closed system. The reaction is as follows:

$$HNO_3 + Cu \rightarrow Cu(NO_3)_2 + NO_2 + H_2O \quad (4)$$

The gas was bubbled into a 1 M $KClO_4$ 5 mL aqueous solution, and this solution was used for both the electrochemical and azo dye measurements. The scheme is shown in Figure

3.11. The concentration of NO_2 gas is confirmed by the Azo dye method. The calibration curve and details of the standard solution are shown in Figure 3.1.

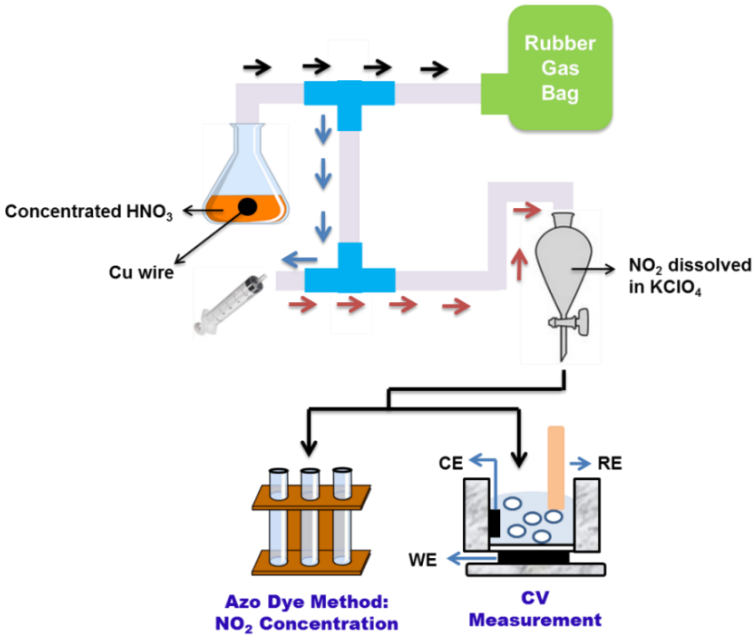

Figure 3.11. Schematic of dissolved NO_2 gas detection using BDD electrodes. (Reprinted with permission from ref. [56]. Copyright 2021 John Wiley and Sons.)

Furthermore, we investigated the oxidation behavior using ~4 mM NO_2 gas at pH 3. The measurement conditions are as in Figure 3.3. Figure 3.12 show CVs for a 0.1M $KClO_4$ solution at pH 3 in the absence and presence of 3.62 mM NO_2. No peak appears in the absence of NO_2, whereas oxidation peaks in the presence of NO_2 can be seen at +0.9 V and +1.5 V (*vs.* Ag/AgCl). At pH 3, NO_2 gas converts into $HONO/NO_2^-$ fractions and the ratio is balanced in the electrolyte[131–134]. At this pH, the CVs show both species as in Figure 3.3.

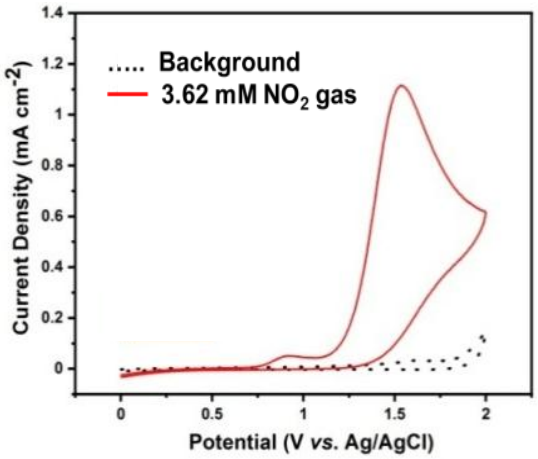

Figure 3.12. Electrochemical behavior of NO_2 on BDD electrodes at pH 3. (Reprinted with permission from ref. [56]. Copyright 2021 John Wiley and Sons.)

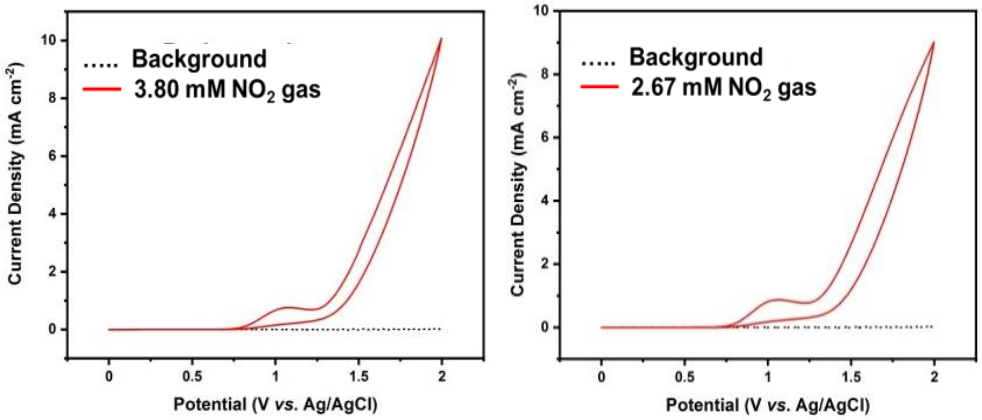

(A) (B)

Figure 3.13. Electrochemical behavior of NO_2 on BDD electrodes at pH 1 (8A) and pH 2 (8B). (Reprinted with permission from ref. [56]. Copyright 2021 John Wiley and Sons.)

Next, we varied the pH and observed the oxidation behavior of NO_2 gas on BDD electrodes. First, at pH 1 (Figure 3.13A) and pH 2 (Figure 3.13B), there is no peak in the absence of NO_2, but a well-defined oxidation peak appears at +1.1 V (*vs.* Ag/AgCl) in the presence of 2.67 – 3.80 mM NO_2. At these pHs, the dominant species is the HONO fraction in the electrolyte[131–134]. As in Figure 4A and 4B, the oxidation profile at these pHs is HONO to $NO_3^{\bullet}$.

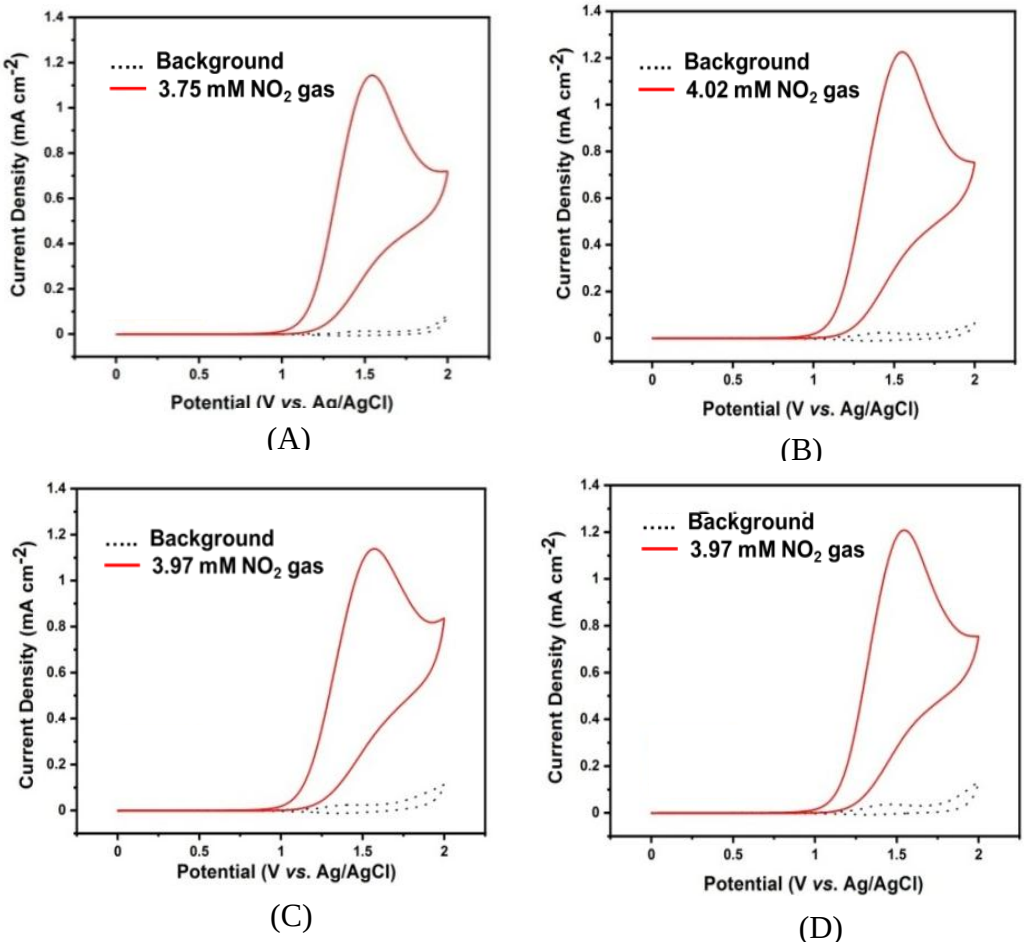

Figure. 3.14. Electrochemical behavior of NO_2 on BDD electrodes at pH 4 (A), pH 5 (B), pH 6 (C) and pH 7 (D). (Reprinted with permission from ref. [56]. Copyright 2021 John Wiley and Sons.)

Then, we carried out CVs at pH 4-7. Figure 3.14A to 3.14D show no peaks in the absence of NO_2, whereas a peak is observed at +1.5 V (*vs.* Ag/AgCl) in the presence of 3.75 – 4.02 mM NO_2. Note that all the species of NO_2 transmute to NO_2^- species in the electrolyte[131–134]. The oxidation peak in these pHs are due to NO_2^- oxidation to NO_3^- as in Figure 3.7A to 3.7D.

This result confirms that the oxidation potential and the peak current using NO_2 gas and NO_2^- have consistent profiles. This suggests that BDD electrodes can be applied directly to NO_2 gas detection.

3.4 Electrodes Materials

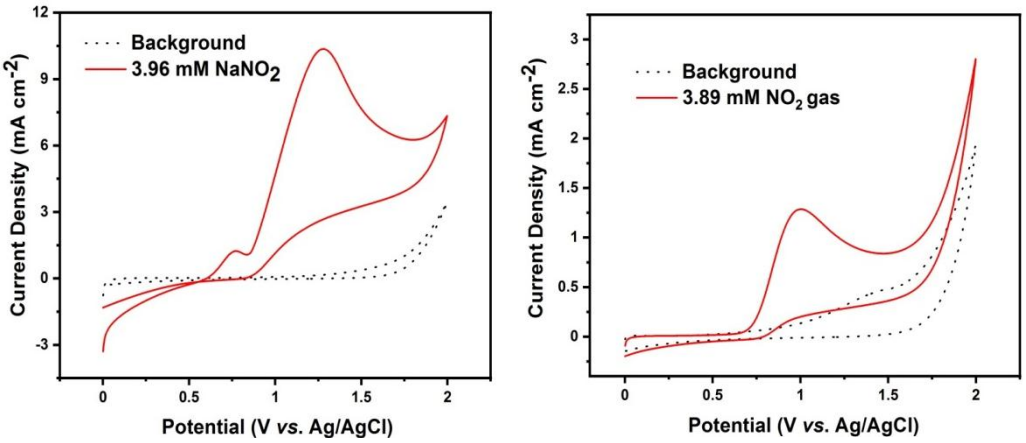

(A) (B)

Figure 3.15. Electrochemical behavior of NO_2 on GC electrodes at pH 1 (A) and pH 7 (B). (Reprinted with permission from ref. [56]. Copyright 2021 John Wiley and Sons.)

Comparisons were conducted using carbon based and metal based electrodes in the same measurement set up. At pH 1, an oxidation of HONO species is observed with GC (Figure 3.15A). The peak potential as well as the peak current when using the GC electrode are almost the same as those with the BDD electrodes since both the GC and BDD electrodes are carbon based. Furthermore, at pH 7, an oxidation of NO_2^- species is observed at a lower potential using the GC electrode compared to the BDD electrode (Figure 3.15B). The difference in peak potential might predominantly depend on the structure of the GC electrode which can easily adsorb species[141]. However, using GC electrodes gives rise to a higher peak current in the absence of NO_2. Hence, a higher signal to background noise ratio (S/B) can be achieved with BDD electrodes compared to GC electrodes as shown in Table 3.3.

Table 3.3. Signal to background noise ratio of oxidation current on carbon and metal based electrodes. (Reprinted with permission from ref. [56]. Copyright 2021 John Wiley and Sons.)

Based Electrodes	Electrodes	S/B	
		pH 1	pH 7
Carbon	BDD	1679	364
	GC	37	10
Metal	Stainless steel	58	12
	Platinum	3	1

Moreover, on metal based electrodes, broader voltammetric signals and higher peak currents are observed with Pt (Figure 3.16A to 3.16B) and stainless steel electrodes (Figure

3.17A to 3.17B) at pH 1 and 7. At pH 1, HONO is oxidized at higher potential on Pt and stainless steel electrodes than on carbon based electrodes. While, at pH 7, NO_2^- is oxidized at lower potential on metal electrodes than on BDD electrodes. However, in the absence of NO_2, the metal electrodes have higher background current. Therefore, when the oxidation peak current is compared to the current in the absence of NO_2 (background), the signal to background noise ratio (S/B) with the BDD electrodes is much higher than that with Pt and stainless steel (Table 3.3), showing the BDD electrodes to be superior in terms of voltammetric gas detection analysis.

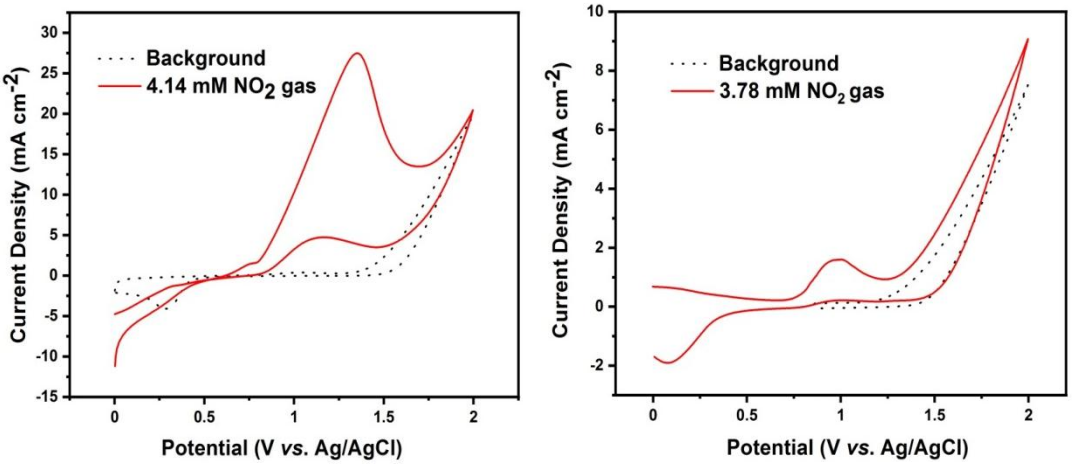

(A) (B)

Figure 3.16. Electrochemical behavior of NO_2 on Pt electrodes at pH 1 (A) and pH 7 (B). (Reprinted with permission from ref. [56]. Copyright 2021 John Wiley and Sons.)

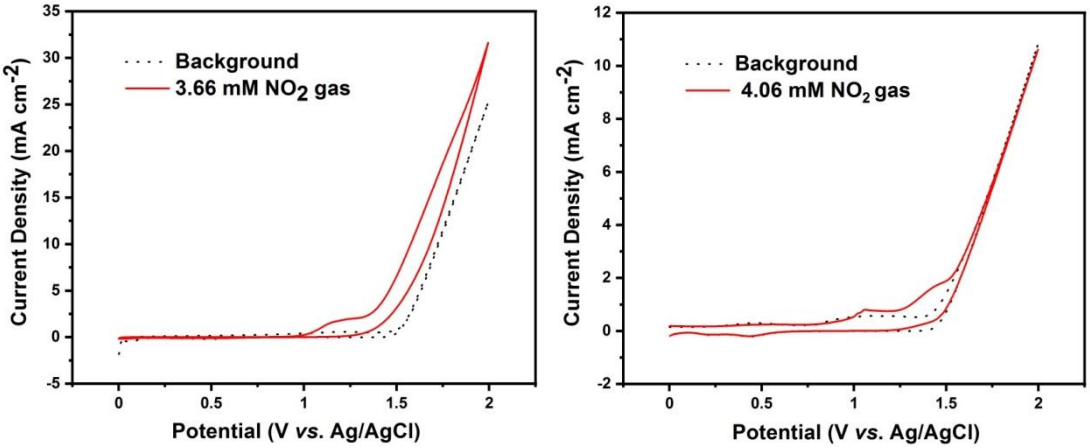

(A) (B)

Figure 3.17. Electrochemical behavior of NO_2 on Stainless Steel electrodes at pH 1 (A) and pH 7 (B). (Reprinted with permission from ref. [56]. Copyright 2021 John Wiley and Sons.)

3.5 Analytical Performance

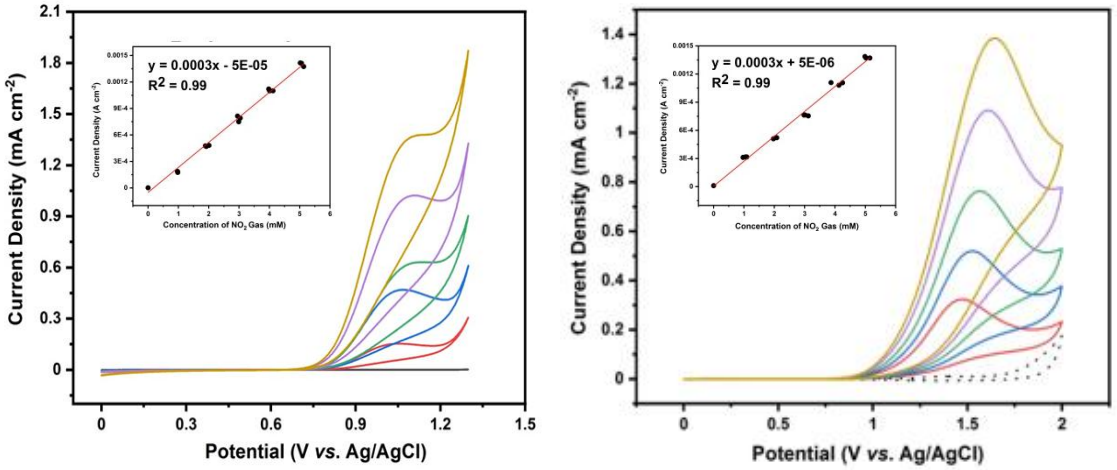

(A) (B)

Figure 3.18. Cyclic voltammograms in the concentration range of ~1 to 5 mM NO_2 in a 0.1 M $KClO_4$ solution at potentials of +1.1 V (vs.Ag/AgCl) (A) and +1.5 V (*vs*. Ag/AgCl) (B) (Insets: Plots of current versus $NaNO_2$ concentration).
(Reprinted with permission from ref. [56]. Copyright 2021 John Wiley and Sons.)

Figure 3.18 shows the current density on BDD electrodes at various concentrations of NO_2. In the inset in Figure 3.18A, the current at +1.1 V (*vs.* Ag/AgCl) is plotted as a function of the concentration of NO_2. The curves have good linearity (R^2 = 0.99) and the curve for the BDD electrode is given by the linear equation y = 0.0003x - 5E-05 in the concentration range of ~1 to 5 mM. The limit of detection (LOD) was determined as mentioned in Chapter 2[110]. A lower detection limit, 11.08 ppb (S/B=3), was obtained with the BDD electrodes compared with the GC and Pt electrodes as shown in Table 3.4.

Table 3.4. Detection Limit on BDD, GC and Pt Electrodes.
(Reprinted with permission from ref. [56]. Copyright 2021 John Wiley and Sons.)

Electrodes	Detection Limit (ppb)	
	HONO	NO_2^-
BDD	11.08	58.60
GC	687.68	16206.90
Pt	210.65	8269.72

Moreover, the inset in Figure 3.18B shows there is a linear relationship (R^2 = 0.99) between the peak current at +1.5 V (*vs.* Ag/AgCl) and the concentration of NO_2, with the equation y = 0.0003x + 5E-06. A lower detection limit, of 58.60 ppb (S/B=3), was achieved

with BDD electrodes compared to GC and Pt electrodes. As we mentioned, BDD electrodes has low background current and sp^3hybridized structure. It leads to low detection limit to detect H_2S gas. However, sp^2 carbon on GC electrodes surface make it easy to adsorb species even if blank sample[29]. In the other hand, Pt electrodes show higher background current due to the conductivity of typical metal electrodes, it usually need surface modification to control the performance[118,142,143].

Moreover, the sensitivity is higher for BDD than for GC and Pt electrodes, and definitely satisfies Japanese government requirements. In Japan, the short-term exposure limit for NO_2 gas is 500 ppb, and the environmental standard value is 40 to 60 ppb[19].

3.6 Interference Test

We didn't do any interference test for NO_2 gas detection on BDD electrodes in the experiment. However, we investigated the interference test theoretically by overlapping CV's of NO_2 and H_2S as shown in Figure 3.19. In low pH, H_2S and NO_2 are oxidized at +1.6 V and +1.0 V (*vs*. Ag/AgCl), respectively (Figure 3.19A). In the other hand, H_2S and NO_2 are oxidized at +0.5 V and +1.5 V (*vs*. Ag/AgCl), respectively (Figure 3.19B) in low pH. Based on this result, it might be no interference of NO_2 gas even if there is H_2S gas due to the difference of electrochemical behavior in the pHs setup.

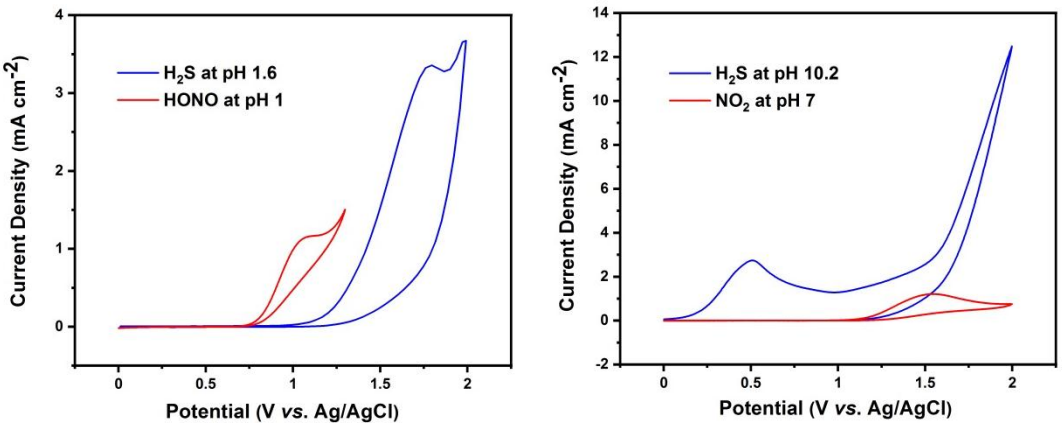

(A) (B)

Figure 3.19. Overlapping CV's for H_2S (blue line) and NO_2 (red line) on BDD electrodes in high pH (A) and low pH (B)

4. Conclusion

In this work, we investigated the electrochemical oxidation behavior of $NaNO_2$ using BDD electrodes. We used NO_2 gas to compare the oxidation behavior with that using other electrodes and measured the detection limits in each case. From this work, it is suggested that an electrochemical oxidation of NO_2 gas detection gives advantages such as high sensitivity, simple reaction and easy control compared to the other methods. Especially, BDD electrodes have several advantages over GC and Pt electrodes: (1) the detection target can be controlled by the pH based on nitrogen containing species ($HONO/NO_2^-$), (2) the electroactive surface area of the BDD electrodes promotes oxidation to $NO_3^{\bullet}$ or NO_3^- and (3) a low detection limit

which cannot be achieved using GC and Pt electrodes. These results suggest that BDD electrodes can be used for detecting NO_2 gas.

Chapter 4

Blood Oxygen Sensor Using Boron Doped Diamond Electrode

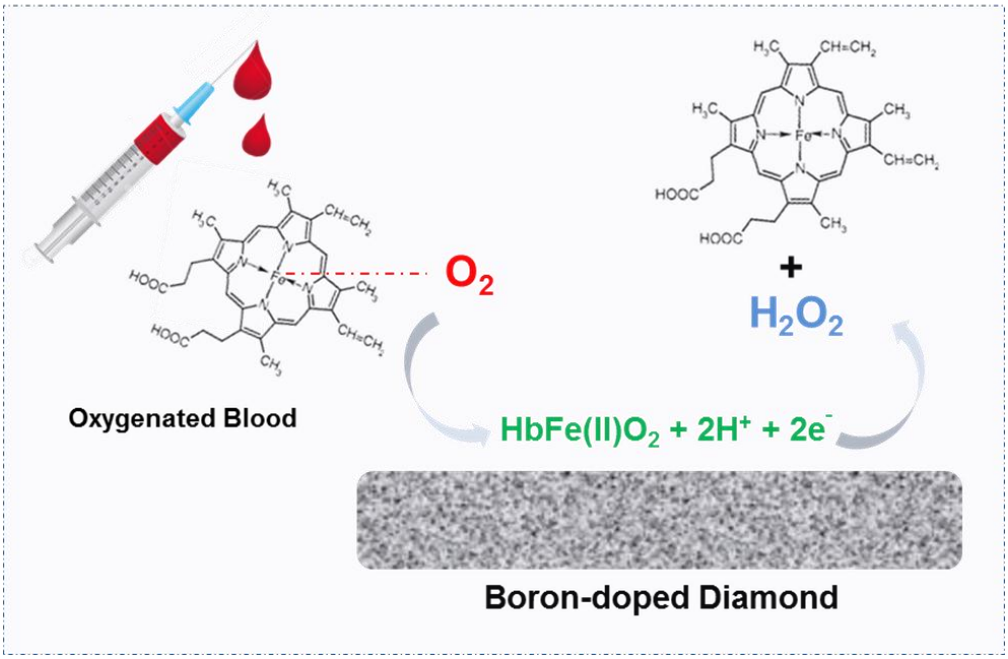

CHAPTER 4.
Blood Oxygen Sensor Using Boron Doped Diamond Electrode

1. Introduction

Monitoring blood oxygen (O_2) levels are crucial to indicate how well the body distributes O_2 from lungs to cells[144,145]. Lack of blood O_2 can be indicated by problems with breathing or circulation. This is called hypoxemia, which can result in shortness of breath, headaches, dizziness, rapid breathing, chest pain, and high blood pressure[146]. In medical applications, monitoring the O_2 level in blood gives an important biomarker for infections, such as COVID-19[147–150], heart failure diagnosis[151], the severity of a stroke[152], and cancers[153,154].

Therefore, there has been a growing interest in various methods for measuring blood O_2 levels. Spectroscopy[155,156] is employed for measuring O_2 in blood. However, this is expensive and the sample incubation is time consuming. Optical detection with a pulse oximeter[157–159] is commonly used, but the measurements are inaccurate due to interference[160] from carbon monoxide[161,162] and also for anemia patients with low saturation[163]. Diffuse optical tomography (DOT)[164] and optical coherence tomography (OCT)[165] are also widely used for blood O_2 levels. However, the analytical accuracy and sensitivity are limited. Optical devices estimate the arterial oxygen saturation (SpO_2). Radioisotope[166], magnetic resonance (MR), and electron resonance[167] techniques also measure O_2 in hemoglobin (% O_2Hb). These techniques are sensitive but are difficult to calibrate and much more expensive.

So far, most of the methods are unable to give a true value for the O_2 concentration (*e.g.,* mmHg or mg L^{-1}). Knowing the percentage of SpO_2 or O_2Hb is insufficient to enable decisions to be made when addressing severe complications, surgical requirements[168], prevention of hypoxemia during surgery[169], or cardiac surgery[170]. There are many factors, such as the patient's condition, that can affect the accuracy of percentage measurements of SpO_2 or O_2Hb. The sources of the errors are the strength of the arterial pulse, movement of the body, lipids and bilirubin, interference due to the color of the skin, and other physical factors[36]. Consequently, the information is insufficient to determine the real condition of the patient.

Electrochemical sensors to measure the actual concentration of O_2 in real time have attracted much attention. These highly sensitive, selective, and stable sensors in real-time measurement, have a low detection limit (LOD) and cost effectiveness[171,172]. The most common types of polarographic oxygen sensors utilize Clark electrodes[173] or microelectrodes[174]. Despite their advantages, these sensors consume oxygen, and it is difficult to acquire the oxygen tension in large areas. Moreover, the sensor needle can cause tissue damage. The next generation of electrochemical sensors use conductometry[175]. However, sensors of this type do not directly measure the O_2 concentration. They measure the difference between the concentration of O_2 in exhaled gas and the air, and they are limited to a small number of applications.

In the last few decades, a number of electrode materials have been studied for their ability to detect blood O_2 in tissue. In most investigations, inert metals such as platinum (Pt)[176] and gold (Au)[177,178] and carbon-based electrodes such as carbon paste electrodes (CPEs)[179,180],

carbon fiber electrodes[181], and carbon epoxy electrodes[182] have been studied. However, these often have problems, such as low sensitivity, lack of precision and durability.

BDD electrodes are commonly used for O_2 sensors in aqueous solutions[183]. BDD electrodes are well known for their superior electrochemical properties, including a wide potential window, low background current, and mechanical stability[127]. The surface of BDD can be easily controlled by an electrochemical treatment[69,88]. These characteristics have led BDD to be used in electrochemical gas sensing applications such as arsine (AsH_3)[60], hydrogen sulfide (H_2S)[61], and nitrogen dioxide (NO_2)[62].

Recently, modification of BDD electrodes with nanoparticles, such as Au[184–186], Pt[187] or gold-palladium[188], has been one of the techniques used to improve the performance. Also, previously, a BDD electrode with an sp^3 surface modified to produce an sp^2 pattern has been used to measure blood O_2 in a buffer solution[189], but the procedure to prepare the BDD is difficult. On the other hand, an investigation into measuring hemoglobin using BDD electrodes has been reported[190]. However, the details of the O_2 reduction behavior were not explained.

In this manuscript, we propose an unmodified 1% boron doped diamond (BDD) electrode as a working electrode to measure the blood O_2 concentration in a bovine hemoglobin solution. This is a simple procedure and low cost. This work focuses on a detailed explanation of the reduction behavior of O_2 in blood on BDD electrodes. Bovine hemoglobin was used for the fundamental study. Specifically, the scan rate dependences were varied to investigate the reduction reaction mechanism. We also give some preliminary results of a comparison between BDD, GC, and Pt electrodes. Then, we applied our BDD method to bovine blood to confirm the O_2 reduction behavior. Furthermore, we compare the blood O_2 concentration measurements using BDD electrode with measurements made using the fiber-optic oxygen sensor device, OxyLite Pro™ [191,192].

2. Experimental

2.1 Preparation of O_2 Gas

Deoxygenated PBS solutions were prepared by bubbling nitrogen (N_2) through them for 15 minutes. Oxygenated PBS solutions were prepared by bubbling O_2 gas through them. O_2 was produced from the reaction between 1 g MnO_2 and 6% H_2O_2 in a closed system. The reaction is as follows:

$$MnO_2\,(s) + 2H_2O_2\,(aq) \rightarrow MnO_2\,(s) + O_2\,(gas) + 2H_2O\,(aq) \qquad (1)$$

The gas was bubbled into a deoxygenated 0.1 M PBS aqueous solution at pH 7.4 and into a deoxygenated 0.1 M PBS aqueous solution containing $1x10^{-6}$ M bovine hemoglobin[190] at pH 7.4. The scheme is shown in Figure 4.1.

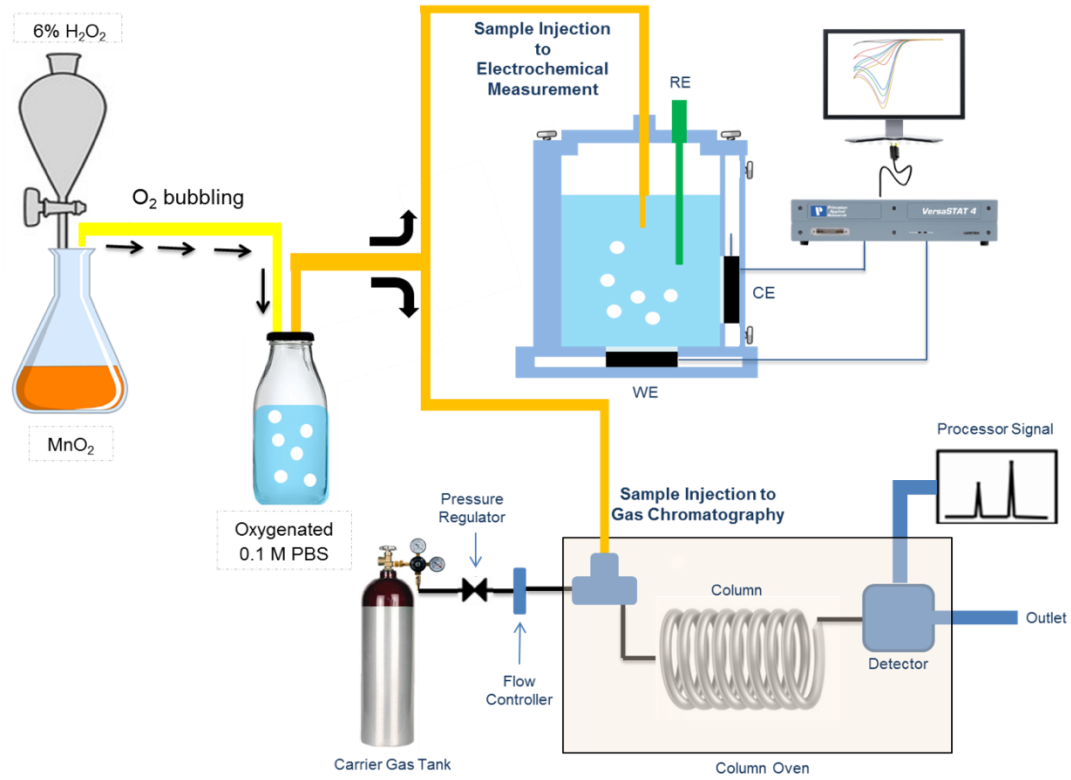

Figure 4.1. Schematic showing the setup for measurements of the O_2 concentration in 0.1 M PBS using gas chromatography and the electrochemical technique

2.2 Chemicals and Materials

All of the chemicals were purchased from FUJIFILM Wako Pure Chemical Corporation and used without further purification. Ultrapure water with a resistivity of 18.2 MΩ cm at 25^0C was obtained from a Simply-Lab water system (DIRECT-Q UV3 system, Millipore Corp.). Bovine hemoglobin was purchased from Sigma Aldrich, and bovine blood was purchased from Cosmo Bio Ltd.

2.3 Electrochemical Measurements

$1x10^{-6}$ M bovine hemoglobin in a 0.1 M phosphate buffer solution (PBS) at pH 7.4 was used for the electrolyte. For the applications to blood samples, 0.1% bovine blood in a 0.1 M PBS solution at pH 7.4 was used as the electrolyte. Electrochemical measurements were conducted at room temperature (25°C) using a three-electrode system in a 5 mL cell. BDD, GC and Pt were used as working electrodes, while 1% BDD was used as the counter electrode and Ag/AgCl (saturated KCl) was used as the reference electrode. The geometric surface area of the working electrode was fixed with an O-ring with an area of 0.636 cm^2 (r = 0.45 cm). This was connected to a potentiostat through a copper plate. Before each measurement, the following pretreatment of the BDD electrodes was conducted. First, the BDD was soaked in aqua regia for 30 min. Then, it was ultrasonicated in pure water for 15

min and dried with N_2 gas. Finally, the BDD was cleaned by chronoamperometry (+3 V *vs.* Ag/AgCl for 5 min and −3 V *vs.* Ag/AgCl for 15 min in 0.1 M H_2SO_4) in order to obtain hydrogen-terminated BDD (H-BDD)[69]. The surfaces of the GC, and Pt were polished with alumina slurry (0.05–1.0 μm). After polishing, they were ultrasonicated in ethanol for 15 min, cleaned with pure water and dried with N_2 gas. Data were recorded by a Versa STAT 4 Potentiostat/Galvanostat (Ametek Inc.).

2.4 Measuring the O_2 Gas Concentration by Gas Chromatography

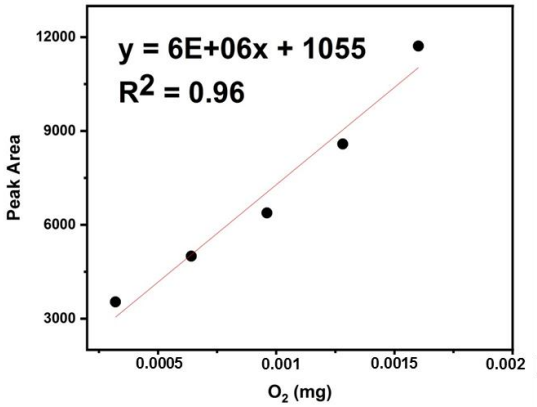

Figure 4.2. A plot of the concentration of O_2 against the peak area from gas chromatography.

The O_2 gas concentrations were quantified using a gas chromatography (GC) system equipped with a thermal conductivity detector or a flame ionization detector (GC2014; Shimadzu Corp.). A molecular sieve 13X (GL Science Corp.) was used as the column filler. First, 120 mL of pure O_2 was added to 5000 mL of N_2 in the gas bag. Volumes of 1 – 5 μL were injected into the gas chromatograph. A plot of the peak area versus the O_2 concentration (mg) was made and linear regression analysis was done to obtain the formula (Figure 4.2). This was used to calculate the O_2 concentration in the subsequent experiments.

We prepared 120 mL pure O_2 gas in 5000 mL N_2 in the gas bag. Then, the gas (1 - 5 μL) was injected into the gas chromatograph. The O_2 concentrations were calculated from the injected O_2 volume divided by the total volume of O_2. The peak area and the O_2 concentration are plotted as in Figure 4.2. The linear equation y = 6E+06x + 1055 (R^2= 0.96) was used to determine the O_2 concentration in the gas chromatography.

2.5 Measuring the O_2 Concentration in a Solution Using BDD Electrodes and Gas Chromatography

We combined two techniques to measure the O_2 concentration; gas chromatography and electrochemical measurements using BDD electrodes. The samples were prepared by bubbling O_2 through 0.1 M PBS solutions at pH 7.4 for from 0 to 105 seconds. These were measured electrochemically using the BDD electrodes and gas chromatography simultaneously, as shown in Figure 1. The reduction current density (A cm^{-2}) from the electrochemical measurements using the BDD electrodes and the O_2 concentrations (mg L^{-1}) determined by gas chromatography (GC2014; Shimadzu Corp.) were plotted to determine the

analytical performance. GC and Pt electrodes were also used in the same measurement setup. The lowest limit of detection (LOD) was determined on the basis of the equations of LOD = 3 SD/slope, where SD is the standard deviation of three background current of blank samples and the slope is obtained from the calibration curve[110].

2.6 Measuring the O_2 Concentration Using OxyLite Pro™.

The O_2 concentrations in the blood samples were measured using the fiber-optic oxygen sensor device OxyLite Pro™ (Oxford Optronix Ltd). OxyLite sensor was aligned to the sensor connector, and then the sensor was attached to the sample for about 30 seconds. The information was automatically monitored, and the data were processed using Lab Chart 8.

2.7 Statistical Analysis

Statistical analyses were performed using Prism 9 for macOS software version 9.3.1 (GraphPad Software, San Diego, CA, USA). The S/B values between BDD and GC or Pt electrode were compared using one-way ANOVA and Dunnett's multiple comparisons test. The comparison of the measurement value between OxyLite Pro and BDD electrode was performed the Deming regression and Bland-Altman plot using Prism 9. The acceptance criteria for rating the Deming regression were defined as a slope of 1.00 $\pm$ 0.15 and and intercept $\leq \pm$ 5 mmHg.

3. Result and Discussion

3.1 Effect of BDD Pretreatment to O_2 Detection

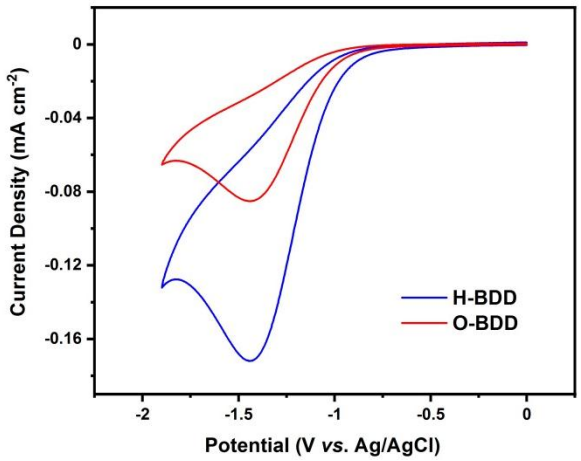

Figure 4.3. CVs of $1x10^{-6}$ bovine hemoglobin in a 0.1 M PBS solution at pH 7.4 in 30 seconds O_2 bubbling using BDD as working electrodes with H-BDD (blue line) and O-BDD (red line) pretreatment.

First, oxygenated 1 x 10^{-6} bovine hemoglobin in 0.1 M PBS was prepared by using 30 seconds O_2 bubbling at pH 7.4. The CVs were recorded at 0.1 V s^{-1}, over the potential range 0 V to 2.0 V (*vs.* Ag/AgCl). The same procedures were done for hydrogen termination (H-BDD) and oxygen termination (O-BDD) preparation as mentioned in chapter 2. As shown in Figure 4.3, the CV's shows similar oxidation potential at +1.5 V *(vs.* Ag/AgCl). However, the current density is higher on H-BDD blue line) than O-BDD (red line). H-BDD termination give improvement of electronic characteristics but it does not change both physical and

chemical surface (inert). While O-BDD change the surface due to adsorption of hydroxyl group[48,50]. Based on this result, H-BDD was used as the following pretreatment to study the electrochemical behavior of O_2 in blood solution on BDD electrodes.

3.2 Reduction Behavior of O_2

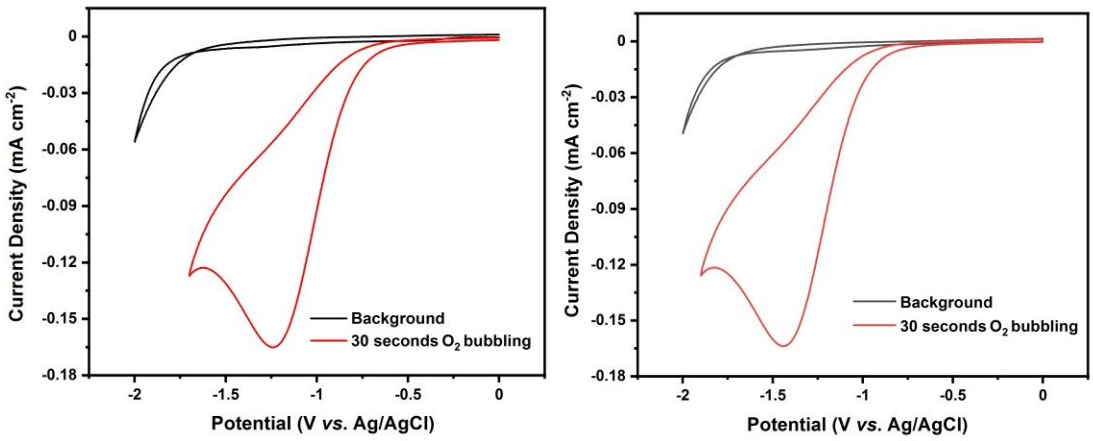

(A) (B)

Figure 4.4. CVs of a 0.1 M PBS solution at pH 7.4 in the absence (black line) and presence (red line) of O_2 (A).). CVs of $1x10^{-6}$ bovine hemoglobin in a 0.1 M PBS solution at pH 7.4 in the absence (black line) and presence (red line) of O_2 (B).

We prepared deoxygenated 0.1 M PBS solutions by N_2 bubbling into the solution and oxygenated 0.1 M PBS solutions by O_2 bubbling into the solution. Figure 4.4A show CVs for O_2 in 0.1 M PBS at pH 7.4 using BDD for the working electrode. A scan rate of 100 mVs^{-1} was applied over the potential range 0 V to -2.0 V (*vs*. Ag/AgCl) (CVs were scanned in the negative direction from 0 V to -2.0 V and then back to 0 V). Whereas no peak appears for the deoxygenated 0.1 M PBS solution, a single reduction peak can be seen at -1.3 V (vs. Ag/AgCl) for the oxygenated 0.1 M PBS (30 seconds O_2 bubbling). Here, the O_2 concentration was 145.13 mg L^{-1}, which was confirmed by gas chromatography.

Figure 4.4B shows CVs for O_2 in $1x10^{-6}$ M bovine hemoglobin in 0.1 M PBS at pH 7.4. No reduction peak was observed in the absence of O_2, whereas a well-defined reduction peak can clearly be seen at -1.4 V (*vs*. Ag/AgCl) in the presence of O_2 (30 seconds bubbling). Here, the O_2 concentration was 143.84 mg L^{-1}, which was confirmed by gas chromatography.

As expected, the O_2 reduction peak has shifted depending on the electrolyte. This might be due to the specific characteristics of the electrode surface, which could be affected by organic compounds such as hemoglobin. Hemoglobin contains heme-containing α and β globular proteins[193]. It also contains carbohydrates and minerals due to the purification process. On BDD electrodes, the compounds support higher molecule distance compared to the PBS solution. Furthermore, the current density of O_2 in PBS is similar to O_2 in hemoglobin. Interaction of O_2 in hemoglobin is diffusion control as shown in Figure 4.5B. It indicated that O_2 is directly reduced on the surface of BDD such as in PBS solution.

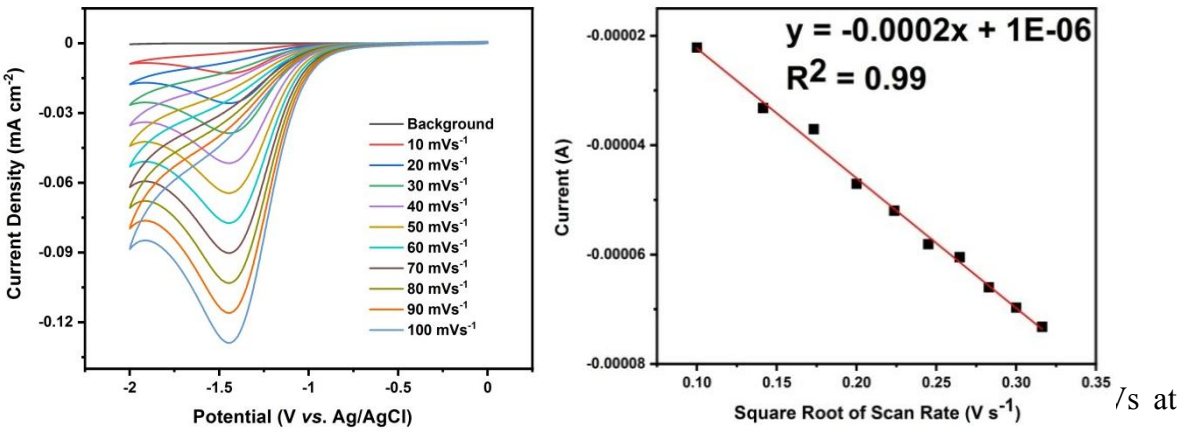

(A) (B)

Figure 4.5. CVs at various scan rates with $1x10^{-6}$ M bovine hemoglobin in a 0.1 M PBS solution at pH 7.4 as the electrolyte. The range of scan rates is 10 – 100 mVs^{-1} (A). The current as a function of the square root of the scan rate (B).

various scan rates were conducted in the range of 10 – 100 mvs^{-1}[194–196]. The potential range used was from 0 V to -2 V (*vs.* Ag/AgCl), as shown in Figure 4.5. The electron number was calculated from the slope of the linear relationship between peak currents and scan rates, as represented by the Randles Sevick Equation[100,101] for an irreversible process (2):

$$I_p = (2.99x10^5)\, n\, (\alpha\, n_\alpha)^{1/2}\, A\, D^{1/2}\, v^{1/2}\, C_A \qquad (2)$$

in which I_p is the peak current (ampere), *n* is the number of electrons, α is the charge transfer coefficient, n_α is the number of electrons involved in the charge transfer step, *D* is the diffusion coefficient ($cm^2\ s^{-2}$), *A* is the area of the electrode surface (0.636 cm^2), *v* is the scan rate ($V\ s^{-1}$), and *C* is the concentration in the bulk solution ($mol\ cm^{-3}$). Detailed calculations are summarized in Table 4.1. As shown in Figure 4.5A, the reduction current increases linearly with the square root of the scan rate over the range 20 – 100 $mVs^{-1,}$ which shows the process is transport controlled. The slope here is -0.0002 (R^2 = 0.99) (Figure 4.5B) and the calculated value for n is ~2 electrons (Table 4.1).

Table 4.1. Calculation of the electron number from the variable scan rate.

Scan Rate (Vs^{-1})	Square Root of Scan Rate ($V\ s^{-1}$)	Potential V (vs. Ag/AgCl)	Current Density ($A\ cm^{-2}$)	Electron number (n)	Average of n
0.01	0.10	-1.45	-3.48E-05	2.58	1.80
0.02	0.14	-1.45	-5.22E-05	2.30	
0.03	0.17	-1.45	-5.83E-05	1.71	
0.04	0.20	-1.45	-7.40E-05	1.86	
0.05	0.22	-1.45	-8.17E-05	1.44	
0.06	0.24	-1.45	-9.13E-05	1.78	
0.07	0.26	-1.45	-9.51E-05	1.36	
0.08	0.28	-1.45	-1.04E-04	1.82	
0.09	0.30	-1.45	-1.10E-04	1.90	
0.1	0.32	-1.45	-1.15E-04	2.02	

This result shows that the contribution to the total reduction reaction of O_2 to H_2O_2 via the transfer of ~2 electrons (3) is consistent with previous reports[190,197]. Based on the behavior, we propose the following mechanism for the reduction reaction for O_2 in hemoglobin at -1.4 V (vs. Ag/AgCl):

$$HbFe(III)O_2 + 2H^+ + 2e^- \rightarrow HbFe(II) + H_2O_2 \qquad (3)$$

3.3 Electrode Materials

Comparisons were made with measurements made using GC and Pt electrodes in the same measurement setup. Reduction of O_2 was observed on the GC electrode (Figure 4.5A). The peak potentials when using GC are almost the same as those with BDD electrodes since they are carbon-based. On the other hand, O_2 was reduced at higher potentials on Pt compared to the carbon-based electrodes (Figure 4.5B).

Higher background currents in the deoxygenated solution on GC electrodes were observed (Figure 4.6A). Therefore, significantly lower signal to background noise ratios (S/B) was obtained with GC electrodes compared to BDD electrodes ($P<0.0001$; one-way ANOVA and Dunnett's multiple comparisons test, $n = 3$), as shown in Table 2. This might be due to the characteristics of GC, which easily adsorbs species on its surface[141]. A higher current density for the background signal occurred with Pt electrodes (Figure 4.6B). Thus, the signal to background noise ratio (S/B) was significantly lower than with BDD electrodes ($P<0.0001$; one-way ANOVA and Dunnett's multiple comparisons test, $n = 3$), as shown in Table 4.2. Pt electrodes need some special condition such as modification or high temperature to enhance the performance[198].

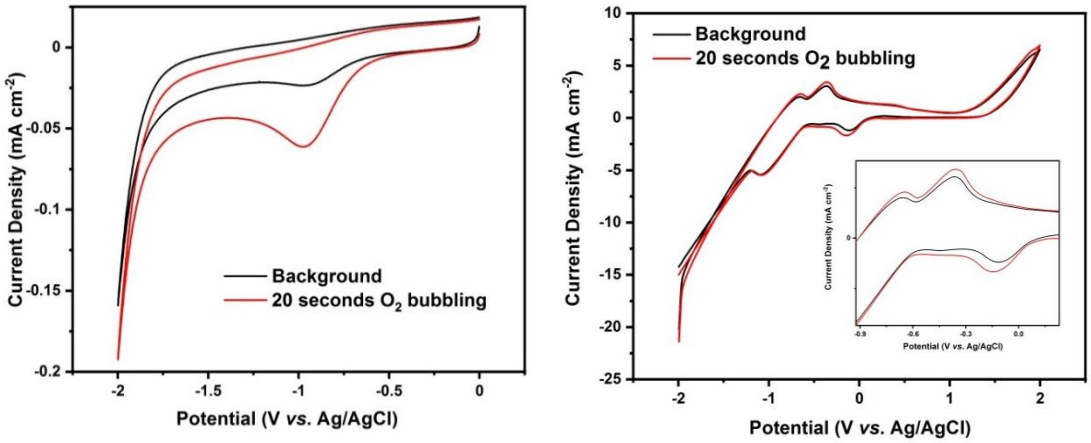

Figure 4.6. Electrochemical behavior of O_2 on a GC electrode (A) and a Pt electrode (B) at pH 7. CVs of a deoxygenated 0.1 M PBS solution containing $1x10^{-6}$ M bovine hemoglobin (black lines) and similar solutions with 20 seconds O_2 bubbling (red lines).

Table 4.2. Signal to background noise ratio of reduction current on BDD, GC and Pt electrodes.

Electrodes	Background (mA cm^{-2})	Current Density (mA cm^{-2})	S/B	Mean ± SD
BDD	-0.005 ± 0.00	-0.114 ± 0.00	21.92	21.9 ± 0.00
GC	-0.024 ± 0.00	-0.061 ± 0.00	2.59	2.59 ± 0.00
Pt	-1.673 ± 0.16	-1.193 ± 0.11	0.71	0.71 ± 0.00

n = 3

In this case, the sp^3 hybridized structure of BDD gives it high chemical and physical stability[55]. Therefore, it gives advantage such as high sensitivity and low detection limit. Hence, a higher signal to background noise ratio (S/B) can be achieved with BDD electrodes compared to GC and Pt electrodes as shown in Table1. The BDD electrode also had a higher signal to background noise ratio than Pt and GC electrodes for detecting hydrogen sulfide[61] and nitrogen dioxide[62]. These results also show BDD electrodes to be the best electrode material for gas detection.

Moreover, the reduction potential on BDD electrodes is higher than GC and Pt electrodes. It might be due to the electrodes' characteristic and different pretreatment. BDD electrodes have semi-metallic characteristic, it needs higher energy to reduced or oxidized species on the surface[199]. GC electrodes have higher conductivity than BDD[55,200], so lower energy is needed to reduced oxygen. Metallic electrodes such as Pt have good conductivity and need low energy to reduced or oxidized target[201], it leads to lower reduction potential than BDD or GC electrodes. Furthermore, BDD electrodes have more stable potential due to the

electrochemical pretreatment. As we see in Figure 4.6, there is a shift potential in the absent and presence of O_2 on GC (Figure 4.6A) and Pt electrodes (Figure 4.6B). It is due to polishing pretreatment make the surface unstable.

3.4 Analytical Performance

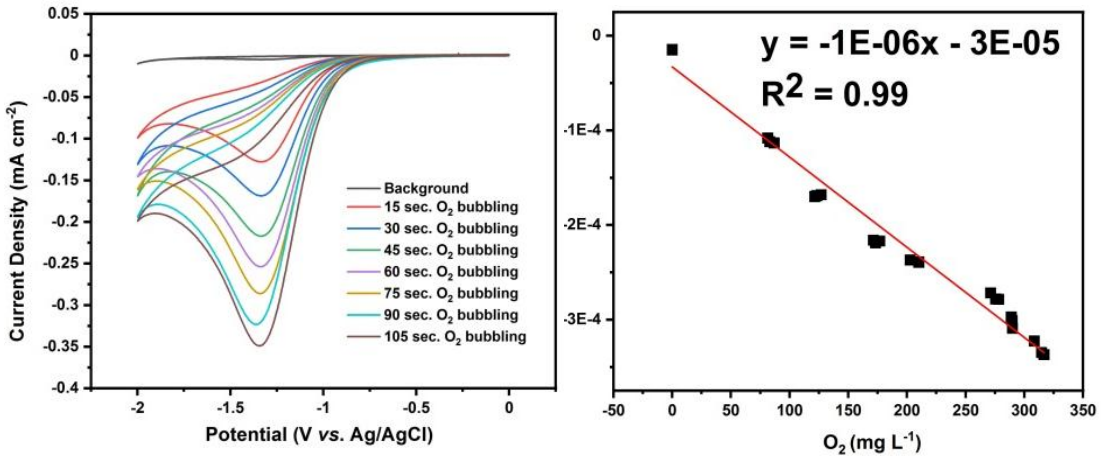

(A) (B)

Figure 4.7. CVs in the concentration range of 93.50 to 320.57 mg L^{-1} O_2 in a 0.1 M PBS solution at pH 7 as the electrolyte (A) Plot of current density versus O_2 concentration (B) on BDD electrodes.

A single sample of a deoxygenated 0.1 M PBS solution at pH 7.4 prepared by N_2 bubbling and five samples of oxygenated 0.1 M PBS solution at pH 7.4 prepared by time dependent O_2 bubbling were used to obtain the calibration curve for O_2 reduction on BDD electrodes. The O_2 concentrations were measured using a combination of a BDD electrode for the current density data and gas chromatography to determine the O_2 concentration, based on the peak area (Table 4.3). The O_2 concentration of each sample was measured using these two methods simultaneously, as shown in Figure 4.1.

Table 4.3. O_2 concentration and reduction current using BDD electrodes.

Bubbling Time (minutes)	Potential (V *vs.* Ag/AgCl)	Current Density (A cm^{-2})	Peak Area from Gas Chromatography	O_2 Concentration (mg L^{-1})
0	-1.3	-0.000015	0	0
	-1.3	-0.000015	0	0
	-1.3	-0.000015	0	0
0.5	-1.3	-0.000113	3661.40	86.88
	-1.3	-0.000112	3550.00	83.17
	-1.3	-0.000108	3496.60	81.39
1	-1.3	-0.000239	7357.90	210.10
	-1.3	-0.000237	7136.20	202.71
	-1.3	-0.000239	7357.90	210.10
2	-1.3	-0.000272	9192.00	271.23
	-1.3	-0.000278	9320.90	275.53
	-1.3	-0.000279	9399.20	278.14
3	-1.3	-0.000309	9750.30	289.84
	-1.3	-0.000301	9744.10	289.64
	-1.3	-0.000297	9720.70	288.86
4	-1.3	-0.000335	10493.90	314.63
	-1.3	-0.000337	10556.70	316.72
	-1.3	-0.000323	10308.90	308.46

Table 4.4. Detection Limit for BDD, GC and Pt electrodes

Electrodes	Limit of Detection (mg L^{-1})
BDD	1.0
GC	85.6
Pt	415.39

Figure 4.7A shows the current density with BDD electrodes at various concentrations of O_2. In Figure 4.7B, the current density (x-axis) at -1.4 V (*vs*. Ag/AgCl) is plotted as a function of the concentration of O_2 (y-axis) determined by gas chromatography. The curves have good linearity (R^2=0.99), and the curve for BDD is given by the linear equation y = -1E-06x – 2E-05 in the concentration range of 88.68 – 314.63 mg L^{-1}. The limit of detection (LOD) was determined as mentioned in Chapter 2[202]. The same procedures were conducted with GC (Figure 4.8) and Pt (Figure 4.9) electrodes. Table 4.4 shows that BDD electrodes have detection limit of 1.0 mg L^{-1} which is lower than both GC (Table 4.5) and Pt electrodes (Table 4.6). It is due to a lower background current of BDD electrodes[55] compared to GC and Pt electrodes as shown in Table 4.3. Furthermore, the sensitivity is higher for BDD than for GC and Pt electrodes. GC electrodes has sp^2 carbon on the surface, it leads strong adsorption of species including blank sample[203]. Moreover, Pt electrodes have sensitive surface to detect O_2 due to metal characteristic. It needs modification or special condition such as high temperature to enhance the performance[187].

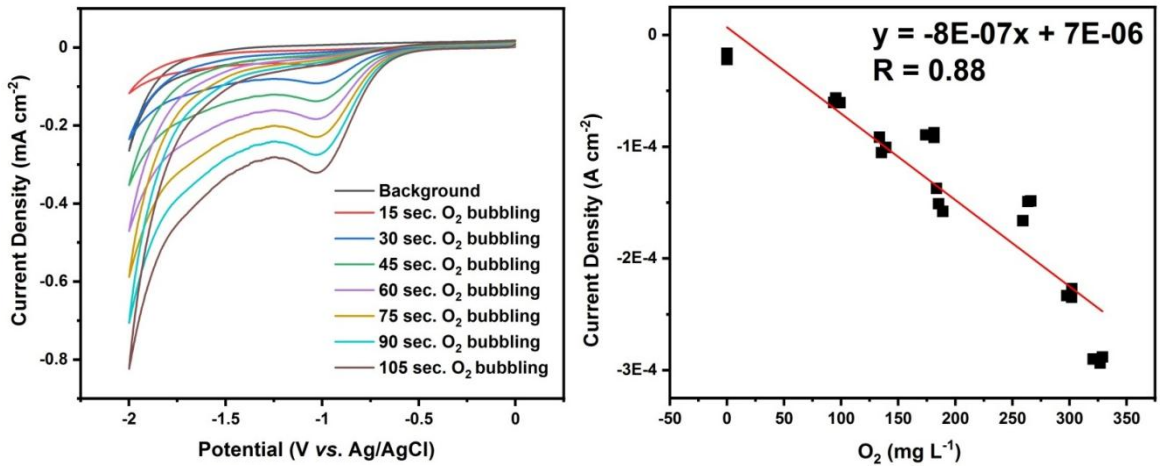

(A) (B)

Figure 4.8. CVs in the concentration range of 93.50 to 320.57 mg L^{-1} O_2 in a 0.1 M PBS solution at pH 7 as the electrolyte (A) Plot of current density versus O_2 concentration (B) on GC electrodes.

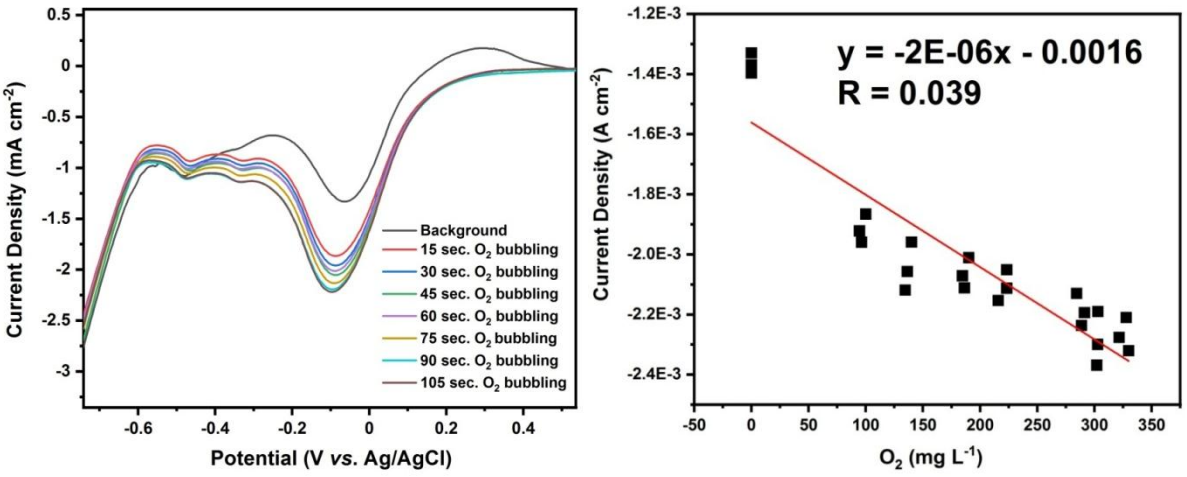

(A) (B)

Figure 4.9. CVs in the concentration range of 94.51 to 321.59 mg L^{-1} O_2 in a 0.1 M PBS solution at pH 7 as the electrolyte (A) Plot of current density versus O_2 concentration (B) on Pt electrodes.

Table 4.5. O_2 concentration and reduction current using GC electrodes.

Bubbling Time (minutes)	Potential (V *vs.* Ag/AgCl)	Current Density (A cm^{-2})	Peak Area from Gas Chromatography	O_2 Concentration (mg L^{-1})
0	-1.0	-0.000022	0	0
	-1.0	-0.000016	0	0
	-1.0	-0.00002	0	0
0.5	-1.0	-0.000061	4024.73	98.99
	-1.0	-0.000056	3913.33	95.28
	-1.0	-0.00006	3859.93	93.5
1	-1.0	-0.000092	6494.57	181.32
	-1.0	-0.000089	6272.87	173.93
	-1.0	-0.000088	6494.57	181.32
2	-1.0	-0.000166	8828.67	259.12
	-1.0	-0.000149	8957.57	263.42
	-1.0	-0.000149	9035.87	266.03
3	-1.0	-0.000227	10113.63	301.95
	-1.0	-0.000235	10107.43	301.75
	-1.0	-0.000233	9984.03	297.63
4	-1.0	-0.000294	10857.23	326.74
	-1.0	-0.000288	10920.03	328.83
	-1.0	-0.00029	10672.23	320.57

Table 4.6. O_2 concentration and reduction current using Pt electrodes.

Bubbling Time (minutes)	Potential (V *vs.* Ag/AgCl)	Current Density (A cm^{-2})	Peak Area from Gas Chromatography	O_2 Concentration (mg L^{-1})
0	-0.15	-0.000846	0	0
	-0.15	-0.000829	0	0
	-0.15	-0.00084	0	0
0.5	-0.15	-0.00057	4055.06	100.00
	-0.15	-0.000795	3943.66	96.29
	-0.15	-0.00079	3890.26	94.51
1	-0.15	-0.000715	7751.56	223.22
	-0.15	-0.000763	7529.86	215.83
	-0.15	-0.000579	7751.56	223.22
2	-0.15	-0.000705	9585.66	284.36
	-0.15	-0.000683	9714.56	288.65
	-0.15	-0.000855	9792.86	291.26
3	-0.15	-0.000724	10143.96	302.97
	-0.15	-0.000838	10137.76	302.76
	-0.15	-0.000941	10114.36	301.98
4	-0.15	-0.000951	10887.56	327.75
	-0.15	-0.000926	10950.36	329.85
	-0.15	-0.00099	10702.56	321.59

3.5 Applications in Blood

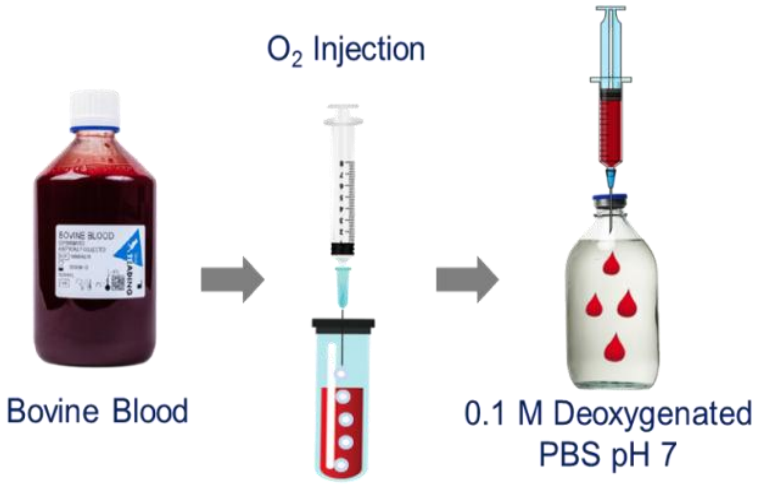

Figure 4.10. Preparation of oxygenated bovine blood solution

First, we prepared deoxygenated bovine blood by N_2 bubbling. Then, O_2 gas was bubbled into bovine blood directly in a closed system to obtain oxygenated bovine blood, as shown in Figure 4.10. Deoxygenated PBS was prepared by N_2 bubbling into the solution. Then, 1 mL of oxygenated bovine blood was injected into 99 mL of deoxygenated PBS electrolyte (1% bovine blood).

3.5.1 Reduction Behavior of O_2 in Blood

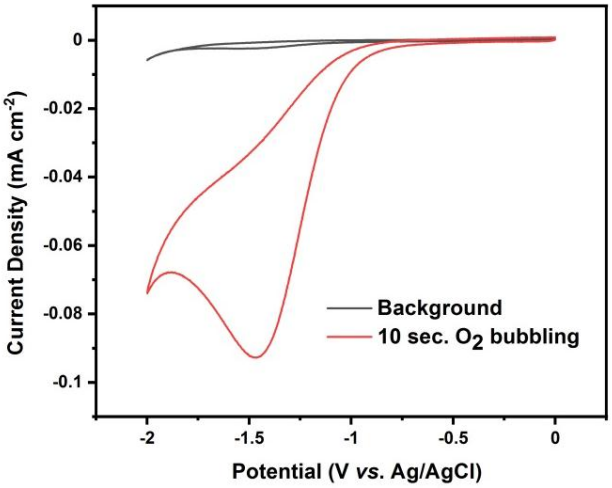

Figure 4.11. CVs of 1% bovine blood in 0.1 M PBS at pH 7 in the absence (black line) and presence (red line) of 10 seconds O_2 bubbling.

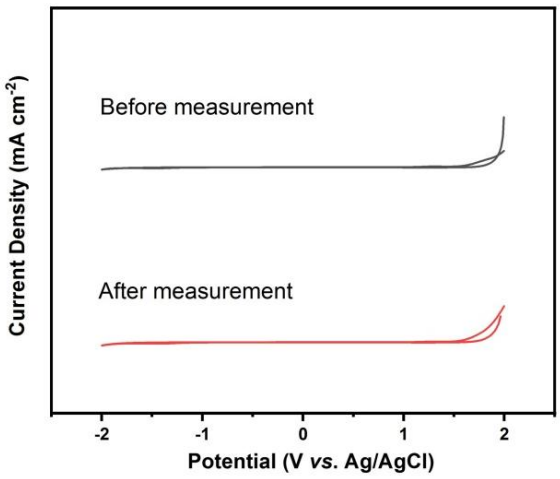

Figure 4.12. CVs of deoxygenated 0.1 M PBS at pH 7.4 before (black line) and after (red line) measurement.

The electrochemical behavior of O_2 in a blood solution on BDD electrodes was investigated. Figure 4.11 shows CVs of 1% bovine blood in 0.1 M PBS at pH 7.4 in the potential range from 0 V to -2 V (*vs*. Ag/AgCl). The black line is for a deoxygenated solution and the red line is for a solution oxygenated with 10 seconds O_2 bubbling. (The O_2 concentration is 75.18 mg L^{-1} confirmed by combination technique of BDD electrodes and gas chromatography).

A well-defined signal can be seen at -1.4 V (*vs*. Ag/AgCl). Note that, at this reduction potential, O_2 is reduced to H_2O_2 on BDD as in Figure 4.4B. Figure 4.12 shows that similar CVs were obtained both before and after measurements made on the bovine blood solution. This suggests that little or no fouling of the BDD surface occurs after using the blood solution.

Moreover, Figure 4.13A show CVs of 1% bovine blood in 0.1 M PBS at pH 7.4 in the potential range from 2 V to -2 V (*vs*. Ag/AgCl). The black line is for deoxygenated blood and the red line is for blood oxygenated with 80.75 mg L^{-1} O_2. A well-defined reduction peak can be seen at -1.4 V (vs. Ag/AgCl) as in Figure 4.5. Other than that, there is an oxidation peak at +1.6 V (*vs*.Ag/AgCl). Bovine blood contains of 80.9% water, 17.3% protein, 0.23% fat, 0.07% carbohydrate, and 0.62% minerals[204]. This peak is attributed to oxidation processes on hemoglobin or other protein[205]. After measurement, Figure 4.13B shows an oxidation peak at around +1.5 V (vs. Ag/AgCl). This peak might be due to the oxidation product of fouling species on the surface of the BDD electrode. These results suggest that, in order to avoid surface fouling, O_2 measurements should be made in the potential range from 0 V to -2 V (*vs*. Ag/AgCl).

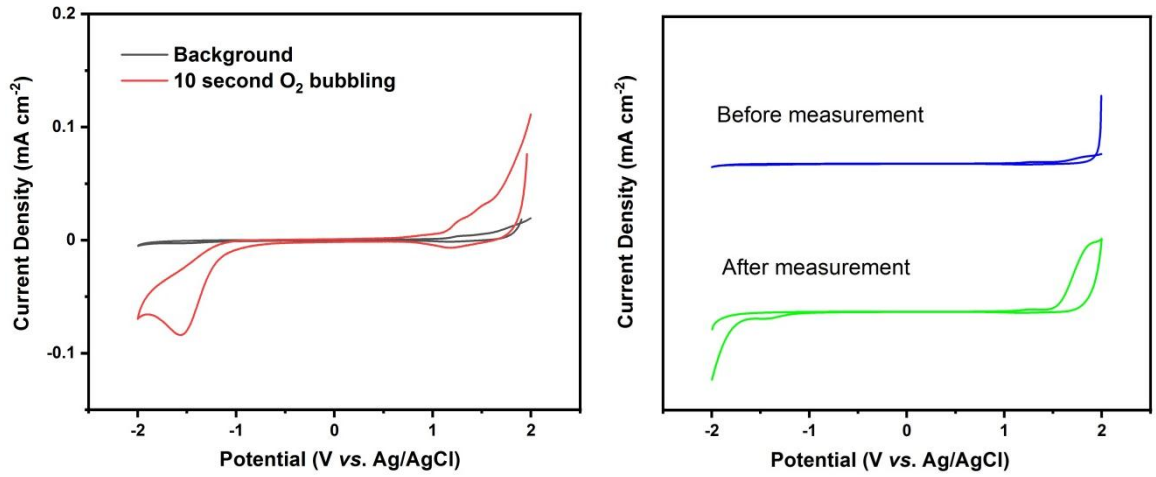

(A) (B)

Figure 4.13. CVs of a deoxygenated (black line) 0.1 M PBS solution at pH 7.4 containing 1% bovine blood and a similar solution oxygenated (red line) with 10 seconds O_2 bubbling over the potential range from +2 V to -2 V (*vs*. Ag/AgCl). The O_2 concentration was 80.76 mg L^{-1}, which was confirmed by gas chromatography (A). CVs of deoxygenated 0.1 M PBS at pH 7.4 before (blue line) and after (green line) measurement (B).

Furthermore, we did an electrochemical pretreatment by chronoamperometry (+3 V *vs*. Ag/AgCl for 5 min and −3 V *vs*. Ag/AgCl for 15 min in 0.1 M H_2SO_4) in order to obtain a H-BDD surface before measuring the O_2 concentration in blood solution. This step was only done before the measurement. It showed that BDD can be used repeatedly and applied to measure O_2 concentrations without the need for pretreatment, as shown in Figure 4.14A. From 10 cycles, BDD electrodes show stable current density even without pretreatment on each measurement (Figure 4.14B). As shown in Figure 4.14, BDD electrodes (Figure 4.14A) show stable reduction current density even without pretreatment. However, CVs on GC (Figure 4.15B) and Pt (Figure 4.15C) electrodes show a decreasing current density without pretreatment (Table 4.7). Based on the result, BDD has more stable than GC and Pt electrodes. It might be due to surface fouling on GC and Pt electrodes from bovine blood composition[204]. Moreover, electrochemical pretreatment of H-BDD is easier than technical pretreatment of polishing for GC and Pt electrodes.

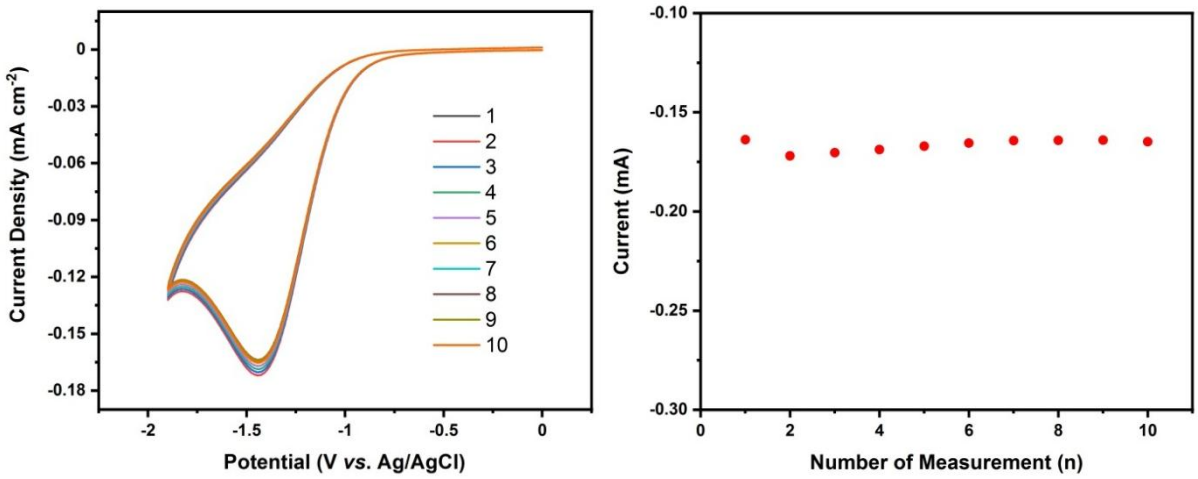

(A) (B)

Figure 4.14. CVs of 1% bovine blood in 0.1 M PBS solution at pH 7.4 in 30 seconds O_2 bubbling with 10 cycles (A). Plots of reduction current of O_2 on BDD electrodes versus the number of measurements (B).

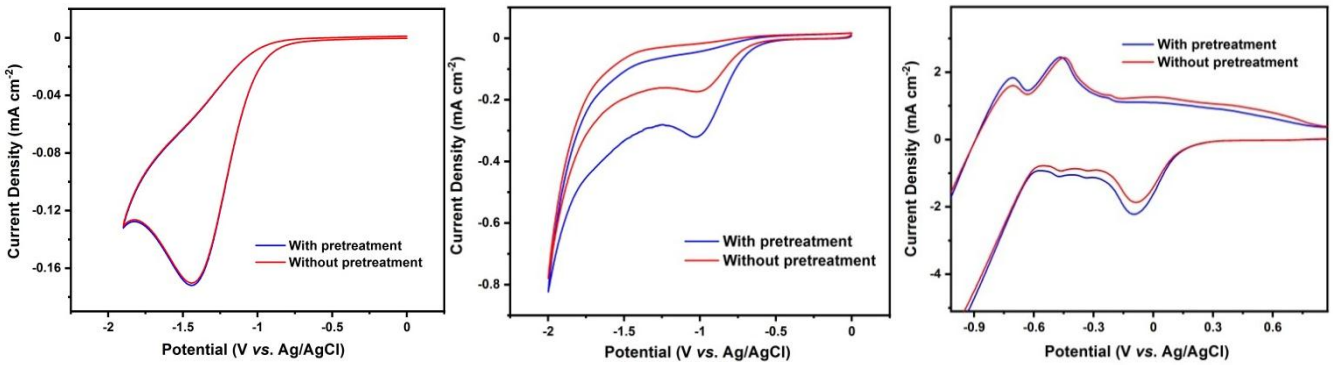

(A) (B) (C)

Figure 4.15. CVs of 1% bovine blood in 0.1 M PBS at pH 7.4 in 30 seconds O_2 bubbling for BDD (A), GC (B), and Pt (C)..

Table 4.7. Decreasing of current density on BDD, GC and Pt electrodes without pretreatment.

Electrodes	Potential (V *vs.* Ag/AgCl)	Current Density (mA cm^{-2})		Decreasing of Current Density (mA cm^{-2})
		With Pretreatment	Without Pretreatment	
BDD	-1.3	-0.172	-0.170	-0.002
GC	-1.0	-0.320	-0.173	-0.147
Pt	-0.15	-2.210	-1.855	-0.355

3.5.2 Comparison with a Different Method for Measuring the O_2 Concentration in Blood

To examine the credibility of the blood O_2 measurements, a comparison of the O_2 concentration in bovine blood was measured using BDD electrodes and an OxyLite Pro (Oxford Optronix Ltd). Five samples (A to E) of oxygenated 1% bovine blood in 0.1 M PBS at pH 7.4 were used as sample solutions The O_2 concentration in each sample was measured three times over three days. The measurements were done simultaneously.

Table 4.8. Comparison of O_2 concentration in bovine blood using the OxyLite sensor and the BDD electrode

Sample	Volume of O_2 (ml)	Day	Average of O_2 Concentration (±)			
			OxyLite Pro		BDD electrodes	
			(mg L^{-1})	(mmHg)	(mg L^{-1})	(mmHg)
A	3	1	66.16	38.54	67.04	39.06
		2	73.05	42.54	65.37	38.09
		3	70.59	41.09	65.77	38.32
B	4	1	108.43	63.06	106.29	61.93
		2	112.19	65.35	104.88	61.11
		3	112.10	65.38	105.24	61.31
C	5	1	143.09	83.26	142.37	82.95
		2	141.01	82.13	142.38	82.96
		3	143.06	83.40	142.12	82.80
D	6	1	176.92	103.06	176.52	102.85
		2	180.56	105.35	175.44	102.22
		3	180.50	105.38	175.74	102.39
E	7	1	260.89	151.73	260.87	152.00
		2	265.60	154.84	260.20	151.61
		3	262.46	153.09	260.44	151.74

Here, the O_2 concentration measured by the BDD electrodes and the OxyLite Pro™ is in mg L^{-1} and mmHg, respectively. In order to convert mg L^{-1} to mmHg or mmHg to mg L^{-1}, we used the ideal gas law equation[206] (4) below:

$$PV = nRT \qquad (4)$$

in which P, V and T are the pressure (Pa), volume (m^3) and absolute temperature (Kelvin) of the gas, respectively, n is the number of gram-moles of gas, and R is the ideal gas constant (8.314 J mol^{-1} K^{-1}). Table 4.8 shows the values of O_2 concentration using both the BDD electrode and the OxyLite Pro for samples A to E in mmHg and mg L^{-1}. As shown in Figure 4.16A, both methods showed excellent agreement. Deming regression analysis to compare the BDD electrode (x-axis) and the OxyLite Pro (y-axis) yielded the following: y = 0.9918x - 2.508 (n = 15). These values met our acceptance criteria (see the Methods section). The mean difference between the BDD and OxyLite Pro determined by the Bland-Altman plot[207] was 1.791 ± 1.846 mmHg (mean ± S.D.). All points were within the 95% confidence interval range of -1.828 to 5.409 mmHg (Figure 4.16B). Overall, the two methods were in good agreement, with OxyLite Pro showing slightly higher values than BDD electrode across all ranges.

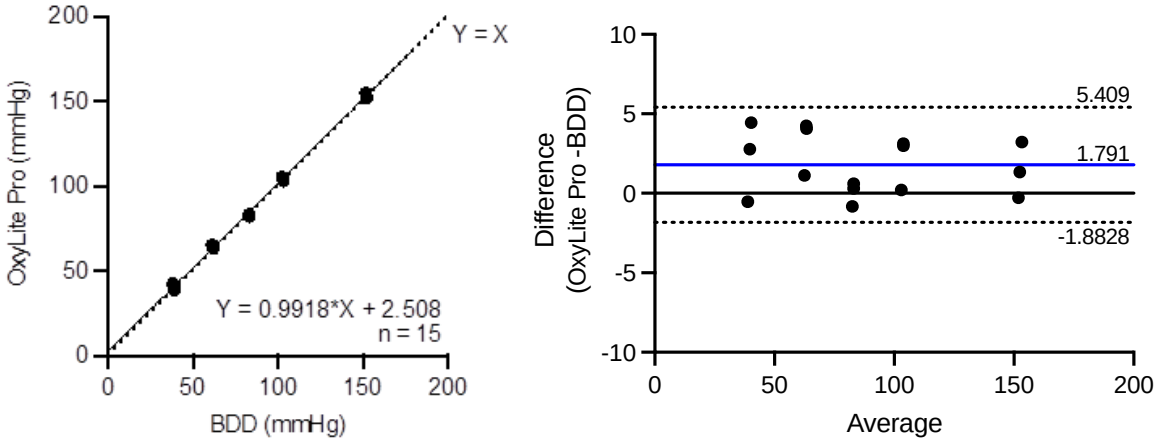

(A) (B)

Figure 4.16. Comparison of the OxyLite Pro sensor and the BDD electrode. (A) describe the scatter plot to show the relationship between methods using Deming regression analysis (solid line; y = 0.9918x - 2.508, dashed line; y = x). (B) indicates Bland-Altman analysis of the difference between the BDD electrode and OxyLite Pro sensor measurements plotted as a function of the mean of these values.

Table 4.9. Comparison of O_2 concentration in 1% and 100% bovine blood.

Volume of O_2 (mL)	n	OxyLite Pro (mmHg)	
		1%	100%
5	1	83.625	84.462
	2	82.335	83.158
	3	83.812	84.650
7	1	152.395	153.919
	2	151.781	153.299
	3	151.009	152.519
Air condition	1	133.728	135.065
	2	132.133	133.454
	3	131.282	132.595

Moreover, the O_2 concentrations obtained using the OxyLite Pro in 1% bovine blood were compared with those in 100% bovine blood. The results are shown in Table 4.9. For example, with five milliliters of O_2 in 100% bovine blood the concentration is similar to the same blood diluted to 1% in PBS. All the measurements are in the range of 82–85 mmHg. Thus, measurements of the O_2 concentration using the BDD electrode are accurate. The O_2 concentration range is ~40 to 150 mmHg and this is an appropriate range for human blood[208].

4. Conclusion

In this work, we studied the electrochemical reduction behavior of blood O_2 using BDD electrodes. The results of this study suggest that BDD electrodes have several advantages: (1) the performance is excellent with a higher signal to background noise ratio (S/B) and a lower detection limit than those obtained using GC and Pt electrodes, (2) the negative reduction potential promotes no surface fouling in applications to blood solutions, and (3) the O_2 concentration can be measured as well as it is measured by conventional methods, with lower cost, real-time measurement, and a simpler procedure. This work suggests that BDD electrodes can be applied in measuring the O_2 concentration not only in blood but also in other aqueous samples such as for environmental applications.

Chapter 5

Summary and Future Perspective

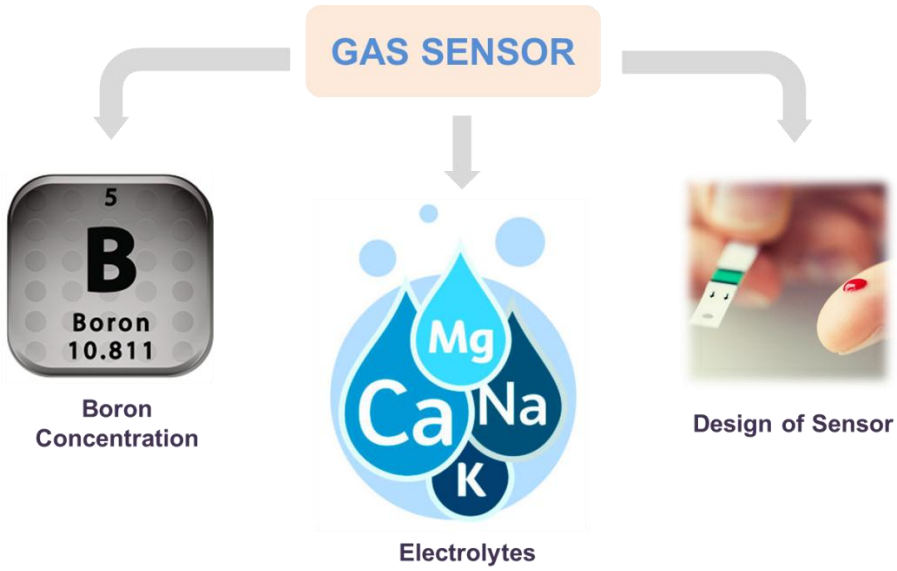

CHAPTER 5.
Summary and Future Perspective

1. Summary

In this thesis, we investigated the advantage of boron doped diamond (BDD) as working electrode in the application of electrochemical gas sensor for hydrogen sulfide, nitrogen dioxide and oxygen.

In **Chapter 2**, we studied an oxidation reaction of dissolved H_2S using boron doped diamond (BDD) electrodes and 0.1 mol L^{-1} $KClO_4$ as an electrolyte. Oxidation of H_2S and HS^- started at potentials of +1.7 V and +0.5 V (*vs.* Ag/AgCl), respectively. Moreover, as demonstrated by X-ray photoelectron spectroscopy, no sulfur fouling was detected on the BDD surface. The scan rate dependence was investigated to study the reduction reaction mechanism, which is attributable to the oxidation of H_2S to $S_2O_6^{2-}$ via 7 electrons and HS^- to $S_2O_6^{2-}$ via 4 electrons. A linear calibration curve was observed in the concentration range of 0.08 – 2.34 mg L^{-1} ($r^2 = 0.99$) with a detection limit of 0.82 μg L^{-1} (S/N = 3) which is lower than glassy carbon and platinum electrodes. In addition, an interference test with CO_2 was performed, which showed there was no significant interference to the sensor.

In **Chapter 3**, the electrochemical oxidation reaction of NO_2 using boron doped diamond (BDD) electrodes is presented. Cyclic voltammetry of NO_2 in a 0.1 M $KClO_4$ solution exhibits oxidation peaks at +1.1 V and +1.5 V (*vs.* Ag/AgCl) which are attributable to oxidation of HONO and NO_2^-, respectively. The scan rate dependence was investigated to study the reduction reaction mechanism, which is attributable to the oxidation of HONO to $NO_3^{\bullet}$ via 3 electrons and NO_2^- to NO_3^- via 2 electrons. A linear calibration curve was observed in the concentration range of ~1 to 5 mM ($R^2 = 0.99$) with a detection limit of 11.08 ppb S/B = 3) for HONO and 58.60 ppb (S/B = 3) for NO_2^- which can't be reach by using glassy carbon, platinum and stainless steel electrodes.

In **Chapter 4**, the electrochemical behavior of oxygen (O_2) in blood was studied using boron doped diamond (BDD) electrodes. Cyclic voltammetry of O_2 in a 0.1 M PBS solution containing $1x10^{-6}$ M of bovine hemoglobin exhibits a reduction peak at -1.4 V (vs. Ag/AgCl). Moreover, the scan rate dependence was investigated to study the reduction reaction mechanism, which is attributable to the reduction of O_2 to H_2O_2 via 2 electrons. A linear calibration curve was observed in the concentration range of 86.88 to 314.63 mg L^{-1} ($R^2 = 0.99$) with a detection limit of 1.0 mg L^{-1} (S/B = 3). The analytical performance was better than those with glassy carbon or platinum electrodes as the working electrode. The O_2 concentration in the blood measured on the BDD electrodes was compared to that measured using the OxyLite Pro™ fiber-optic oxygen sensor device. Both methods gave similar values of O_2 concentration in the range of ~40 to 150 mmHg. This result confirms that BDD electrodes could potentially be used to detect O_2 concentration in blood.

2. Future Perspective

We successful develop BDD electrodes as gas sensors for H_2S, NO_2 and O_2. Here, we show how BDD electrodes can be a good candidate as working electrodes for gas sensors. This could open a new chance to develop gas sensor by using cheap and high durability material with a simple procedure. The electrochemical oxidation and reduction are easily

controlled by the applied potentials. BDD show good sensitivity and lower detection limit (LOD) which cannot be achieved by using other electrodes such as glassy carbon and platinum.

In this work, we use 1% BDD electrodes to detect gases. It is better if we compare with various boron concentrations on diamond surface (low and high concentrations) since it gives special characteristic such as wider potential window and lower background current. Moreover, it is also important to use other electrolytes to study the electrochemical behavior. It can lead to the better performance of the electroanalytical properties such as lower oxidation or reduction potential. In addition, improvement on the design of the system is needed. It is better to use additional converter or other instruments to confirm O_2 concentration in the air as shown in Figure 5.1. Finally, interference test should be more investigated in real sample such as gas from industries.

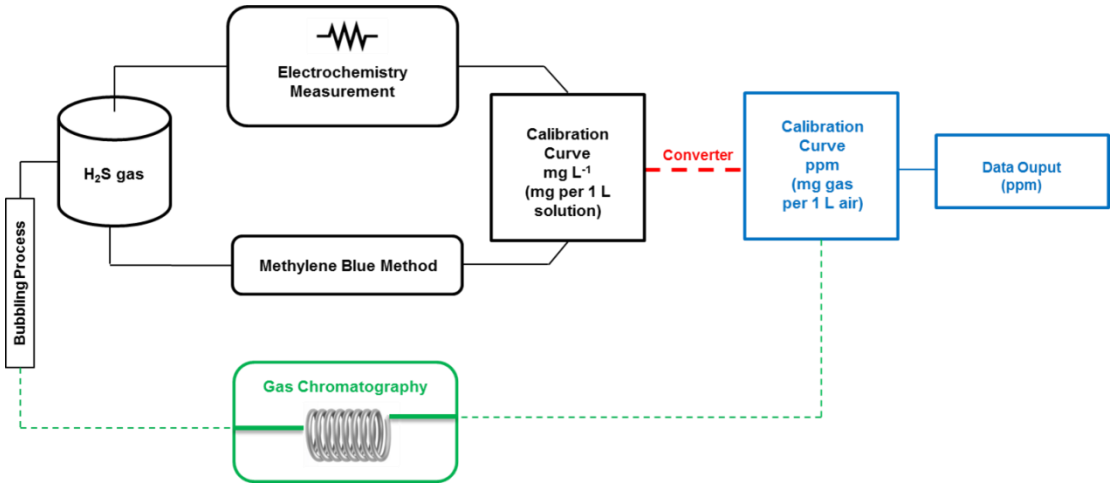

Figure 5.1 Design application system of gas detection using boron doped diamond (BDD) electrodes

REFERENCE

[1] M. Javaid, A. Haleem, S. Rab, R. Pratap Singh, R. Suman, *Sens. Intl.* **2021**, *2*, 100121.

[2] H. Seok Jo, S. An, H. J. Kwon, A. L. Yarin, S. S. Yoon, *Sci. Rep.* **2020**, *10*, 1–12.

[3] U. Yaqoob, M. I. Younis, *Sensors* **2021**, *21*, 1–40.

[4] C. Monn, *Atmos. Environ.* **2001**, *35*, 1–32.

[5] R. A. Rohde, R. A. Muller, *PLoS One* **2015**, *10*, 1–14.

[6] A. J. Cohen, M. Brauer, R. Burnett, H. R. Anderson, J. Frostad, K. Estep, K. Balakrishnan, B. Brunekreef, L. Dandona, R. Dandona, V. Feigin, G. Freedman, B. Hubbell, A. Jobling, H. Kan, L. Knibbs, Y. Liu, R. Martin, L. Morawska, C. A. Pope, H. Shin, K. Straif, G. Shaddick, M. Thomas, R. van Dingenen, A. van Donkelaar, T. Vos, C. J. L. Murray, M. H. Forouzanfar, *Lancet* **2017**, *389*, 1907–1918.

[7] R. J. Reiffenstein, W. C. Hulbert, S. H. Roth, *Annu. Rev. Pharmacol. Toxicol.* **1992**, *32*, 109–134.

[8] R. O. Beauchamp, J. S. Bus, J. A. Popp, C. J. Boreiko, D. A. Andjelkovich, P. Leber, *Crit. Rev. Toxicol.* **1984**, *13*, 25–97.

[9] D. C. Dorman, M. L. Foster, *Hydrogen Sulfide*, **2016**.

[10] Y. Ogasawara, K. Ishii, T. Togawa, S. Tanabet, **1991**, *116*, 1359–1363.

[11] C. Gru, P. M. Sarradin, H. Legoff, S. Narcon, J. C. Caprais, F. H. Lallier, *Analyst* **1998**, *123*, 1289–1293.

[12] T. Ramstad, A. H. Bates, T. J. Yellig, S. J. Borchert, K. A. Mills, *Analyst* **1995**, *120*, 2775–2780.

[13] P. R. Bérubé, P. D. Parkinson, E. R. Hall, *J. Chromatogr. A* **1999**, *830*, 485–489.

[14] Z. Mao, A. Anani, R. E. White, S. Srinivasan, A. J. Appleby, *J. Electrochem. Soc.* **1991**, *138*, 1299–1303.

[15] Y. Yan, N. Miura, N. Yamazoe, *Chem. Lett.* **1994**, 1753–1756.

[16] J. A. Bennett, J. E. P. Iii, M. A. Neiswonger, *J. Electroanal. Chem.* **2011**, *654*, 1–7.

[17] K. Stemmler, M. Ammann, C. Donders, J. Kleffmann, C. George, *Nature* **2006**, *440*, 195–198.

[18] N. M. Elsayed, *Toxicology* **1994**, *89*, 161–174.

[19] S. Tanaka, T. Esaka, *Mater. Res. Bull.* **2000**, *35*, 2491–2502.

[20] K. Kikugawa, T. Kato, Y. Okamoto, *Free Radical Biol. Med.* **1994**, *16*, 373–382.

[21] R. R. Reston, E. S. Kolesar, *Journal of Microelectromechanical Systems* **1994**, *3*, 134–146.

[22] A. M. Winer, J. W. Peters, J. P. Smith, J. N. Pitts, *Environ. Sci. Technol.* **1974**, *8*, 1118–1121.

[23] E. J. Dunlea, S. C. Herndon, D. D. Nelson, R. M. Volkamer, F. San Martini, P. M. Sheehy, M. S. Zahniser, J. H. Shorter, J. C. Wormhoudt, B. K. Lamb, E. J. Allwine, J. S. Gaffney, N. A. Marley, M. Grutter, C. Marquez, S. Blanco, B. Cardenas, A. Retama, C. R. R. Yillegas, C. E. Kolb, L. T. Molina, M. J. Molina, *Atmos. Chem. Phys.* **2007**, *7*, 2691–2704.

[24] S. - C Chang, J. R. Stetter, *Electroanalysis* **1990**, *2*, 359–365.

[25] J. M. Sedlak, K. F. Blurton, *Talanta* **1976**, *23*, 811–814.

[26] J. S. Do, W. B. Chang, *Sens. Actuators, B* **2001**, *72*, 101–107.

[27] Z. Duan, Y. Zhang, Y. Tong, H. Zou, J. Peng, X. Zheng, *J. Electron. Mater.* **2017**, *46*, 6895–6900.
[28] N. Spãtaru, T. N. Rao, D. A. Tryk, A. Fujishima, *J. Electrochem. Soc.* **2001**, *148*, E112.
[29] C. E. Banks, A. Goodwin, C. G. R. Heald, R. G. Compton, *Analyst* **2005**, *130*, 280–282.
[30] R. Zhu, M. Desroches, B. Yoon, T. M. Swager, *ACS Sensors* **2017**, *2*, 1044–1050.
[31] M. Erecińska, I. A. Silver, *Respir. Physiol.* **2001**, *128*, 263–276.
[32] D. S. Martin, M. P. W. Grocott, *Crit. Care Med.* **2013**, *41*, 423–432.
[33] M. Morgante, M. Gianesella, S. Casella, L. Ravarotto, C. Stelletta, E. Giudice, *Comp. Clin. Pathol.* **2009**, *18*, 229–232.
[34] P. Leonard, N. R. Grubb, P. S. Addison, D. Clifton, J. N. Watson, *Journal of Clinical Monitoring and Computing* **2004**, *18*, 309–312.
[35] T. O. McBride, B. W. Pogue, E. D. Gerety, S. B. Poplack, U. L. Österberg, K. D. Paulsen, *Appl. Opt.* **1999**, *38*, 5480.
[36] G. Mardirossian, R. E. Schneider, *Anesth.Prog.* **1992**, *39*, 194–196.
[37] M. Elas, K. H. Ahn, A. Parasca, E. D. Barth, D. Lee, C. Haney, H. J. Halpern, *Clin. Cancer. Res.* **2006**, *12*, 4209–4217.
[38] D. R. Collingridge, J. M. Piepmeier, S. Rockwell, J. P. S. Knisely, *Radiother. Oncol.* **1999**, *53*, 127–131.
[39] W. L. Markus, P. A. Bruttel, *J. Am. Oil Chem. Soc.* **2014**, 792–795.
[40] J. H. T. Luong, K. B. Male, J. D. Glennon, *Analyst* **2009**, *134*, 1965–1979.
[41] R. G. Compton, J. S. Foord, F. Marken, *Electroanalysis* **2003**, *15*, 1349–1363.
[42] J. V Macpherson, *Phys.Chem.Chem.Phys.* **2015**, *17*, 2935–2949.
[43] G. Ogata, Y. Ishii, K. Asai, Y. Sano, F. Nin, T. Yoshida, T. Higuchi, S. Sawamura, T. Ota, K. Hori, K. Maeda, S. Komune, K. Doi, M. Takai, I. Findlay, H. Kusuhara, Y. Einaga, H. Hibino, *Nat. Biomed. Eng.* **2017**, *1*, 654–666.
[44] A. Hanawa, K. Asai, G. Ogata, H. Hibino, Y. Einaga, *Electrochim. Acta* **2018**, *271*, 35–40.
[45] T. Watanabe, Y. Honda, K. Kanda, Y. Einaga, *Phys. Status Solidi. A* **2014**, *211*, 2709–2717.
[46] Z. J. Ayres, A. J. Borrill, J. C. Newland, M. E. Newton, J. V. Macpherson, *Anal. Chem.* **2016**, *88*, 974–980.
[47] I. Duo, A. Fujishima, C. Comninellis, *Electrochem. Commun.* **2003**, *5*, 695–700.
[48] S. C. B. Oliveira, A. M. Oliveira-Brett, *Electrochim. Acta* **2010**, *55*, 4599–4605.
[49] C. A. Rossi Salamanca-Neto, F. A. Yoshida, E. R. Sartori, J. Tobias Moraes, *Anal. Methods* **2018**, *10*, 3347–3352.
[50] H. Notsu, I. Yagi, T. Tatsuma, D. A. Tryk, A. Fujishima, *J. Electroanal. Chem* **2000**, *492*, 31–37.
[51] M. Murata, T. A. Ivandini, M. Shibata, S. Nomura, A. Fujishima, Y. Einaga, *J. Electroanal. Chem.* **2008**, *612*, 29–36.
[52] A. Suzuki, T. A. Ivandini, A. Kamiya, S. Nomura, M. Yamanuki, K. Matsumoto, A. Fujishima, Y. Einaga, *Sens. Actuators, B* **2007**, *120*, 500–507.
[53] M. Chiku, T. A. Ivandini, A. Kamiya, A. Fujishima, Y. Einaga, *J. Electroanal. Chem.* **2008**, *612*, 201–207.

[54] A. Preechaworapun, T. A. Ivandini, A. Suzuki, A. Fujishima, O. Chailapakul, Y. Einaga, *Anal. Chem.* **2008**, *80*, 2077–2083.
[55] Y. Einaga, *J. Appl. Electrochem.* **2010**, *40*, 1807–1816.
[56] Z. Wang, P. Lin, G. A. Baker, J. Stetter, X. Zeng, **2011**, 7066–7073.
[57] S. Ernst, L. Aldous, R. G. Compton, *J. Electroanal. Chem* **2011**, *663*, 108–112.
[58] C. A. Martínez-Huitle, N. Suely Fernandes, S. Ferro, A. De Battisti, M. A. Quiroz, *Diamond and Related Materials* **2010**, *19*, 1188–1193.
[59] M. Rycewicz, M. Ficek, K. Gajewski, S. Kunuku, J. Karczewski, T. Gotszalk, I. Wlasny, A. Wysmołek, R. Bogdanowicz, *Carbon* **2021**, *173*, 832–841.
[60] T. A. Ivandini, D. Yamada, T. Watanabe, H. Matsuura, N. Nakano, A. Fujishima, Y. Einaga, *J. Electroanal. Chem* **2010**, *645*, 58–63.
[61] Y. Triana, M. Tomisaki, Y. Einaga, *J. Electroanal. Chem* **2020**, *873*, 114411.
[62] Y. Triana, * Irkham, Y. Einaga, *Electroanalysis* **2021**, 1–10.
[63] M. Wang, N. Simon, C. Decorse-Pascanut, M. Bouttemy, A. Etcheberry, M. Li, R. Boukherroub, S. Szunerits, *Electrochim. Acta* **2009**, *54*, 5818–5824.
[64] B. P. Chaplin, D. K. Hubler, J. Farrell, *Electrochim. Acta* **2013**, *89*, 122–131.
[65] L. A. Hutton, J. G. Iacobini, E. Bitziou, R. B. Channon, M. E. Newton, J. V. Macpherson, *Anal. Chem.* **2013**, *85*, 7230–7240.
[66] S. Ghodbane, D. Ballutaud, A. Deneuville, C. Baron, *Phys. Stat. Sol.* **2006**, *203*, 3147–3151.
[67] R. Boukherroub, X. Wallart, S. Szunerits, B. Marcus, P. Bouvier, M. Mermoux, *Electrochem. Commun.* **2005**, *7*, 937–940.
[68] G. R. Salazar-Banda, L. S. Andrade, P. A. P. Nascente, P. S. Pizani, R. C. Rocha-Filho, L. A. Avaca, *Electrochim. Acta* **2006**, *51*, 4612–4619.
[69] S. Kasahara, K. Natsui, T. Watanabe, Y. Yokota, Y. Kim, S. Iizuka, Y. Tateyama, Y. Einaga, *Anal. Chem.* **2017**, *89*, 11341–11347.
[70] R. Hoffmann, A. Kriele, H. Obloh, J. Hees, M. Wolfer, W. Smirnov, N. Yang, C. E. Nebel, *Appl. Phys. Lett.* **2010**, *97*, 1–4.
[71] C. Yamaguchi, K. Natsui, S. Iizuka, Y. Tateyama, Y. Einaga, *Phys. Chem. Chem. Phys.* **2019**, *21*, 13788–13794.
[72] T. A. Ivandini, Y. Einaga, *Bull. Chem. Soc. Jpn.* **2021**, *94*, 2838–2847.
[73] K. Maebashi, K. Iwadate, K. Sakai, A. Takatsu, K. Fukui, M. Aoyagi, E. Ochiai, T. Nagai, *Forensic Sci. Int.* **2011**, *207*, 91–95.
[74] S. L. Malone Rubright, L. L. Pearce, J. Peterson, *Nitric Oxide* **2017**, *71*, 1–13.
[75] A. F. L. Godoi, A. M. Grasel, G. Polezer, A. Brown, S. Potgieter-Vermaak, D. C. Scremim, C. I. Yamamoto, R. H. M. Godoi, *Sci. Total Environ.* **2018**, *610–611*, 583–590.
[76] M. Maasikmets, E. Teinemaa, A. Kaasik, V. Kimmel, *Biosyst. Eng.* **2015**, *139*, 48–59.
[77] T. Xu, N. Scafa, L. P. Xu, S. Zhou, K. Abdullah Al-Ghanem, S. Mahboob, B. Fugetsu, X. Zhang, *Analyst* **2016**, *141*, 1185–1195.
[78] V. Stanić, T. H. Etsell, A. C. Pierre, R. J. Mikula, *Electrochim. Acta* **1998**, *43*, 2639–2647.
[79] P. Jeroschewski, K. Haase, A. Trommer, P. Gründler, *Electroanalysis* **1994**, *6*, 769–772.

[80] G. Schiavon, G. Zotti, R. Toniolo, G. Bontempelli, *Anal. Chem.* **1995**, *67*, 318–323.
[81] N. S. Lawrence, J. Davis, L. Jiang, T. G. J. Jones, S. N. Davies, R. G. Compton, *Electroanalysis* **2000**, *12*, 1453–1460.
[82] A. N. Buckley, I. C. Hamilton, R. Woods, *J. Electroanal. Chem* **1987**, *216*, 213–227.
[83] P. G. Komorowski, *Electrochim. Acta* **1994**, *39*, 2285–2289.
[84] J. E. Doeller, T. S. Isbell, G. Benavides, J. Koenitzer, H. Patel, R. P. Patel, J. R. Lancaster, V. M. Darley-Usmar, D. W. Kraus, *Anal. Biochem.* **2005**, *341*, 40–51.
[85] A. M. O'Mahony, D. S. Silvester, L. Aldous, C. Hardacre, R. G. Compton, *J. Phys. Chem. C* **2008**, *112*, 7725–7730.
[86] Q. Huang, W. Li, T. Wu, X. Ma, K. Jiang, X. Jin, *Electrochem. Commun.* **2018**, *88*, 93–96.
[87] M. D. Brown, J. R. Hall, M. H. Schoenfisch, *Anal. Chim. Acta* **2019**, *1045*, 67–76.
[88] S. J. Cobb, Z. J. Ayres, J. V. Macpherson, *Annu. Rev. Anal. Chem.* **2018**, *11*, 463–484.
[89] K. Asai, T. A. Ivandini, Y. Einaga, *Scientific Reports* **2016**, *6*, 1–10.
[90] T. A. Ivandini, B. V. Sarada, C. Terashima, T. N. Rao, D. A. Tryk, H. Ishiguro, Y. Kubota, A. Fujishima, *J. Electroanal. Chem* **2002**, *521*, 117–126.
[91] S. Falina, S. Kawai, N. Oi, H. Yamano, T. Kageura, E. Suaebah, M. Inaba, Y. Shintani, M. Syamsul, H. Kawarada, *Sensors* **2018**, *18*, 1–10.
[92] K. Waterston, D. Bejan, N. J. Bunce, *J. Appl. Electrochem.* **2007**, *37*, 367–373.
[93] E. Bitziou, M. B. Joseph, T. L. Read, N. Palmer, T. Mollart, M. E. Newton, J. V. Macpherson, *Anal. Chem.* **2014**, *86*, 10834–10840.
[94] S. J. Broderius, L. L. Smith, *Anal. Chem.* **1977**, *49*, 424–428.
[95] Z. Pawlak, A. S. Pawlak, *Talanta* **1999**, *48*, 347–353.
[96] K. Park, H. Lee, S. Phelan, S. Liyanaarachchi, N. Marleni, D. Navaratna, V. Jegatheesan, L. Shu, *Int. Biodeterior. Biodegrad.* **2014**, *95*, 251–261.
[97] P. C. Caliari, M. J. Pacheco, L. F. Ciríaco, A. M. C. Lopes, *J. Braz. Chem. Soc.* **2017**, *28*, 557–566.
[98] J. Xu, K. Natsui, S. Naoi, K. Nakata, Y. Einaga, *Diamond Relat. Mater.* **2018**, *86*, 167–172.
[99] Irkham, T. Watanabe, Y. Einaga, *Anal. Chem.* **2017**, *89*, 7139–7144.
[100] A. J. Bard, L. R. Faulkner, *Electrochemical Methods: Fundamentals and Applications*, Wiley, New York, **2001**.
[101] P. Zanello, *Inorganic Electrochemistry: Theory, Practice, and Application*, The Royal Society Of Chemistry, Cambridge, UK, **2003**.
[102] N. S. Lawrence, M. Thompson, C. Prado, L. Jiang, T. G. J. Jones, R. G. Compton, *Electroanalysis* **2002**, *14*, 499–504.
[103] G. H. Kelsall, I. Thompson, *J. Appl. Electrochem.* **1993**, *23*, 427–434.
[104] A. V. Kroll, V. Smorchkov, A. Y. Nazarenko, *Sens. Actuators B* **1994**, *21*, 97–100.
[105] H. Zanin, P. W. May, D. J. Fermin, D. Plana, S. M. C. Vieira, W. I. Milne, E. J. Corat, *ACS Appl. Mater. Interfaces* **2014**, *6*, 990–995.
[106] P. J. Vandeberg, J. L. Kowagoe, D. C. Johnson, *Anal. Chim. Acta* **1992**, *260*, 1–11.
[107] J. Szynkarczuk, P. G. Komorowski, J. C. Donini, *Electrochim. Acta* **1995**, *40*, 487–494.
[108] Ramasubramanian N., *J. Electroanal. Chem* **1975**, *64*, 21–37.
[109] A. Ahnood, H. Meffin, D. J. Garrett, K. Fox, K. Ganesan, A. Stacey, N. V. Apollo, Y.

T. Wong, S. G. Lichter, W. Kentler, O. Kavehei, U. Greferath, K. A. Vessey, M. R. Ibbotson, E. L. Fletcher, A. N. Burkitt, S. Prawer, *Adv. Biosys.* **2017**, *1*, 1–10.
[110] A. Shrivastava, V. Gupta, *Chronicles of Young Scientists* **2011**, *2*, 21.
[111] N. S. Lawrence, R. P. Deo, J. Wang, **2004**, *517*, 131–137.
[112] P. K. Jiwanti, Y. Einaga, *Phys. Chem. Chem. Phys.* **2019**, *21*, 15297–15301.
[113] W. E. Luttrell, *J. Chem. Health Saf.* **2014**, *21*, 28–30.
[114] D. Brannegan, M. Ashraf-Khorassani, L. T. Taylor, *J. Chromatogr. Sci.* **2001**, *39*, 217–221.
[115] N. A. Marley, J. S. Gaffney, R. V. White, L. Rodriguez-Cuadra, S. E. Herndon, E. Dunlea, R. M. Volkamer, L. T. Molina, M. J. Molina, *Rev. Sci. Instrum.* **2004**, *75*, 4595–4605.
[116] F. M. Black, J. E. Sigsby, *J. Environ. Sci. Technol.* **1974**, *8*, 149–152.
[117] J. E. Sigsby, F. M. Black, T. A. Bollar, D. L. Klosterman, *J. Environ. Sci. Technol.* **1973**, *7*, 51–54.
[118] B. G. Snider, D. C. Johnson, *Anal. Chim. Acta* **1979**, *105*, 9–23.
[119] K. Wang, H. Yan, J. Liu, X. Sun, E. Wang, *Electroanalysis* **2004**, *16*, 1318–1323.
[120] K. C. Ho, W. T. Hung, *Sens. Actuators B* **2001**, *79*, 11–16.
[121] C. Y. Lin, W. T. Hung, C. T. Wu, K. C. Ho, *Sens. Actuators, B* **2009**, *136*, 32–38.
[122] N. Miura, G. Lu, N. Yamazoe, *Sens. Actuators, B* **1998**, *52*, 169–178.
[123] J. M. Sedlak, K. F. Blurton, *J. Electrochem. Soc.* **1976**.
[124] K. Y. Lee, C. Amatore, J. K. Kochi, *J. Phys. Chem. C* **1991**, *95*, 1285–1294.
[125] R. Zhang, X. Liu, T. Zhou, L. Wang, T. Zhang, *J. Colloid Interface Sci.* **2018**, *524*, 76–83.
[126] B. Liu, X. Liu, Z. Yuan, Y. Jiang, Y. Su, J. Ma, H. Tai, *Sens. Actuators, B* **2019**, *295*, 86–92.
[127] Y. Einaga, *Bull. Chem. Soc. Jpn* **2018**, *91*, 1752–1762.
[128] Y. Honda, T. A. Ivandini, T. Watanabe, K. Murata, Y. Einaga, *Diamond Relat. Mater.* **2013**, *40*, 7–11.
[129] N. Badiadka, S. Kenchaiah, *Eurasian J. Anal. Chem.* **1976**, *21*, 302–305.
[130] N. Kamoshida, S. Kasahara, N. Ikemiya, N. Hoshi, M. Nakamura, Y. Einaga, *Diamond Relat. Mater.* **2019**, *93*, 50–53.
[131] E. Riordan, N. Minogue, D. Healy, P. O'Driscoll, J. R. Sodeau, *J. Phys. Chem. A* **2005**, *109*, 779–786.
[132] J. Wang, G. M. Swain, *J. Electrochem. Soc.* **2003**, *150*, E24.
[133] D. O'Sullivan, J. R. Sodeau, *J. Phys. Chem. A* **2010**, *114*, 12208–12215.
[134] K. Kim, H. Y. Chung, J. Ju, J. Kim, *Sci. Total Environ.* **2017**, *590–591*, 107–113.
[135] D. A. Armstrong, R. E. Huie, W. H. Koppenol, S. V. Lymar, G. Merényi, P. Neta, B. Ruscic, D. M. Stanbury, S. Steenken, P. Wardman, *Chem. Intl.* **2016**, *38*, 1–294.
[136] Y. Kameoka, R. L. Pigford, *Ind. Eng. Chem., Fundam.* **1977**, *16*, 163–169.
[137] C. Zou, B. Yang, D. Bin, J. Wang, S. Li, P. Yang, C. Wang, Y. Shiraishi, Y. Du, *J. Colloid Interface Sci.* **2017**, *488*, 135–141.
[138] M. Y. Mihaylov, V. R. Zdravkova, E. Z. Ivanova, H. A. Aleksandrov, P. S. Petkov, G. N. Vayssilov, K. I. Hadjiivanov, *J. Catal.* **2020**, 1–14.
[139] D. J. Goebbert, E. Garand, T. Wende, R. Bergmann, G. Meijer, K. R. Asmis, D. M.

Neumark, *J. Phys. Chem. A* **2009**, *113*, 7584–7592.
[140] O. Husson, *Plant Soil* **2013**, *362*, 389–417.
[141] B. R. Kozub, N. V. Rees, R. G. Compton, *Sens. Actuators, B* **2010**, *143*, 539–546.
[142] F. Opekar, *Electroanalysis* **1992**, *4*, 133–138.
[143] A. V. Kalinkin, M. Y. Smirnov, V. I. Bukhtiyarov, *Kinetics and Catalysis* **2016**, *57*, 826–830.
[144] R. Ewald, *Arch. Intern. Med.* **1971**, *128*, 7–9.
[145] C. R. Taylor, E. R. Weibel, *Respir. Physiol.* **1981**, *44*, 1–10.
[146] R. L. Hoiland, A. R. Bain, M. G. Rieger, D. M. Bailey, P. N. Ainslie, *Am. J. Physiol: Regul., Integr. Comp. Physiol.* **2016**, *310*, 398–413.
[147] M. J. Tobin, F. Laghi, A. Jubran, *Am. J. Respir. Crit. Care. Med.* **2020**, *202*, 356–360.
[148] M. Coen, G. Allali, D. Adler, J. Serratrice, *J. Med. Virol.* **2020**, *92*, 1705–1706.
[149] S. Dhont, E. Derom, E. Van Braeckel, P. Depuydt, B. N. Lambrecht, *Respir. Res.* **2020**, *21*, 1–9.
[150] K. Haryalchi, A. Heidarzadeh, M. Abedinzade, S. Olangian-tehrani, S. G. Tehran, *Reg. Anesth. Pain Med.* **2021**, *11*, 19–21.
[151] R. M. Bersin, M. Kwasman, D. Lau, C. Klinski, K. Tanaka, P. Khorrami, T. Demarco, C. Wolfe, K. Chatterjee, *Heart* **1993**, *70*, 443–447.
[152] S. M. Cohn, A. B. Nathens, F. A. Moore, J. C. Puyana, E. E. Moore, G. J. Beilman, T. Investigators, *J. Trauma* **2007**, *62*, 44.
[153] D. A. Benaron, B. E. Rubinsky, D. M. Otten, C. J. Levinson, A. L. Murphy, J. W. Price, J. P. Weersing, J. L. Duckworth, U. B. Hörchner, E. L. Kermit, *J. Biomed. Opt.* **2015**, *10*, 1–9.
[154] K. Cai, A. Shore, A. Singh, M. Haris, T. Hiraki, *NMR Biomed.* **2012**, *25*, 1125–1132.
[155] N. J. Crane, Z. D. Schultz, I. R. A. W. Levin, *J. Trauma* **2007**, *61*, 797–803.
[156] H. Matsumoto, N. Yoshimura, *Anesth. Analg.* **1996**, *83*, 513–518.
[157] M. Nitzan, I. Nitzan, *Med. Hypotheses* **2013**, *81*, 293–296.
[158] R. Ahmad, P. Kuppusamy, *Chem. Rev.* **2010**, *110*, 3212–3236.
[159] Steven J. Barker, Kevin K. Tremper, *Int. Anesthesiol. Clin.* **1987**, *25*, 155–175.
[160] N. K. Pandya, S. Sharma, *Capnography And Pulse Oximetry*, **2020**.
[161] R. G. Buckley, S. E. Aks, J. L. Eshom, R. Rydman, J. Schaider, P. Shayne, *Ann. Emerg. Med.* **1994**, *24*, 252–255.
[162] N. B. Hampson, *Chest* **1998**, *114*, 1036–1041.
[163] J. W. Severinghaus, S. O. Koh, *J. Clin. Monit.* **1990**, *6*, 85–88.
[164] B. J. Tromberg, *Med. Phys.* **2008**, *35*, 2443–2451.
[165] D. J. Faber, E. G. Mik, *Opt. Lett.* **2005**, *30*, 1015–1017.
[166] G. Mees, R. Dierckx, C. Vangestel, *Eur. J. Nucl. Med. Mol. Imaging.* **2009**, *36*, 1674–1686.
[167] K. A. Krohn, J. M. Link, R. P. Mason, *J. Nucl. Med.* **2008**, *49*, 129–148.
[168] J. M. Murkin, S. J. Adams, R. J. Novick, M. Quantz, D. Bainbridge, I. Iglesias, A. Cleland, B. Schaefer, B. Irwin, S. Fox, *Anesth. Analg.* **2007**, *104*, 51–58.
[169] S. Ramaswamy, S. Chang, V. Mehta, *Anaesthesia* **2015**, *70*, 518–522.
[170] S. Shaefi, P. Shankar, A. L. Mueller, B. P. O'Gara, K. Spear, K. R. Khabbaz, A. Bagchi, L. M. Chu, V. Banner-Goodspeed, D. E. Leaf, D. S. Talmor, E. R.

Marcantonio, B. Subramaniam, *Anesthesiology* **2021**, *134*, 189–201.
[171] C. Clark, C. Leland, G. Misrahy, R. P. F. Chroni-, *J. Appl. Physiol* **2021**.
[172] L. Nei, *ECS Trans.* **2007**, *2*, 33–38.
[173] C. Clark, Y. Springs, S. Public, *J. Appl. Physiol* **1953**.
[174] Donald G. Buerk, *Measuring Tissue PO2 with Microelectrodes*, **2004**.
[175] V. Brinzari, M. Ivanov, B. K. Cho, M. Kamei, G. Korotcenkov, *Sens. Actuators, B* **2010**, *148*, 427–438.
[176] L. Rivas, S. Dulay, S. Miserere, L. Pla, S. B. Marin, J. Parra, E. Eixarch, E. Gratacós, M. Illa, M. Mir, J. Samitier, *Biosens. Bioelectron.* **2020**, *153*, 112028.
[177] N. Holmstrom, P. Nilsson, J. Carlsten, *Biosens. Bioelectron.* **1998**, *13*, 1287–1295.
[178] M. S. El-deab, T. Ohsaka, *Electrochem. Commun.* **2003**, *5*, 214–219.
[179] F. B. Bolger, S. B. Mchugh, R. Bennett, J. Li, K. Ishiwari, J. Francois, M. W. Conway, G. Gilmour, D. M. Bannerman, M. Fillenz, M. Tricklebank, J. P. Lowry, *J. Neurosci. Methods* **2011**, *195*, 135–142.
[180] F. B. Bolger, R. Bennett, J. P. Lowry, *Analyst* **2011**, *136*, 4028–4035.
[181] B. J. Venton, D. J. Michael, R. M. Wightman, *J. Neurochem.* **2003**, 373–381.
[182] G. Bazzu, G. G. M. Puggioni, S. Dedola, G. Calia, G. Rocchitta, R. Migheli, M. S. Desole, J. P. Lowry, R. D. O. Neill, P. A. Serra, *Anal. Chem.* **2009**, *81*, 2235–2241.
[183] D. A. Tryk, K. Hashimoto, A. Fujishima, *J. Electrochem. Soc.* **1998**, *145*, 1870–1876.
[184] Y. Zhang, V. Suryanarayanan, I. Nakazawa, S. Yoshihara, T. Shirakashi, *Electrochim. Acta* **2004**, *49*, 5235–5240.
[185] Y. Zhang, S. Asahina, S. Yoshihara, T. Shirakashi, *Electrochim. Acta* **2003**, *48*, 741–747.
[186] T. A. Ivandini, E. Saepudin, H. Wardah, Harmesa, N. Dewangga, Y. Einaga, *Anal. Chem.* **2012**, *84*, 9825–9832.
[187] L. Hutton, M. E. Newton, P. R. Unwin, J. V. Macpherson, *Anal. Chem.* **2009**, *81*, 1023–1032.
[188] T. A. Ivandini, M. S. P. Luhur, M. Khalil, Y. Einaga, *Analyst* **2021**.
[189] T. L. Read, S. J. Cobb, J. V Macpherson, *ACS Sens.* **2019**, *4*, 756–763.
[190] J. Zhang, M. Oyama, *Microchem. J.* **2004**, *78*, 217–222.
[191] N. Marina, I. N. Christie, A. Korsak, M. Doronin, A. Brazhe, P. S. Hosford, J. A. Wells, S. Sheikhbahaei, I. Humoud, J. F. R. Paton, M. F. Lythgoe, A. Semyanov, S. Kasparov, A. V. Gourine, *Nat. Commun.* **2020**, *11*, 1–9.
[192] M. Gehrung, S. E. Bohndiek, J. Brunker, *J. Biomed. Opt.* **2019**, *24*, 1.
[193] K. Nishi, K. Yamasaki, M. Otagiri, *Serum Albumin, Lipid and Drug Binding*, **2020**.
[194] S. Sakthinathan, A. K. Keyan, R. Rajakumaran, S. M. Chen, T. W. Chiu, C. Dong, S. Vinothini, *Catalysts* **2021**, *11*, 1–21.
[195] D. Moitra, C. Anand, B. K. Ghosh, M. Chandel, N. N. Ghosh, *ACS Appl. Energy Mater.* **2018**, *1*, 464–474.
[196] P. R. Solanki, S. Srivastava, M. A. Ali, R. K. Srivastava, A. Srivastava, B. D. Malhotra, *RSC Advances* **2014**, *4*, 60386–60396.
[197] T. Pavon, *Sustain. Environ. Res.* **2013**, *23(4)*, 259–266.
[198] Y. F. Huang, M. T. M. Koper, *Journal of Physical Chemistry Letters* **2017**, *8*, 1152–1156.

[199] J. Xu, M. C. Granger, Q. Chen, J. W. Strojek, T. E. Lister, G. M. Swain, *Anal. Chem.* **1997**, *69*, 591A-597A.
[200] T. Nagaoka, T. Yoshino, *Anal. Chem.* **1986**, *58*, 1037–1042.
[201] A. M. Feltham, M. Spiro, *Chem. Rev.* **1971**, *71*, 177–193.
[202] A. Shrivastava, V. Gupta, *Chron. Young Sci.* **2011**, *2*, 21.
[203] I. jr Tinoco, O. C. Uhlenbeck, M. D. Levine, *Nature* **1971**, *230*, 362–367.
[204] R. T. Duarte, M. C. Carvalho Simões, V. C. Sgarbieri, *J. Agric. Food Chem.* **1999**, *47*, 231–236.
[205] O. Nekrassova, N. S. Lawrence, R. G. Compton, *Analyst* **2004**, *129*, 804–805.
[206] Kevin M. Tenny, J. S. Cooper, *Ideal Gas Behavior*, **2017**.
[207] E. A. Lakota, C. B. Landersdorfer, R. L. Nation, J. Li, K. S. Kaye, G. G. Rao, A. Forrest, *Antimicrob. Agents Chemother.* **2018**, *62*, 307–310.
[208] John. B West, *Respiratory Physiology*, Lippincot Williams And Wilkins, California, **2004**.

LIST OF PUBLICATION AND CONFERENCES

1. Papers

Published papers presented in this thesis are:

(1) Y. Triana, M. Tomisaki, Y. Einaga,
Oxidation Reaction of Dissolved Hydrogen Sulfide Using Boron Doped Diamond
Journal of Electroanaytical Chemistry , Elsevier, **2020**, *873*, 114411.

(2) Y. Triana, Irkham, Y. Einaga,
Electrochemical Oxidation Behavior of Nitrogen Dioxide for Gas Detection Using Boron Doped Diamond Electrodes
Electroanalysis, Wiley Online Library, **2021**, 1–10.

Submitted paper presented in this thesis is:

Y. Triana, G. Ogata, M. Tomisaki, Irkham, Y. Einaga,
A Blood Oxygen Sensor using a Boron-Doped Diamond Electrode
Analytical Chemistry, Americal Chemical Society (ACS)

2. Online Conferences

International conferences are:

(1) Y. Triana, Y. Einaga,
"The Application of Boron-Doped Diamond (BDD) Electrodes for Gas Sensor"
The 2nd International Webinar in Collaboration with Sakura Science Alumni, Balikpapan, Indonesia (on-line), 2021/06/30

(2) Y. Triana, M. Tomisaki, Y. Einaga,
Electrochemical Gas Sensing by Boron-Doped Diamond Electrodes: Hydrogen Sulfide Detection
Nanotechnologies for 21st Centuries, Cooperation Event Between Albania, Spain and Japan, Madrid, Spain (on-line), 2021/10/07

(3) Y. Triana, Irkham, Y. Einaga,
Electrochemical Sensing of Nitrogen Dioxide for Gas Detection on Boron Doped Diamond Electrodes
The International Chemical Congress of Pacific Basin Societies, Pacifichem, Honolulu, Hawai (on-line), 2021/12/16

Domestic conference is:

Y. Triana, M. Tomisaki, Y. Einaga,
Electrochemical Sensing of Dissolved Hydrogen Sulfide on Boron Doped Diamond Electrodes
34th Diamond Symposium, Tokyo, Japan (on-line), 2021/01/12

ACKNOWLEDGMENT

Praise and gratitude to Allah SWT, because of the permission I was able to complete the thesis book entitled "*Application of Boron Doped Diamond Electrodes to Electrochemical Gas Sensors*". This dissertation book was made as an initial series of final assignments to complete PhD in Engineering at Graduate School of Integrated Design Engineering, Keio University, Tokyo Japan.

Through this opportunity, I would like to give my highest honor and special thanks to **Ministry of Finance, Indonesia Republic** who gives me fully funded support by LPDP Scholarship for my doctoral program. I also would like to express biggest gratitude and thanks to **Prof. Dr. Yasuaki Einaga** as a supervisor who has provided guidance, direction and encourage for every detail research process and gave facilities for me. I had no problem to do experiments and publish papers even in the period of COVID-19 situation in Japan. You are my role model to be a better lecturer and researcher in the future. Also, I would like to thank:

1. Prof. Dr.sc.nat. Daniel Citterio, Prof. Taku Hasobe, Ph.D, and Dr. Teruhiko Matsubara, as my reviewers of doctoral defenses. All your questions and suggestions made this dissertation book perfect.
2. Dr. Gengki Ogata, Dr. Takashi Yamamoto, and all Einaga's laboratory group members for the attention and supports in any condition.
3. Mrs. Ruriko Einaga and Ms. Karin Einaga (Prof. Dr. Yasuaki Einaga's family) for supports, understanding, and attentions for my staying period in Japan.
4. Prof. Masato Tominaga from Saga University for big attention and supports me to be the best.
5. Prof. Ir. Budi Santosa, M.Sc., Ph.D, management staffs, lecturers and all colleagues at Institut Teknologi Kalimantan (ITK) for supports my lecturer career.
6. My most beloved late father Mr. Hadi Waluyo bin Dul Manap and beloved mother Mrs. Sukesi binti Sumo Mukiran. You own my heart and my praying is for you every second. Thank you for loving me and let us meet again in Allah's heaven.
7. My best friend and beloved husband, Andi Purwanto, S.H. Thank you for being with me in Japan since April 2019. Your patient and understanding about me are the best two things in the world.
8. My father in law Mr. Supadianto and mother in law Mrs. Ismiatun for understanding my situation and keep my spirit to finish my study.
9. My other family members and all best friends in Indonesia and Japan who give me spirit and nice relationships.

Finally, I hope that this book can be useful for the development of electrochemical gas sensor using BDD electrodes.

Japan, Februari 2022

Yunita Triana

BIBILIOGRAPHY

YUNITA TRIANA, was born on October 23, 1988 in Balikpapan, East Kalimantan. She is the third child from the couple of Mr. Hadi Waluyo and Mrs. Sukesi. The author started his education in 1996 at SDN 020 Balikpapan. In the same year she continued Junior High School at SLTP Negeri 5 Balikpapan. She continued his education to Senior High School at SMA Negeri 4 Balikpapan in 2003. In 2006, she continued bachelor education in Department of Chemistry, Mulawarman University, Samarinda, East Kalimantan and graduated in 2010. In 2013, she took master education in Department of Chemistry, Institut Teknologi Sepuluh Nopember (ITS), Surabaya. The author is a lecturer in Department of Materials and Metallurgical Engineering, Institut Teknologi Kalimantan (ITK) since September 2015. In 2018, she continued doctoral program at School of Integrated Design Engineering, Keio University, Japan by using LPDP Scholarship from Ministry of Finance, Indonesia Republic. During her PhD program, she published four papers, joined four conferences and active to be a speaker in national and international webinars.